Interfacial and insulating properties of GaN metal-oxide-semiconductor structure with Al_2O_3 gate oxide

（Al_2O_3 絶縁膜を用いた GaN MOS 構造における

界面と絶縁膜の特性評価）

March 2019

Yuta Fujimoto

Graduate School of Materials Science

Nara Institute of Science and Technology

Contents

Chapter 1 Introduction **1**
1.1 Background...1
1.2 Fundamentals of Galium Nitride (GaN) in Group III-Nitride 5
1.2.1 Crystal structure of GaN 5
1.2.2 Comparison of physical properties as power semiconductor ..6
1.3 Power devices using GaN-based semiconductors and their technical issues…......12
1.3.1. Current status of GaN Metal Oxide Semiconductor field Effect Transistor...12
1.3.2 Influence of gate insulation in GaN MOSFET 14
1.4 Problems of power GaN MOSFET fabrication process technology 16
1.5 Objectives and Outline of This Thesis 20
References 22

Chapter 2 Characteristics of GaN MOS capacitor by HPWVA............................**25**
2.1 Introduction 25
2.2 Atomic Layer Deposition (ALD) 26
2.3 High Pressure Water Vapor Annealing (HPWVA)..28
2.4 Experimerntal method 33
2.4.1 Device fabrication 33
2.4.2 Capacitance –Voltage (C-V) method 35
2.4.2.1 Outline of C-V method...35
2.4.2.2 Ideal curve and interface states in MOS structures 39
2.4.3 Experimental apparatus 42
2.4.3.1 X-ray photoelectron spectroscopy (XPS).....................42
2.4.3.2 Temperature-Programmed Desorption (TPD)...............44
2.4.3.3 Secondary Ion Mass Spectrometry (SIMS)..................44
2.4.3.4 Atomic force microscopy (AFM).................................45
2.5 Electrical characterization of GaN MOS capacitor...46
2.5.1 C-V charactarization 46
2.5.2 I-V charactarizaion 52
2.6 Investigation of HPWVA effect with GaN MOS capacitor 56
2.6.1 Change the ALD-Al_2O_3 film quality 56
2.6.2 Diffusion of active species derived from HPWVA.................59
2.6.3 Oxdation of GaN in Al_2O_3/GaN Interface..............................61

2.7 Grain growth of GaOx in HPWVA under high pressure....................................63
2.8 Discussion on reaction model of HPWVA....................................67
2.9 Electrical characterization in high temperature condition....................................69
2.9.1 I-V charactarization 69
2.9.2 C-V charactarization 72
2.10 Summary....................................74
References 78

Chapter 3 Investigation of atomic structure in Al_2O_3/GaN interface 84
3.1 Introduction 84
3.2 Two-Dimensional Photoelectron Spectroscopy 85
3.3 Device fabrication....................................87
3.4 Investigation of atomic structure in Al_2O_3/GaN interface....................................88
3.4.1 STEM 88
3.4.2 Photoelectron Diffraction Pattern (PIAD)....................................89
3.5 Discussion on interfaical atomic sructure model....................................94
3.6 Summary....................................96
References 98

Chapter 4 Effect of ALD precursor on Al_2O_3/GaN MOS capacitors 100
4.1 Introduction 100
4.2 DMAH precursor of ALD-Al_2O_3 100
4.3 Device fabrication....................................102
4.4 Electrical characterization of MOS capacitor with DMAH 103
4.4.1 Comparison of characteristics between TMA and DMAH 103
4.4.2 Comparison of characteristics of DMAH samples with PDA...106
4.5 Investigation of the effect with the ALD-Al_2O_3 with DMAH 110
4.6 Summary....................................114
References 115

Chapter 5 Conclusion....................................117
5.1 Conclusions 117
5.2 Suggestions for future work 120
References 122

Achivement....................................123
Acknowledgments 126

Abbreviation list

Abbreviation	Official Appellation
CMOS	Complementary metal oxide semiconductor
MOSFET	Metal - oxide - semiconductor field effect transistor
LED	Light emitting diode
SBD	Schottky diode
HEMT	High electron mobility transistor
2DEG	Two dimensional electron gas
T-ALD	Thermal atomic layer deposition
JFET	Junction gate field-effect transistor
DIGS	Unified disorder induced gap state model
HPWVA	High pressure water annealing
PIAD	Photoelectron intensity angle distribution
DMAH	Dimethylaluminum hydride
CVD	Chemical vapor deposition
V_{FB}	Flat band voltage
D_{it}	Interface trap density
UPW	Ultra pure water
SCW	Super critical water
TMA	Trimethylaluminum
AC	Alternating-current
DC	Direct-current
C_G	Gate capacitance
C_S	Semiconductor capacitance
C_{OX}	Oxide capacitance
V_G	Gate voltage
C_{FB}	Flat band capacitance
N_F	Fixed charge density
C_{LF}	Capacitance the low-frequency
C_{HF}	Capacitance the high-frequency
C_{trap}	Trap capacitance
XPS	X-ray photoelectron spectroscopy
TOA	Take-off angles
TPD	Temperature-Programmed Desorption

SIMS	Secondary Ion Mass Spectrometry
AFM	Atomic force microscopy
ΔV_{th}	Hysteresis
TZDB	Time-zero dielectric breakdown test
FN plot	Fowler-Nordheim
PF plot	Poole-Frenkel
TAT plot	Trap Assisted Tunneling
SCC-FE	Space-charge-controlled field emission
E_{BD}	Breakdown electric field
TDDB	Time-dependent dielectric breakdown
FFP	Forward focusing peaks
DIANA	Display type spherical mirror analyzer
TEM	Transmission Electron Microscope
SEM	Scanning Electron Microscope
SE	Schottky emission
ABF-STEM	Annular bright-field scanning transmission electron microscopy
IMFP	Mean free path
PDA	post deposition anneal

Chapter 1
Introduction

1.1 Background

In recent years, the dependence on electrical energy has been increasing due to the progress of advanced information society. Because of the spread of information-related equipment, the rapid economic development of developing countries, and the increase of world population, global energy demand is expected to increase in the future. On the other hand, the global warming problem, which is concerned about the depletion of fossil fuels such as petroleum and natural gas as current major energy sources, increased abnormal weather and extinction of species is getting worse. In addition, there are no signs for it to be resolved yet. Therefore, it is expected not to use fossil fuel and to utilize clean energy with less environmental burden. Clean energy includes solar power generation, wind power generation, geothermal power generation, and the like. There are advantages such as suppressing emission of carbon dioxide, which is considered to be the cause of global warming, and inhibit emission of harmful radioactive waste. However, due to high power generation cost and the difficulty of stable supply, it is not a main energy source.

Figure 1-1 shows the recent trends in CO_2 emissions [1]. The CO_2 emissions show a slightly increasing trend, and the amount of "energy conversion" centered on power plants has increased to over 40% of the total. From these facts, it is suggested that our electricity consumption accounts for at least 50% of the total CO_2 emissions. Therefore, considering the convenience, economy and environmental friendliness of electrical energy, it is expected that demand will increase in the future, and device development for energy

conservation is required.

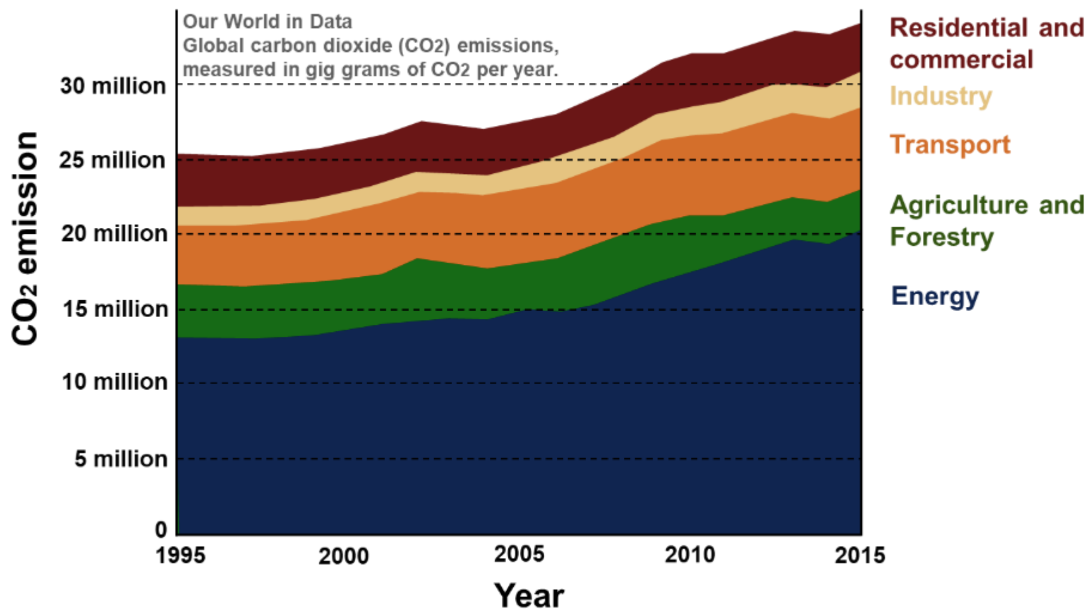

FIG. 1-1. The recent trends in CO_2 emissions. Each sectors shows the source of CO_2 emissions such as residential and commercial, industry, transport, agriculture and forestry, and energy [1].

For the history of semiconductors, transistors were invented by Shockley, Brattain, Bardeen et al., Bell Laboratories, which was known as the world's largest research center at that time in 1947 [2]. From 1960s, silicon has become the dominant semiconductor with the complementary metal oxide semiconductor (CMOS) process [3, 4]. The major driving force for the growth of the industry was scaling as described by the famous Moore's law [5]. This invention is counted as one of the greatest inventions of the 20th century and is believed to be the most fundamental one that supports modern life. After that, semiconductor technology has made rapid progress with numerous inventions. Among them, metal oxide semiconductor field effect transistor (MOSFET) can be mentioned as a big invention. With the advent of MOSFETs, the miniaturization of the

electronic circuit rapidly progressed. With the development of science and technology, our social life have been enriched and the amount of energy has been increasing.

The key to this energy saving is a power conversion element called a power device [6]. The market of power semiconductor devices in the world has grown from $ 11 billion in 2005 to $ 19 billion in 2018. The market did not monotonically increase, but responded sensitively to the market fluctuations for applied fields and grew up and down repeatedly. Trends of the power semiconductor device market are shown in the FIG. 1-2. Industry, consumer, and automobiles are the major markets since 2010 and these are growth fields. In 2013 these account for 80% of the total in 3 fields.

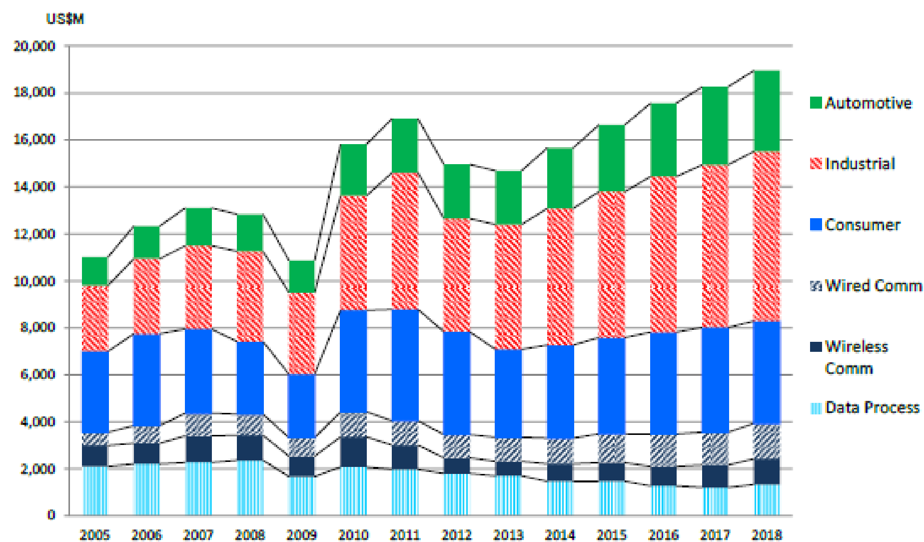

FIG. 1-2. Trends of the power semiconductor device market until 2018. The amount in the market was by automotive, industrial, consumer, wired comm., wireless comm. and data process [6].

The power device facilitates conversion from direct current to alternating current (or alternating current to direct current) and, voltage and frequency conversion. In addition, performance such as high breakdown voltage, large current, low loss and high speed

operation is required, and these have a trade-off relationship. In order to apply the power device to a wide range of power needs ranging from a small capacity to a large capacity, various types of devices have been used and developed. The application of power devices begins with power conversion during power generation and extends to home appliances equipped with inverters such as bullet trains, automobiles, air conditioners, and refrigerators that require motor rotation control. However, the generated electric power is not used directly. It is converted many times to the target voltage, current, frequency by the power device. Therefore, if the performance of power devices is improved and the power loss due to power conversion in each process can be reduced, it is considered that power usage efficiency improves and it can contribute greatly to solving society's energy crisis and global warming problem.

Currently used power semiconductor devices are mainly made of silicon (Si). The high performance by making fully use of micro technology of large scale integrated circuits was tried. However, it is getting close to the performance limit due to the physical characteristics value of Si, and drastic performance improvement of Si power semiconductor device cannot be expected from now on. Therefore, a wide band gap semiconductor having physical properties superior to Si attracts attention. Wide band gap semiconductor is a generic term for semiconductors with large width indicating energy gap between the conduction band and the valence band. Silicon carbide (SiC), gallium nitride (GaN), diamond, and the like can be cited as a wide band gap semiconductor and attracted attention as a next generation power semiconductor device material. Among them, GaN has received particular attention [7].

1.2 Fundamentals of Gallium Nitride in Group III-Nitride

1.2.1 Crystal structure of GaN

Wide-gap semiconductors such as GaN and SiC are attractive materials for realizing the next-generation power conversion system by replacing Si devices. A wide-gap semiconductor is a semiconductor having a double or more band gap compared with Si (1.12 eV) and typical materials are SiC of group IV-IV compound semiconductor and GaN of III-V group nitride semiconductor. III-V semiconductors, which are GaN and related materials. These have a hexagonal wurtzite structure due to the relatively strong ionic of the chemical bonds between cations and anion atoms in the crystal. FIG. 1-3(a) shows definitions of lattice constants and orientations in a hexagonal wurtzite type crystal. c-axis direction [0001] has strong ionic and it is possible to obtain polarization characteristics along the c-axis [8]. "c-plane" which is the (0001) orientation perpendicular to the c-axis is called "polar plane" with polarization effect. Indeed, GaN-based power devices are generally fabricated on c-planes of GaN-based materials. On the other hand, the normal direction of the c-axis defined as the a-axis and the other direction weakens the ionicity in the crystal. As shown in FIG. 1-3(b), the "nonpolar" orientation of the (11-20) plane and the (1-100) plane called the a-plane and the m-plane respectively show no polarization effect. These a-plane and m-plane are used for LEDs to control polarization in order to suppress carrier separation by an internal electric field [9].

In addition, as shown in FIG. 1-3(c), the lattice constant of the wurtzite crystal of GaN is also defined by a and c, c is 5.186 Å and a is 3.189Å. Each lattice constant depends on the ionic in the crystal, and generally, the lattice constant decreases as the ionic property becomes stronger. Comparing the ion intensities between other cations of III- V group and anions, it is observed as AlN> GaN> InN.

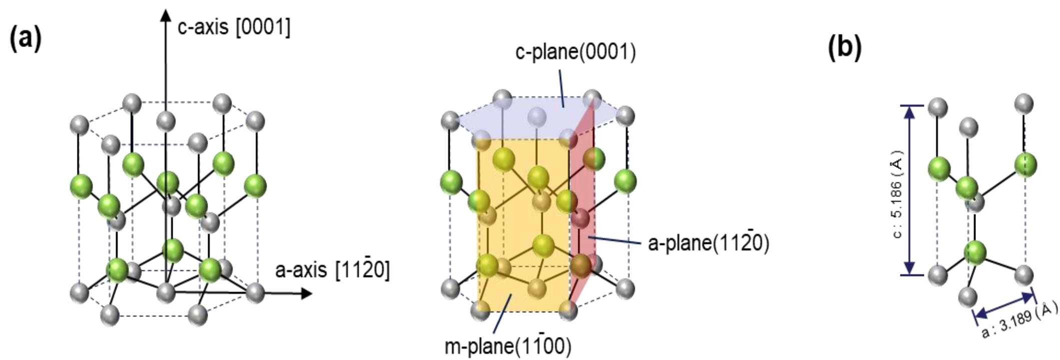

FIG. 1-3. (a) Schematic illustrations of the wurtzite crystal structures and its directions and orientations. (b) Definition of lattice constants of wurtzite crystal. GaN lattice constants are c = 5.186 and a =3.189

1.2.2 Comparison of physical properties as power semiconductor

The switch of the electric circuit is turned-on (R = 0) or turned-off (R = ∞). In an ideal switching process, there is no voltage drop nor leakage current. Note that Power (P) is Voltage (V)× Current (I). However, as shown by the solid line in FIG. 1-4, as the actual switch, the on-voltage and the conductance have a finite resistance against the off-state current. Finite resistance at V, I and P causes voltage drop and power loss in the on state. The resistance value at this time is called "on resistance ($R_{on}A$)" and the conduction loss is called "conduction loss".

The $R_{on}A$ is the resistance to express the characteristics regardless of the device size. The current density is defined by the unit of A/cm^2 in the ON state, the unit of the $R_{on}A$ is Ωcm^2.

In addition, the actual switches have finite transient characteristics of voltage and current during turn-on and turn-off. Increased power loss during turn-on and turn-off transitions is called "switching loss". The longer the transient time, the greater the switching loss. Furthermore, the total amount of switching losses can be larger even at

higher frequency operation. Therefore, from the viewpoint of circuit requirements, it is indispensable to realize a switching transistor having low $R_{on}A$, small leakage current, and excellent switching characteristics.

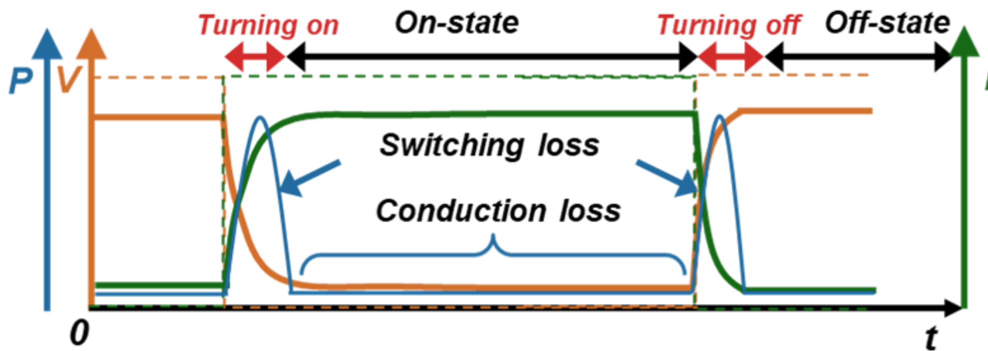

FIG. 1-4. On state and off state of the switching transistor. P (blue line) is V (orange line) × I (green line). The conduction loss is called "conduction loss" and increased power loss during turn-on and turn-off transitions is called "switching loss"

Figure 1-5 shows how physical characteristics values affect the device in view of requirements of power electronics system [10]. If it is a wide gap and high breakdown voltage, the R_{on} can be made small, high output operation can be achieved and power loss can be suppressed. Also, high thermal conductivity improves heat dissipation, stable operation in a high temperature environment of 200 º C or more and miniaturization of the cooling device (water cooling to air cooling etc.) are also possible. High electron mobility and carrier density can achieve high frequency operation and high electron density, and downsizing and cost reduction of the device can be realized. Therefore, a high voltage operating device with a lower R_{on} can minimize the cooling device. Furthermore, if the device can operate at a higher temperature, the reduction of the cooling system can realize not only a reduction in the cost and volume of the system but also an improvement in efficiency due to a reduction in heat loss in the power system.

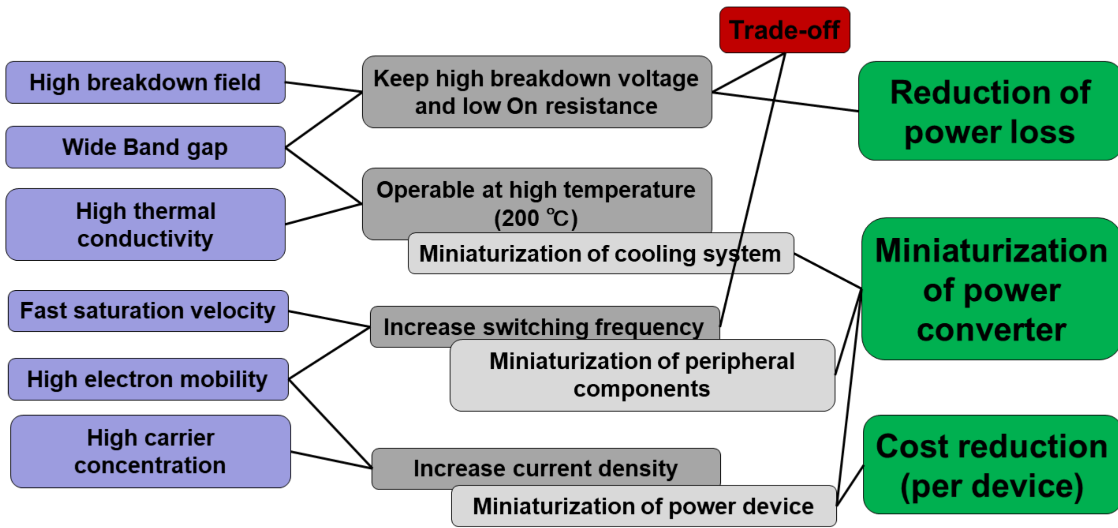

FIG. 1-5. Influence of physical properties in power electronics systems. The purple group shows the physical properties of power device semiconductors. The gray and green group indicates the influence of the power device and system.

TABLE 1-1 compares band gap, breakdown electric field, electron mobility, electron saturation veocity, transition type, thermal conductivity, Johnson figure of merits, Baliga figure of merits of Si, 4H-SiC, 6H-SiC, GaN, AlN and InN [11]. The Johnson figure of merit (JFM) is one of the most widely used performance indexes for high frequency power applications and it is expressed by the equation (1.1) using the dielectric breakdown electric field E_c and the saturated electron velocity v_s [12]. Baliga figure of merit (BFM) proposed by Baliga shows the performance in low frequency applications reflecting the conduction loss of the transistor and is expressed by the equation (1.2) using the electron mobility μ_e and the band gap Eg [13].

$$\mathrm{JFM} = \left(\frac{E_c v_s}{2\pi}\right)^2 \qquad (1.1)$$

$$\mathrm{BFM} = \varepsilon_r \varepsilon_0 \mu_e E^3{}_g \qquad (1.2)$$

Physical characteristics factors which are important in application to power semiconductors are wide band gap, high dielectric breakdown electric field, high thermal

conductivity, high electron saturation speed, and high carrier mobility. GaN is a direct transition type semiconductor having a wurtzite crystal structure and has a band gap of 3.4 eV, dielectric breakdown electric field of 3.3 MV/cm, electron mobility of 1000 to 2000 cm^2/Vs, electron saturation. It has a speed (2.8×10^7 cm/s) and shows excellent physical properties exceeding not only Si but also SiC. The band gap of GaN is 3 times the band gap of Si, and the electric breakdown field is 10 times higher. Although the electron mobility of GaN and SiC is lower than that of Si, the influence of mobility on R_{on} can be suppressed by using an optimized device structure [14].

Particularly, because GaN and its related materials have less impurity diffusion, the electron mobility is much higher than Si and SiC. In addition, GaN based hetero structures generally show a high electron density about ten times over their channels. Comparing these performance indices with Si as a reference, the JFM of GaN has a high value of 270-480 times of Si and 17-34 times of BFM. Furthermore, in comparison with the group III-V group, AlN exhibits the largest band gap in the III-V group and InN shows the smallest because the stronger ionic nature in the semiconductor increases the band gap. Although GaN and other III-V have direct band gap, Si and SiC have indirect ones. With direct bandgap, electron can be emitted from the valence band to the conduction band, which is an important element for realizing the efficient light emitting diode (LED). The higher saturation velocity and the higher breakdown electric field also giving the superior transport properties in the high electric field condition, that is, the high-frequency operation.

TABLE 1-1. Physical properties of Si, GaN, and 4H-SiC, 6H-SiC, AlN, InN [11].

300 K	Si	4H-SiC	6H-SiC	AlN	InN	GaN
Bandgap Eg (eV)	1.1	3.3	2.9	6.1	0.7	3.4
Breakdown electric field E_{BD} (MV/cm)	0.3	3.0	4	6-15	1	3.3
Electron mobility μ_e (cm^2/Vs)	1350	700	600	1100	3600	1200(Bulk) 2000(HEMT)
Electron saturation velocity v_e (cm/s)	1.0×10^7	2.0×10^7	1.5×10^7	1.5×10^7	1.5×10^7	2.5×10^7
Transition type	Indirect	Indirect	Indirect	Direct	Direct	Direct
Thermal conductivity Θ_K (W/cmK)	1.5	4.9	5.0	2	1	1.5
Johson figure of merit JFM	1	324	400	900-5600	11	270-480
Baliga figure of merit BFM	1	12	6	100	0.8	34

Figure 1-6 shows the electric field distribution in the depletion layer of Si and GaN SBD [15]. The breakdown voltage corresponds to the area of the triangle. GaN shows a vertically elongated triangle as compared with Si because of its large dielectric breakdown electric field. As a result, GaN can shorten the drift layer compared to Si, and because of the high carrier concentration, the $R_{on}A$ can be made smaller by two or more orders. Therefore, as an advantage of GaN with respect to Si, it is possible to reduce the thickness of the drift layer and to realize a low $R_{on}A$. Figure 1-7 shows the comparison between the performance limit line of Si, SiC, and GaN estimated from the physical value and the GaN-based power semiconductor [16]. Because GaN and SiC have 10 times the breakdown electric field compared to Si, $R_{on}A$ of these materials can be made three orders smaller than Si. GaN has already developed high breakdown voltage devices exceeding the performance limit line of SiC [17].

In recent years, the practical application of inverters for railway vehicles using SiC power semiconductors has been started and research on crystal growth technology and device technology on GaN vertical device structure is actively studied. By using GaN, it

is possible to realize a power device capable of operating at ultra low loss, small size, and high temperature. In the future, the hybridization of gasoline cars and full-scale introduction of electric vehicles are anticipated and power devices are expected to be used for various purposes more than ever. Therefore, expectation of energy saving effect is high through the realization of GaN power devices [18, 19].

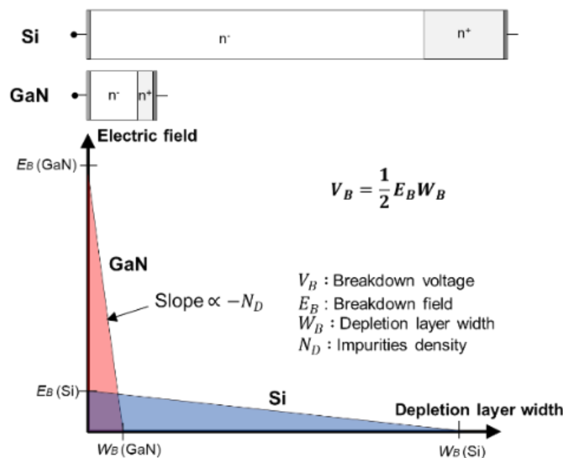

FIG. 1-6. Electric field distribution in depletion layer of Si and GaN SBD. GaN shows a vertically elongated triangle as compared with Si.

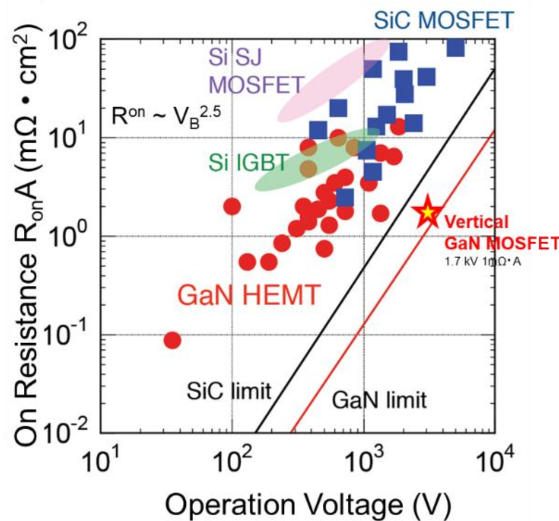

FIG. 1-7. Relation between characteristic $R_{on}A$ and operation voltage [16]. The theoretical limit value of GaN exceeds SiC. This shows the characteristics of Si SJ MOSFET, SiC MOSFET, Si IGBT and GaN HEMT [16].

1.3 Power devices using GaN-based semiconductors and their technical issues

1.3.1 Current Status of GaN Metal Oxide Semiconductor Field Effect Transistor

Table 1-2 summarizes the structures and corresponding characteristics of the high electron mobility transistor (HEMT) and the vertical GaN MOSFET [20]. A transistor with high breakdown voltage, low resistance, high-frequency operation is a feature of the GaN HEMT structure [21-23]. Also, it is a vertical type GaN power device that aims at ultra-high voltage transistor due to the high breakdown voltage of GaN bulk crystal [24]. The benefit of the HEMT structure is that not only the $R_{on}A$ can be greatly reduced by high carrier concentration and high mobility but also the operating frequency is high due to high saturated electron velocity, and the two dimensional electron gas (2DEG) concentration is 1×10^{13} cm^{-2} or more, which can reduce the parasitic resistance at the source/drain region. However, it is difficult to improve the breakdown voltage in the HEMT structure wherein the electric field is applied in the lateral direction in the plane. Also, from the viewpoint of miniaturization, it is limited to applications of up to several hundred volts due to the short channel. From the viewpoint of power device application, while the HEMT structure is advantageous for its low resistance, it has disadvantages such as becoming a "normally on" device in which the channel is in a conducting state even if no gate voltage is applied.

In a power device for high breakdown voltage and large current, a vertical structure is advantageous in that it is a relatively easy structure to have a high breakdown voltage and a high current density per chip area. The dielectric breakdown of GaN is expected to

become very high and it is expected that ultrahigh voltage transistors exceeding SiC can be realized if the vertical structure utilizes a GaN bulk substrate [25]. Ultra high breakdown voltage operation has already been demonstrated in vertical devices and breakdown field strengths of 3.5 MV/cm to 3.75 MV/cm have been observed from the operating characteristics of Schottky barrier diodes. This is much larger than the 2.8 MV/cm of 4 H-SiC, suggesting the possibility that GaN essentially has merit in ultra-high voltage operation. Recently, as shown in FIG. 1-7, the demonstration of vertical GaN MOSFET that can withstand 1.7 kV of voltage and 1.0 mΩ・A which exceeds the theoretical performance limit that is constrained by the drift resistance of 4H-SiC has been reported [26]. In addition, the latest research have reported operation that shows high $R_{on}A$ while having high breakdown voltage in vertical GaN MOSFET [27]. However, for practical application, it is indispensable to form a free-standing substrate of high quality and the establishment of large-diameter bulk crystal growth technique is necessary.

TABLE 1-2. Structures and their characteristics of MOS HEMT and vertical GaN MOSFET.

Schematic image of GaN MOSFET	**MOS HEMT**	**Vertical MOSFET**
	Source Gate Drain Oxide AlGaN 2DEG Current n-GaN epitaxial layer Si Substrate	Source Gate Oxide p n+ n+ p n-GaN epitaxial layer Current n+-GaN sub metal Drain
Characteristics of each MOSFETs	✓ Low resistance ✓ High frequency operation	✓ High output ✓ Device for high breakdown voltage
Crystal growth method and quality	✓ Heteroepitaxial crystals on Si substrate	✓ High quality bulk crystal Growth technology is under study
On resistance and operating frequency	✓ High channel operation ✓ low channel resistance and low parasitic resistance	✓ Drift layer = high breakdown voltage ✓ Drift current limits performance

1.3.2 Influence of Gate Insulation in GaN MOSFET

Figure 1-8 (a) shows the band diagrams of the Schottky gate and insulated gate in the ON state. The gate leakage current of the Schottky greatly increases and it is impossible to interrupt the flow of electrons in the positive bias state. However, the gate insulating film has a large conduction band offset at the insulator/GaN interface and gate leakage current can be reduced even with a positive bias. As a result, the insulated gate structure allows a normally-off operation which needs application of a positive gate bias to turn on. Therefore, an insulated gate structure is very important for improving operating performance [28]. Figure 1-8 (b) shows the band diagram of GaN and the main insulator material of HfO_2, ZrO_2, La_2O_3, Ga_2O 3, Si_3N_4, Al_2O_3, and SiO_2 as candidates for the gate dielectric film [29]. In order to realize a good insulated gate, it is necessary to consider several material properties such as the insulator, band gap, band discontinuity to GaN, breakdown field and dielectric constant. In order to keep the leakage current low, it is necessary to select materials with wider band gap than GaN. High breakdown field is also necessary for operation under high voltage. Furthermore, because the gate insulated film expands the distance between the gate metal and the channel, it is also necessary to increase the dielectric constant of the insulating film. SiO_2 has the largest band gap among the materials, however its dielectric constant is about 4. HfO_2 is known as a "high-k" material with a dielectric constant higher than 20. However, the bandgap of the reported HfO_2 film is about 5-6 eV, which cannot prepare a sufficiently large band offset for the GaN-based material. Ga_2O_3 is the only material derived from GaN. However, the reported band gap of Ga_2O_3 showed a relatively small band gap similar to Si_3N_4 and HfO_2. In addition to these properties, a low electronic state density at the insulator / semiconductor interface is necessary. An electronic state is an interface state generally caused by a

chemical bond structure between an insulator and a semiconductor and a chemical reaction can be formed within a band gap. Therefore, it is indispensable to realize well-controlled interface characteristics in insulated gate devices. Amorphous Al_2O_3 having a high dielectric constant of 8 to 10, which is as large as 2.1 eV in conduction band discontinuity with GaN was focused. Al_2O_3 has a wide band gap (6.0 - 8.8 eV) and a higher dielectric constant than SiO_2 (3.9) having the same band gap. In addition, it has high dielectric breakdown electric field (8-10 MV/cm) and is thermally and chemically stable. As a deposition method of Al_2O_3 dielectric film, atomic layer deposition (ALD) method which ensures excellent film thickness uniformity, controllability, and step coverage is investigated. Al_2O_3 is a promising as a gate dielectric material for GaN-based MOS devices.

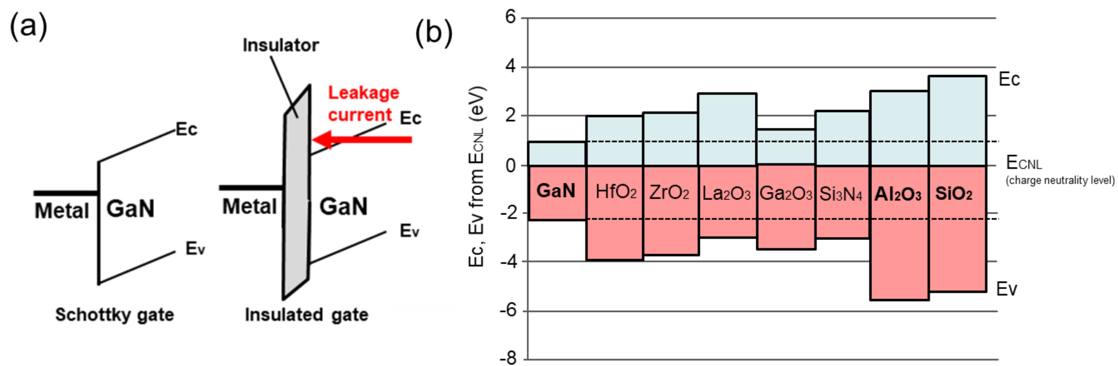

FIG. 1-8. (a) Band diagrams of Schottky and insulated-gate under the forward gate bias. The gate insulator has a large conduction band offset and gate leakage current can be reduced. (b) Band lineup of GaN and major insulators materials such as HfO_2, ZrO_2, La_2O_3, Ga_2O 3, Si_3N_4, Al_2O_3, and SiO_2.

1.4 Problems of GaN MOSFET fabrication process technology

For the practical application of GaN MOSFETs, there is a various problem that threshold voltage instability by traps at MOS structure, controllability of threshold voltage by ion implantation, high Ron by drift layer of GaN and expensive and quality of GaN substrate. One of the problems of GaN MOS is that the $R_{on}A$ which causes conduction loss is large. Figure 1-9 shows a cross sectional view of a typical vertical type n-type MOS. When the device is off, p-type and the n-type drift layer prevent current from current flow between drain and source. When the device is on state, the surface of the p-type layer just under the gate insulating film turns to n-type, and a current path is formed from the drain to the source at GaN MOSFET. On state resistance is used as an index showing the power loss in the on state [30]. It was shown that the channel resistance (R_{ch}) is determined by carrier density and mobility, the accumulation layer resistance (R_a) of on the surface of the n-type layer, JFET resistance (R_j) occurring in junction gate field-effect transistor by conducting in the vertical direction, drift resistance (R_{drift}) is determined by the film thickness of the drift layer and impurity concentration, contact resistance (R_c) and the substrate resistance (R_{sub}). For methods to improve the process for lowering resistance, there are reduction of R_{ch} by enhancing the mobility, reduction of R_{sub} by using a thin wafer and reduction of R_j by cell pitch miniaturization. Reduction of the substrate resistance can be improved by devising the process, but there is a physical limit. In principle, R_j can be zeroed by adopting a trench MOS structure.

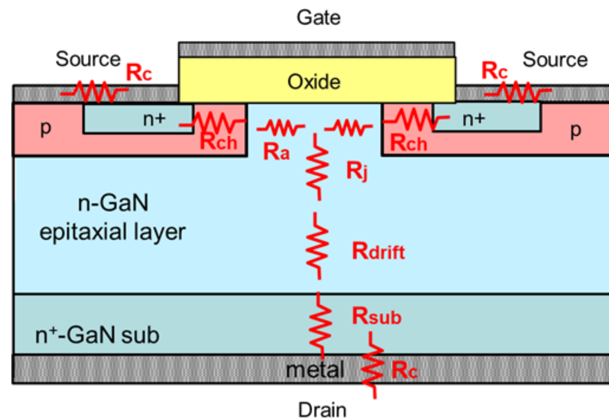

FIG. 1-9. Cross-sectional view of vertical MOSFET. The vertical MOSFET contains each resistance component such as R_c, R_{ch}, R_a, R_j, R_{drift} and R_{sub}.

The basic classifications of these traps and charges of oxide/GaN are shown in FIG. 1-10 [31]. The first trap is interface state, which is located at the insulator/GaN interface with energy states within the GaN bandgap and usually attributed to the dangling bonds or interface defects such as excess GaN, broken GaN bonds, excess oxygen and impurities at the dielectric/semiconductor. Fixed oxide charges which are located at or near the interface and are immobile under an applied electric field. Bulk trapped charges which can be created, for example, by hot-electron injection; these traps are distributed inside the dielectric layer. The positive fixed charges was also observed at MOS interface of the transition region between the dielectric layer and semiconductor. Their origins are possibly from either the ionized donors in the interface or a polarization-charge inversion at the surface due to the chemical bonds with dielectric film.

Figure 1-11 shows the interface state density distribution based on the DIGS (unified disorder induced gap state model) proposed by Hasegawa and Ohno in 1986 to show each defect distribution. The DIGS density distribution shows negative and positive charge and these states relate as acceptor-like state and donor-like state, respectively. At the energy

represented by the neutral charge (E_{CNL}), the state density shows the minimum value. It has been reported that as an origin of traps, nitrogen defects (V_N) in GaN is donor type and Al defects derived from Al_2O_3 film is acceptor type. However, the origins of defects in the interface have not yet been clarified.

The most problematic of MOS structure is low reliability such as low mobility and threshold instability. Carriers trapped at the interface existing at the MOS interface and fixed charges in the film cause mobility degradation and threshold instability. SiO_2 film can be thermal oxidized to form the gate insulating film of Si and SiC MOS devices. Some reports have shown that oxidation techniques of dry oxidation at 1050°C at SiO_2/SiC MOS devices reduced the interfaces state density up to 10^{11} eVcm^{-2} and post-oxidation anneal process (NO_x) at temperatures ranging from 1000 °C to 1300 °C is effected SiO_2/SiC interface [31, 32]. Otherwise, some recent reports have shown the effectiveness of dry O_2 annealing at high temperature (about 800°C) in reducing the D_{it} which were ~ 5×10^{11} cm^{-2} eV^{-1} at the energy level of $E_C-E = 0.2$ eV of both SiO_2/GaN [33]. However, in the case of Al_2O_3/GaN MOS capacitor, crystallization of Al_2O_3 begins at high temperature oxidization anneal of 800 °C and it is difficult to achieve the low D_{it} under 10^{12} cm^{-2} eV^{-1} [34].

In addition. to improve the interface properties, it was reported that that the N_2-plasma treatment was effective on the GaN surface to terminate the N-vacancy-related near-surface traps in AlGaN/GaN MOS HEMT [37]. However, it is not a highly desirable method for modifying the interface due to the possibility of damaging the GaN surface by plasma and the necessity of a lower temperature annealing. Therefore, for a high quality MOS interface, fundamental research is required which makes use of the semiconductor interface control technology.

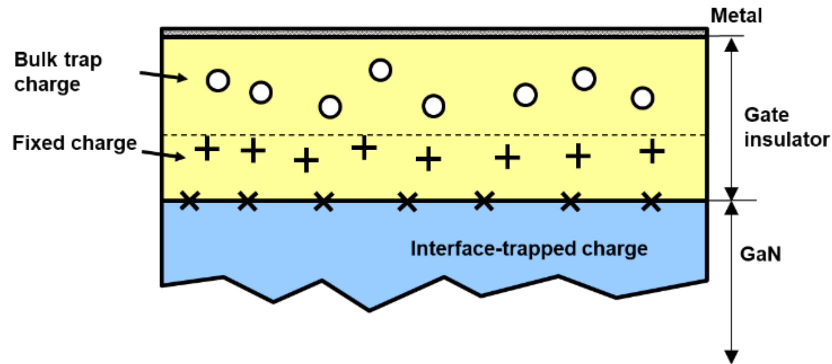

FIG. 1-10. Terminology for charges associated between gate insulator and GaN substrate. Gate insulator includes the bulk trap charge and fixed charge. The interface between gate insulator and GaN has interface-trapped charge.

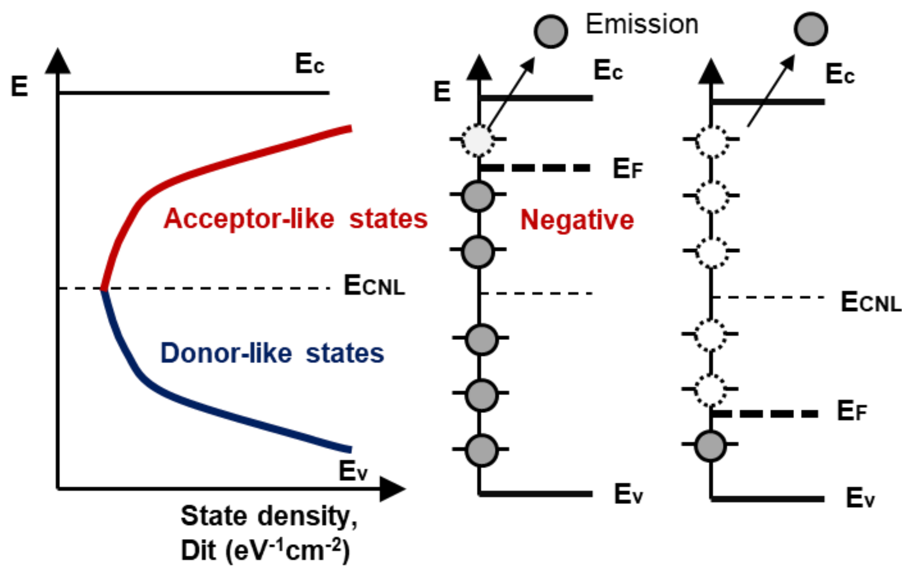

FIG. 1-11. Bonding and antibonding states of the DIGS model of interface state density distribution. The DIGS density distribution is negative and positive, respectively, when the electrons occupy both types of states. These show acceptor state and donor state. The state density shows the minimum value at the energy represented by the neutral charge (E_{CNL}).

1.5 Objectives and outline of this thesis

GaN-based MOSFETs are very attractive for realizing ultra-low loss power transistors having excellent physical properties and applicable to next generation power electronics. In recent years, GaN-based metal oxide semiconductor MOSFETs using Al_2O_3 insulator have been reported by many groups. However, there are few reports on the relationship between the MOS interface state and the characteristics in the GaN-based MOSFET, the understanding of insulator/GaN is still developing [39-41]. In this research, the insulator and interface quality of Al_2O_3/GaN was improved and investigated in detail.

This paper is organized as follows. In Chapter 2, "high pressure water annealing (HPWVA)" which is heat treatment after deposition using high temperature and high pressure water atmosphere was proposed. First, the principle and conditions of high pressure water treatment will be described in detail. In order to investigate the trapping state at the Al_2O_3/GaN interface and mechanism of HPWVA, electrical characteristics evaluation and physical characteristics evaluation were used. The effect on Al_2O_3/GaN interface will be explained by varying the conditions of the HPWVA.

In Chapter 3, the atomic structure at the Al_2O_3/GaN interface using two-dimensional photoelectron spectroscopy. The local interfacial structure of the Al_2O_3/GaN interface is clarified by using the photoelectron intensity angle distribution (PIAD) of SPring-8 which can directly access the local atomic structure of the selected elemental atom site.

In Chapter 4, interface quality and its physical properties by introducing a new ALD precursor for GaN MOSFET was improved. Electrical characteristics of MOS capacitor using dimethylaluminum hydride (C_2H_7Al : DMAH) as a new precursor in atomic layer deposition method are evaluated. In addition, the HPWVA was applied to realize the high

quality Al_2O_3/GaN MOS capacitor.

Chapter 5 summarizes the conclusion and future prospects of this study. In addition, problems of the proposed method for fabrication of GaN MOSFET was described. Finally, my research achievement and acknowledgment in this paper were listed.

References

[1] H. Ritchie and M. Roser: CO_2 and other Greenhouse Gas Emissions. Published online at OurWorldInData.org. (2018).

[2] A. Kunioka and K. Uemura: Shinban kiso-handotai kouigaku, Asakura (1996).

[3] P. Seidenberg: A History of Change in the Technology of the Semiconductors. Facets New Perspectivies on the History of Semiconductors, pp. 36–74 (1997).

[4] R. J. Baker, CMOS: circuit design, layout, and simulation. John Wiley & Sons, (2011).

[5] Gordon E. Moore, Cramming more components onto integrated circuits. EMG. **38,** 8 (1965).

[6] K. Iwamuro: High performance of next-generation power semiconductors in the electronics series and its industrial development, CMC (2015).

[7] M.Hikita, M.Yanagihara, Y.Uemoto, GaN power device, Panasonic Technical Jornal, **55,** 2 (2009).

[8] D. B. Holt, B. G. Yacobi: Extended Defects in Semiconductors, Cambridge University Press, (2007).

[9] K. Motoki: Development of nitride semiconductor Crystal substrate and device, SEI technical review, (2012).

[10] B. Gil: III-Nitride Semiconductors and their Modern Devices, oxford science publications, oxford university press, (2013).

[11] M. E. Levinshtein, S. L. Rumyantsev, and M. S. Shur, Properties of Advanced SemiconductorMaterials GaN, AlN, SiC, BN, SiC, SiGe, John Wiley & Sons, Inc., New York, pp.93-148, (2001).

[12] E. O. Johnson, *RCA rev.*, **26**, 163 (1965).

[13] B. J. Baliga, IEEE Electron Device Lett. **10**, 455 (1989).

[14] M. S. Shur, B. Gelmont, and M. A. Khan, J. Electron. Mater. **25**, 777 (1996).

[15] A. Lidow, J. Strydom and M. Rooij: GaN transistors for efficient power conversion. 2nd Edition, pp 266 (2014).

[16] K. Okumura, Juornal of Japanse Appl. Phys.lett., **45**, 7565 (2006).

[17] S. Pearton, GaN and ZnO-based Materials and Devices, Springer, pp 209 (2014).

[18] T. Kachi, Jpn. J. Appl. Phys., **53**, 100210 (2014).

[19] S. Chowdhury, Phys. Status Solidi A, **212**, 1066 (2015).

[20] Japan Science and Technology Agency: Technological Issues and Future Prospects of GaN and Related Semiconductor Devices, March, (2017).

[21] B. M. Green, K. K. Chu, E. M. Chumbes, J. A. Smart, J. R. Shealy, L. F. Eastman, IEEE Electron Device Lett, **21**, 6 (2000).

[22] M. Asif Khan, A. Bhattarai, J. N. Kuznia, D. T. Olson, Appl. Phys. Lett., **63**, 1214 (1993).

[23] J. A. Alamo and J. Joh, Microelectronics Reliability, **49**, 1200 (2009).

[24] T. Oka, Y. Ueno, T. Ina, and K. Hasegawa, Appl. Phys. Exp., **7**, 021002 (2014).

[25] H. Ishida, D. Shibata, H. Matsuo, M. Yanagihara, Y. Uemoto, T. Ueda, T. Tanaka, and D. Ueda, Technical Digest of IEEE International Electron Device Meeting, pp. 145-148, (2008).

[26] D. Shibata, R. Kajitani, M. Ogawa, K. Tanaka, S. Tamura, T. Hatsuda, M. Ishida, and T. Ueda, Technical Digest of IEEE International Electron Device Meeting, pp. 248-251, (2016).

[27] T. Oka, T. Ina, Y. Ueno, and J. Nishii, Appl. Phys. Exp., **8**, 054101, (2015).

[28] J. Robertson, J. Appl. Phys., **28,** 265 (2004).

[29] J. Robertson, and B. Falabretti, Mater. Sci. and Eng. B **135**, 267 (2006).

[30] G. Liu, B. R. Tuttle and S. Dhar, Appl. Phys. Rev. **2,** 021307 (2015).

[31] A. Benfdila and K. Zekentes African Phys. Rev. **4**, 0005 (2010)

[32] T. Kimuraa, T. Ishikawab, N. Soejimac, K. Nomurad and T. Sugiyamae, Materials Science Forum **740**, 737 (2013)

[33] Nguyen Xuan Truyen, Noriyuki Taoka, Akio Ohta, Katsunori Makihara, Hisashi Yamada, Jpn. J. Appl. Phys. **57**, 04FG11 (2018)

[34] Yujin Hori, Chihoko Mizue, and Tamotsu Hashizume, Jpn. J. Appl. Phys. **49,** 080201 (2010)

[35] S.M. Sze, Kwok. K. NG, Physics of Semiconductor Device, Willy, pp 213 (2006)

[36] J. Neugebauer and C. G. Van de Walle Phys. Rev. B, **50**, 8067 (1994).

[37] T. Hashizume, S. Ootomo, H. Hasegawa, Applied Physics Letters, **83**, 2952 (2003).

[38] Y.Hori, C.Mizue, and T. Hashizume, Phys. Stat. Sol. C, **9**, 356 (2012)

[39] M. Choi, A. Janotti, and C. G. Van de Walle, J. Appl. Phys., **113,** 044501(2013)

[40] Chris G. Van de Walle J. Appl. Phys., **113**, 044501, (2013)

[41] M. Choi, A. Janotti, and Chris G. Van de Walle, ACS Appl. Mater. Interfaces, **6**, 4149 (2014)

Chapter 2 Characteristics of MOS Capacitor by HPWVA

2.1 Introduction

In this chapter, GaN MOS capacitor was fabricated using ALD-Al_2O_3 as a gate insulator and a high quality Al_2O_3 film and interface was produced. ALD have superior film thickness uniformity, film thickness controllability, and step coverage, compared to chemical vapor deposition (CVD) and sputtering method, and is promising as a method for forming a gate dielectric film. In particular, a high-quality metal/oxide semiconductor (MOS) structure is indispensable for the production of the next generation of GaN-based field effect transistors with stable threshold voltages, low leakage currents, and high breakdown voltages [1-3]. Having low densities of fixed charges and interfacial traps results in higher performance, including better control of the flat band voltage (V_{FB}) and mobility. In addition, the high breakdown field enables a high on-state gate voltage swing and high off-state blocking voltage. For GaN based power devices, Al_2O_3 is a promising gate dielectric, because it has a reasonably high dielectric constant, large conduction-band offset in Al_2O_3/GaN, and good thermal stability [4-7]. In order to develop GaN power devices, it is therefore important to control and reduce the number of defects in the Al_2O_3 gate dielectric and at the interface between the Al_2O_3 and the GaN. Some recent reports have shown the effectiveness of dry O_2 annealing at high temperature (about 800°C) in reducing the interface trap density (D_{it}) of both SiO_2/GaN and Al_2O_3/GaN [8, 9].

However, it is not yet clear what treatment has the greatest effect on the interface characteristics. Here, a post deposition treatment “HPWVA” which utilizes the strong

oxidizing power of water vapor [10, 11] was proposed. HPWVA is more effective than dry oxidation in promoting reoxidation at lower temperatures [12]. There have also been reports of HPWVA about reforming CVD-SiO_2 film, terminating dangling bonds in poly-Si and improvement in the reliability of IGZO-based oxide semiconductors [13-17]. Our group has also reported the improved electrical performance of GaN-on-Si MOS capacitors with HPWVA [17]. The present study focuses on the effect of HPWVA on Al_2O_3/GaN and evaluates the electrical characteristics of the MOS capacitors. In particular, the reactions caused by HPWVA and its effects were analyzed.

2.2 Atomic Layer Deposition (ALD)

The ALD method is a type of thin film growth technique of oxide film and nitride film by gas phase. The principle was proposed by Suntol et al. in the 1970 's [18]. It is a technology capable of uniformly growing from an atomic level to complicated device structures and three-dimensional shapes such as nanoparticles. For example, Intel used an Hf-based gate insulator using the ALD method for a 45 nm generation CMOS device [19]. The disadvantage of the ALD method is that the growth rate is slow, but the growth rate such as in the gate insulator of MOS devices with scaling progress is often not particularly important. For display applications, spatial ALD, which enables large area and high growth rate, is also under development [20, 21].

ALD cycle for Al_2O_3 is schematically shown in FIG. 2-1 [22, 23]. In the top left corner, the metal surface with existing hydroxyl surface is exposed to the metal–organic precursor. Trimethyl aluminum (TMA) is used as the metal–organic precursor and water for the co-reactant. The precursor decomposes by reacting with the hydroxyl surface groups, leaving a CH_3 terminated surface. The precursor reacts only with hydroxyl groups

and will not react with itself, creating self-limiting growth. Once all hydroxyl sites have been reacted additional exposure to the precursor will not result in additional growth, creating one monolayer. The system is purged with inert gas to remove excess precursors, reactants or by-products. The CH_3 terminated surface is then exposed to the co-reactant reacts on the surface to leave one monolayer of Al_2O_3. The self-limiting nature of the chemistries implemented in ALD process produce high quality, dense and nearly pinhole-free films with thickness control at the atomic level, excellent thickness uniformity and unequalled conformity. ALD has been demonstrated to produce films that are perfectly conformal even for nano porous substrates. ALD films have been demonstrated to be effective diffusion barriers for corrosion protection [24]. The density of ALD Al_2O_3 films is 3.0–2.5 g/cm^3, depending on deposition temperature.

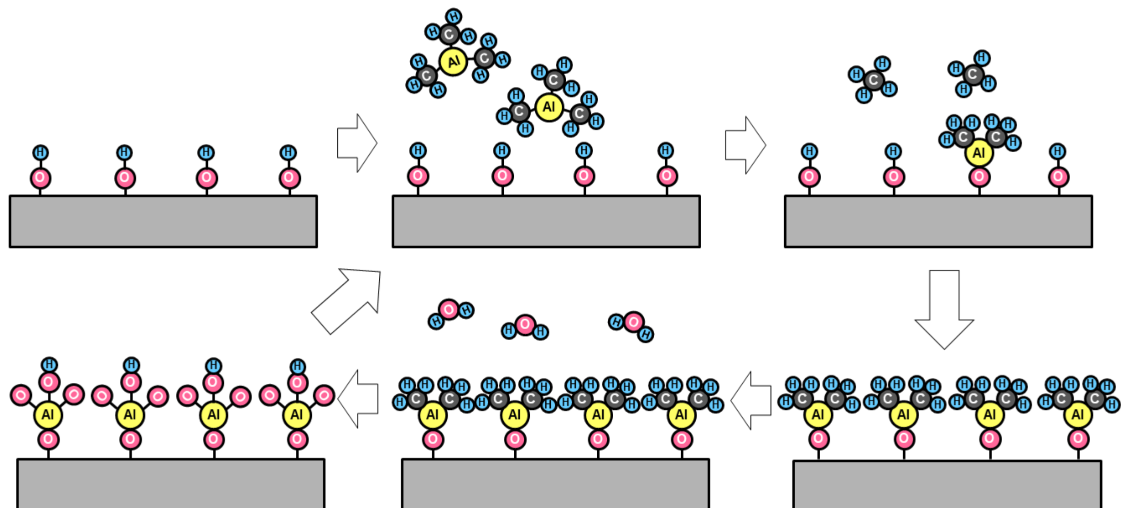

FIG. 2-1 ALD process: schematic of one cycle of Al_2O_3 ALD growth. TMA is pulsed into the chamber to deposit one layer of Al. The TMA is then evacuated form the chamber, and H_2O is introduced. Al the necessary surface hydroxyl groups may not exist before the first H_2O pulse. The first water pulse will both hydroxyl late the surface and thermally oxidize a thin layer in the body of the film.

It is necessary to set the growth temperature to an appropriate ALD temperature. At a temperature lower than the CVD process, the precursor of the organometallic

decomposes on the substrate surface and does not become a self-limiting reaction, causing uneven film growth and an increase in carbon concentration as an impurity. The temperature range that the precursor adsorbs on the surface but does not decompose is called ALD window. TMA is an ideal ALD precursor with a wide ALD window (room temperature to 450 °C).

The gas flow sequence in the ALD process in this study is shown in FIG. 2-2. In ALD, raw material gas and purge gas are supplied in pulses. For III-V semiconductors such as GaAs, it is expected to have a effect of removing Ga oxide called "self-cleaning effect" by first supplying TMA [25]. For all ALD gas flow sequences, These were 4 stages of TMA supply, N_2 gas purge, oxidant flow supply, and N_2 gas purge. With this flow as one cycle, film formation was continuously performed until a desired film thickness was obtained.

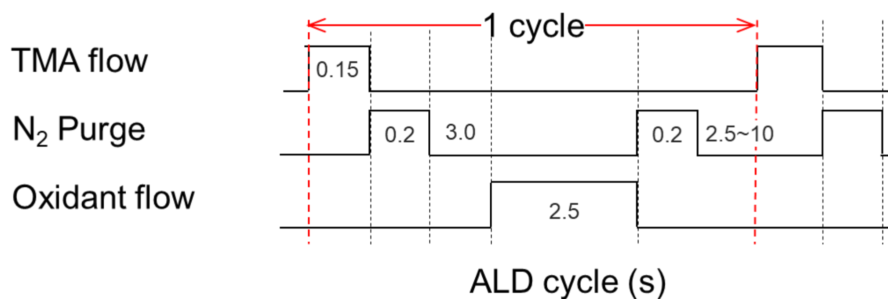

FIG. 2-2 The gas flow sequence in the ALD process. TMA first was adopted and it was set to 4 stages of TMA supply, N_2 gas purge, oxidant flow supply, and N_2 gas purge.

2.3 High Pressure Water Vapor Annealing (HPWVA)

Annealing processes using NH_3 gas or high temperature have been previously reported as interfacial reforming processes [26, 27]. However, surface damage by plasma

and harmful gas such as NH_3 are used. Development of a simple process with low damage was desired. HPWVA using high temperature and high pressure water was recently proposed. High pressure water vapor annealing is an annealing treatment developed by Sameshima et. al. as a dangling bond termination in poly-Si [12, 13, 28] The advantage of this annealing is that it is environmentally friendly, plasma-less, processing at a relatively low temperature (up to 400 ° C), and a simple apparatus. There have also been reports of reforming CVD-SiO_2 film, terminating dangling bonds in poly-Si and of high-k film on Si, and improvement of reliability of IGZO-based oxide semiconductor [14, 15]. Moreover, it has been shown that the interface state density (D_{it}) decreases also at the SiO_2/SiC interface as a power device application [29]. In this study, the improvement of the Al_2O_3 film and the termination of the D_{it} at the Al_2O_3/GaN interface was investigated.

The phase diagram of water is shown in FIG. 2-3. High pressure water has properties such as low density, low ion product, and low dielectric constant compared with water at normal temperature and pressure. As the temperature rises, the ion product of the high pressure water greatly increases and shows a maximum value around 250 ° C. In addition, the hydrolysis reaction is dominated as the electrolyte solvent. If the temperature is further raised, the ion product sharply decreases and radical reaction becomes dominant. OH radicals have the strongest oxidizing power and is the most reactive among the molecular species. In FIG. 2-4, under the conditions in this study, it is considered that the reaction of monomers of water molecules with hydrogen bonds cuts off and radicals are predominant [30]. Furthermore, in the supercritical state (374 ° C, 22 MPa), the relative dielectric constant of water decreases, it has gas diffusivity and liquid solubility and it can provide ion reaction field and radical reaction field.

Therefore, HPWVA is more advantageous than other dry oxidation treatments due to

re-oxidation and an increase in diffusion rate in a high pressure state. It is considered to be effective for reforming oxygen vacancies in Al_2O_3 film and interface

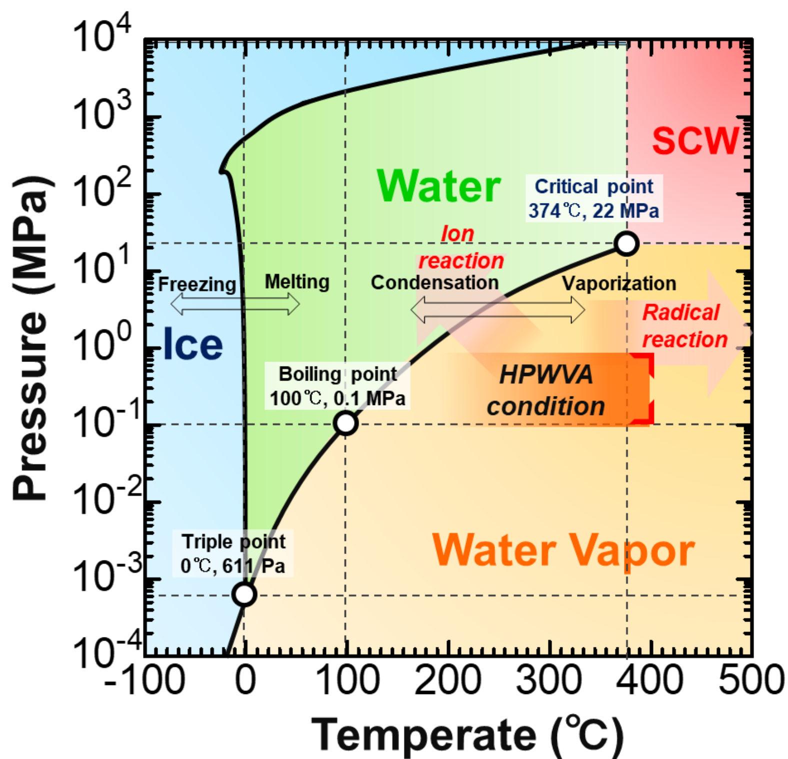

FIG. 2-3 The phase diagram of water. The ion product sharply increased at high pressure water condition and radical reaction becomes dominant at supercritical condition. It was carried out under HPWVA condition in this study.

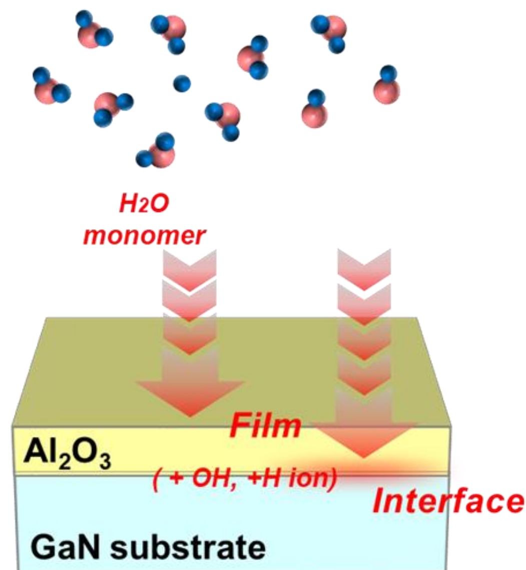

FIG. 2-4 Schematic diagram of HPWVA for Al_2O_3/GaN MOS structure. The reaction of H_2O monomers are predominant in the condition of around 400 °C and 0.5 ~ 1.0 MPa.

Schematic diagram of HPWVA chamber system is shown in the FIG. 2-5 and time change of pressure, temperature of chamber and heater of HPWVA equipment (400°C, 0.5MPa, 30 min) was shown in FIG. 2-6. The temperature inside the chamber was detected through a thermocouple, and the temperature of the heater was adjusted so that the inside of the chamber was at a desired temperature.

This is the flow of the annealing process:

1. Samples placing on the holder were set in the chamber.
2. The ultra pure water (UPW) was weighed and it was put into the chamber and the chamber was sealed. Pressure of HPWVA changed with amount of UPW.
3. The pressure in the chamber increased with increasing temperature. The heater temperature was once raised to 800 ºC and the temperature inside the chamber reached 400 °C at 70 min.

4. the temperature and pressure in chamber were kept. The annealing time depended on this process time.
5. The leak valve was opened after processing at a predetermined temperature and pressure and water vapor was discharged. Air cooling was carried out and the sample was removed at 50 °C or less.

Withstanding pressure upper limit of this HPWVA chamber was 1.0 MPa and maximum temperature was 400 °C.

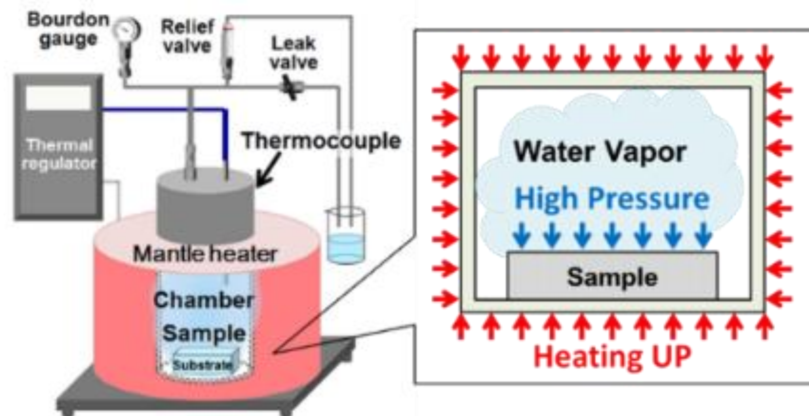

FIG. 2-5 Schematic diagram of HPWVA chamber system. By introducing water and applying a temperature to the chamber of the sealed space, a phase state of high pressure and high temperature is created.

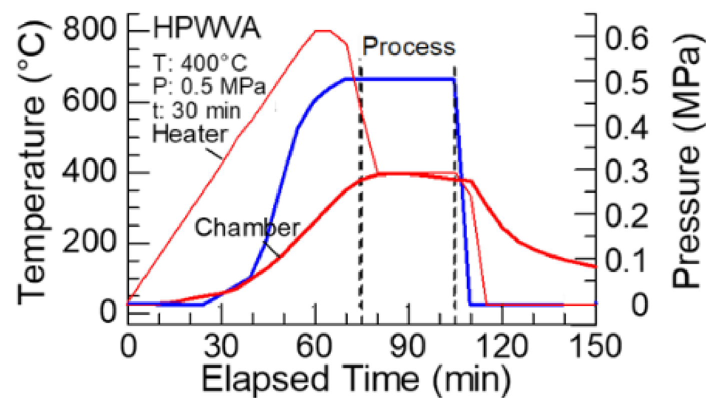

FIG. 2-6 Time change of pressure, temperature of chamber and heater of HPWVA equipment (400 °C, 0.5 MPa, 30 min)

For the purpose of enabling processing under high pressure condition, a device capable of withstanding pressure of 30 MPa was designed. Figure 2-7 shows the temperature and pressure profiles of super critical water (SCW) equipment (400 °C, 0.5 MPa, 30 min). The SCW equipment was designed that the temperature can be raised up to 410 ° C in the temperature control, and the chamber temperature reaches 400 ° C at a total heating time for 140 min. After the heater temperature reached the target value, the processing time was kept constant, then the heater was turned off. When the temperature had dropped to about 200 ° C, the leak valve was opened, the pressure was released and naturally cooled.

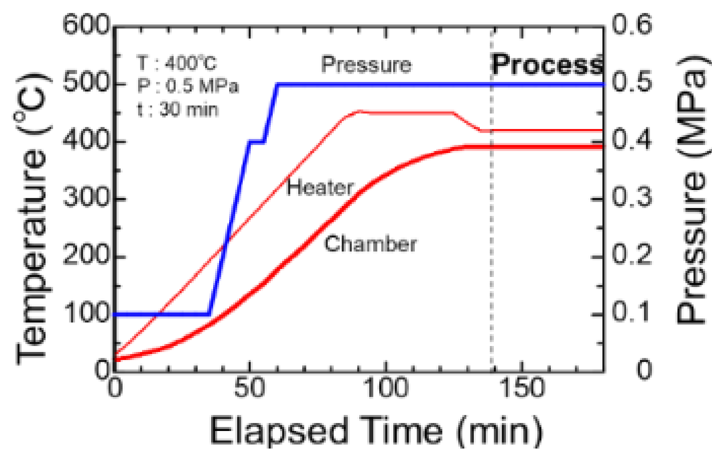

FIG. 2-7 Time change of pressure, temperature of camber and heater of SCW equipment (400 °C, 0.5 MPa, 30 min)

2.4 Experimental method

2.4.1 Device fabrication

In this study, MOS capacitor was fabricated as an element for evaluating ALD-Al_2O_3 film on GaN (0001) substrate. Figure 2-8 shows the schematic image of Al_2O_3/GaN MOS capacitor. Homoepitaxial layer (2 μm, Si :5 × 10^{16} cm^{-3}) on c-plane (0001) free-standing GaN substrates was utilized. After performing the standard RCA cleaning process, an

Al_2O_3 film with a nominal thickness of 40 nm was deposited on the n^+-GaN (0001) surface using T-ALD. Hattori et al. reported that the HF treatment as the wet-etching process of GaN (0001) surface is more effective for the flatness in addition to relative cleanness than HNO_3 and NaOH [31-33]. The Al_2O_3 film was deposited at 300°C by repeating cycles of TMA introduction as aluminum precursor, and then O_3 supply. The deposition rate of the Al_2O_3 film was 0.91 Å/cycle. Then, HPWVA was performed on samples under a constant pressure of 0.5 MPa at an annealing temperature of 400 °C for 30 min. For the top electrode, 100 nm-thick Al was deposited by electron beam (EB) evaporation. After removing the oxide from the back of the GaN substrate, 10/100 nm-thick Ti/Al as a bottom electrode was deposited for the back-side ohmic contact. Details of the fabrication process are described below.

・RCA cleaning [34]

SPM Cleaning (Removal of Organics) Substrate was immersed in SPM solution (H_2SO_4: H_2O_2 = 1: 1) warmed to 80 ° C for 25 minutes to remove organic fragment. After rinsing with UPW, it was immersed in diluted-HF) for 5 minutes to remove the chemical oxide film. SC1 cleaning (particle remover) Substrate was immersed in SC1 solution (NH_4OH: H_2O_2: H_2O = 1: 1: 5) warmed to 80 ° C. for 15 minutes to remove the particles. After rinsing with UPW, it was immersed in DHF for 5 minutes to remove the chemical oxide film. SC2 cleaning (metal impurity removal) The substrate was immersed in an SC2 solution (HCl: H_2O_2: H_2O = 0.5:1:5) warmed to 80 ° C. for 15 minutes. After rinsing with ultrapure water, it was immersed in DHF for 5 minutes to remove the oxide film and GaN surface bonding switched to the OH bond [35]. Finally, the substrate was dried with N_2 blow.

・Deposition process of ALD-Al_2O_3

The sample was quickly introduced into an ALD chamber after RCA process. The Al_2O_3 film was deposited at 300°C by repeating TMA as aluminum precursor and O_3 supply. The deposition rate of the Al_2O_3 film was 0.91 Å/cycle. Time cycle of ALD process was performed under the conditions shown in FIG. 2-2.

・Deposition process of electrode

Al electrodes of top electrode were formed on the surface in a high vacuum of ~ 7×10^{-4} Pa or less using an EB deposition. Gate electrodes with diameters of 100 ~ 500 μm were formed using a metal mask. An electrode size of 500 μm was used for C-V measurement and an electrode size of 100 μm was used for J-E measurement. Resist was applied to the surface to protect the top surface and the substrate was immersed in buffered HF to remove the back oxide. After removing the resist, Ti/Al electrodes as bottom electrode were formed.

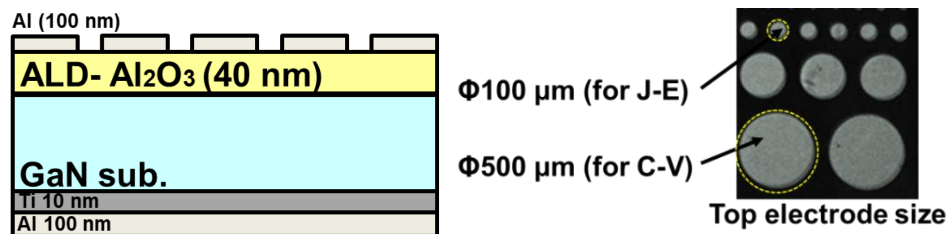

FIG. 2-8 The cross section of Al_2O_3/GaN MOS capacitor. An electrode size of 500 μm was used for C-V measurement and an electrode size of 100 μm was used for J-E measurement.

2.4.2 Capacitance – Voltage (C-V) method

2.4.2.1 Outline of C-V method

Various defects exist in Al_2O_3/GaN MOS capacitor and interface states are formed within the band gap. The interface state within this gap affects the electrical characteristics

of the MOS device and it is necessary to evaluate its characteristics and quantity by C-V method [36, 37]. As shown in FIG. 2-9, MOS capacitor consists of a semiconductor, an insulator, a gate electrode on the insulator, and an ohmic electrode on the substrate side. As shown in FIG. 2-9, the MOS capacitor received an alternating-current (AC) signal and a direct-current (DC) gate bias between MOS capacitor electrodes to measure the gate capacitance (C_G). Charge change amount per voltage change can be obtained from voltage displacement due to the AC signal. When a bias is applied to the gate, a voltage is applied to the semiconductor side and the oxide film. Therefore, C_G is the series capacitance of the capacitance C_S on the semiconductor side and the capacitance of the oxide film (C_{OX}). Gate voltage (V_G) gives a static change such as carrier accumulation and depletion layer width. By repeating the C_G measurement while sweeping the DC bias, the C-V characteristic can be obtained.

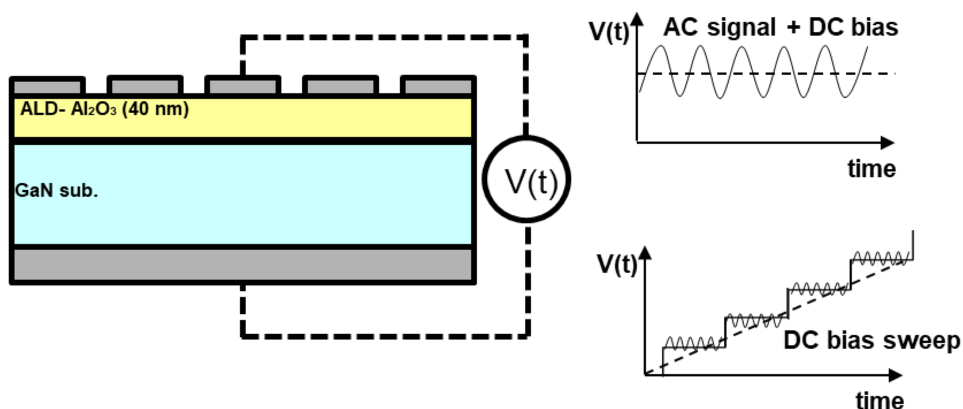

FIG. 2-9 Schematic diagram of Al_2O_3/GaN MOS capacitor and C-V measurement. The MOS capacitor applies an AC signal and a DC gate bias to measure the gate capacitance.

Figure 2-10 shows a band diagram of an ideal MOS structure. In the ideal case, the work function of the gate metal is equal to the work function of the semiconductor, and it

becomes a "flat band" state. At $V_G > 0$, the energy band deflects upward, resulting in "accumulation" of electrons at the insulator/semiconductor interface. On the other hand, when $V_G < 0$, the band bends downward, resulting in "depletion" of electrons in the semiconductor layer. Charges such as oxide traps, interface state charges and fixed charges affect the bending of the band. In reality, there is an energy difference between the gate metal and the work function of the semiconductor [38]. If the work function of the gate metal is greater than the work function of the semiconductor and there is a negative charge at the interface, under conditions that do not consider Fermi level pinning, the energy band at the interface will bend upward as shown FIG. 2-10 (b). Under the opposite condition, as shown in FIG. 2-10 (c), the energy band turns downward in an equilibrium state [38].

There is a difference of work function between a metal and a semiconductor, and when a Fermi level matches by forming a MOS structure, energy band is bended on the surface of the semiconductor. The flat band voltage is the voltage applied to the metal and semiconductor required to flatten the bend of this band. Ideally, the flat band voltage should be equal to the difference in work function between metal and semiconductor (ϕ_{MS}), but due to various the fixed charge at the oxide/semiconductor interface (Q_{it}), the work function difference was shifted [38].

Figure 2-10 (d) shows the energy band in the flat band state of MOS structure ($Q_{it} \neq 0$). In those cases, the V_{FB} which should be applied in order to flatten the bands, can be described by the equation (2.1) [39],

$$V_{FB} = \phi_M - \phi_s - \frac{Q_{it}}{C_{ox}} \tag{2.1}$$

where ϕ_M and ϕ_s are the work functions of the gate metal and the semiconductor, respectively, and Q_{it} is the fixed charge at the oxide/semiconductor interface. C_{ox} is the

insulator capacitance per unit area.

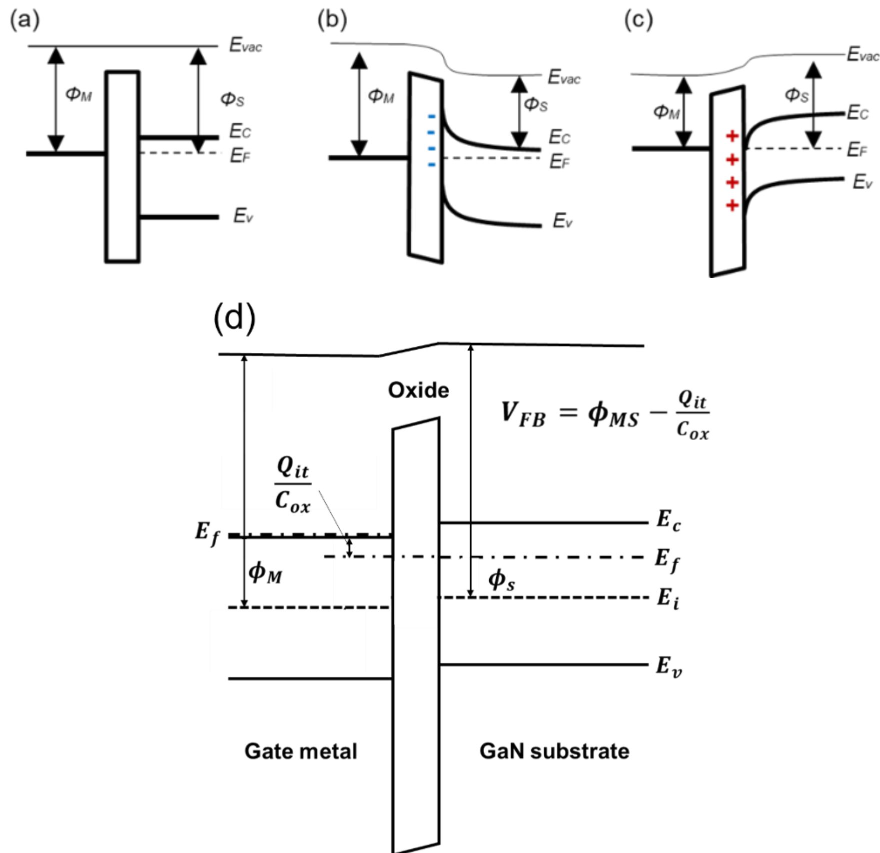

FIG. 2-10 (a) Band diagrams of ideal MOS junction at equilibrium and (b) and (c) for real cases of between negative state and positive state. (d) Energy band in the flat band state of MOS structure ($Q_{it} \neq 0$)

As shown in FIG. 2-11, C-V characteristics affected by the distributed interface states is shown. As described in Chapter 1, the upper and lower states are the acceptor like state and the donor like state, respectively. When the electron occupies both states, it has negative charge and a positive charge, respectively. The occupation rate of each state is influenced by the Fermi-Dirac function. These polarities depend on the position of the Fermi level at the interface and the change in the interface state charge affects the C-V characteristic of the MOS capacitor. The interface state hinders the surface potential

control by the gate voltage. Consequently, the continuous distribution interface state causes the "stretch-out" behavior of the C-V curve [39].

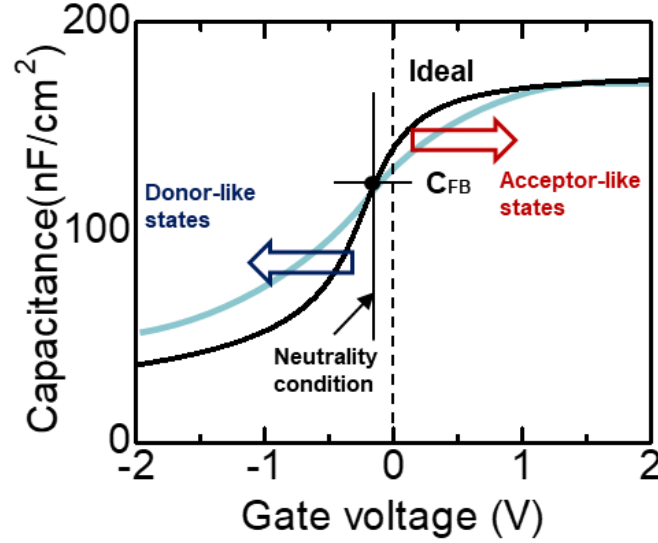

FIG. 2-11 C-V characteristics affected by the distributed interface states. Black curve is ideal curve and ideal C_{FB} was shown. C-V curve shifts to the positive direction by an acceptor like state and C-V curve shifts to the negative direction by an donor like state.

2.4.2.2 Ideal C- V curve and interface states in MOS structures

Ideal C-V curve of MOS structure was obtained. An experimental capacitance (C_{ex}) and an experimental voltage (V_{ex}) were measured by high frequency measurement of C-V method such as 1 MHz. The semiconductor work function (ϕ_s) is arbitrarily assumed [40,41]. Carrier concentration (N_d) was calculated from gradient of $1/(C_{ex})^2$ plot as shown in the equation (2.2) [41].

$$N_d = -\frac{2}{q\varepsilon_s\varepsilon_0 A^2\left(\frac{\Delta 1/C_{ex}^2}{\Delta V_G}\right)} \tag{2.2}$$

Fermi potential (ϕ_f) and intrinsic debye length (λ_n) in semiconductor were calculated as shown the equation (2.3) and (2.4) [41].

$$\phi_f = \frac{kT}{q} \ln\left(\frac{N_d}{n_i}\right) \tag{2.3}$$

$$\lambda_n = \sqrt{\frac{\varepsilon_s \varepsilon_0 kT}{2q^2 n_i}} \tag{2.4}$$

Maximum capacitance C_{ox} in accumulation region of experimental C-V curve was extracted. The dimensionless semiconductor surface electric field $F(U_s, U_F)$ is defined by the equation (2.5) [42, 43].

$$\mathrm{F}(U_s,\ U_f) = \sqrt{e^{U_f}(e^{U_s} + U_s - 1) + e^{-U_f}(e^{U_s} - U_s - 1)} \tag{2.5}$$

The U_s and U_F are normalized potentials, defined by $U_s = \frac{q\phi_s}{kT}$ and $U_f = \frac{q\phi_f}{kT}$, where the surface potential ϕ_s, and the Fermi potential ϕ_f are defined. The symbol $\widehat{U}_s$ stands for the sign of the surface potential and is given by $\frac{|U_s|}{U_s}$.

Capacitance of the wide gap semiconductors ($C_{s,\text{ wide gap}}$) corresponding to φ_s with C_{ox} was calculated as shown in the equation (2.6) [42].

$$C_{s,\,widegap} = \widehat{U}_s \frac{\varepsilon_s \varepsilon_0}{2L_{Di}} \frac{\left[e^{-U_f}(e^{U_s} - 1)\right]}{\mathrm{F}(U_s, U_f)} \tag{2.6}$$

Total capacitance (C_t) is defined by $C_t = (1/(1/C_{ox}) + (1/C_s))$. The gate voltage is related to voltage, the surface potential, and the flat band voltage (V_{FB}) through the relationship [42].

$$V_t = V_{FB} - \phi_s - \widehat{U}_s \frac{kT\varepsilon_s t_{ox} \mathrm{F}(U_s, U_f)}{q\varepsilon_{ox} L_{Di}} \tag{2.7}$$

The above is the derivation formula of the ideal C-V curve.

Flat band capacitance (C_{FB}) is extracted using the C_{OX}, the dielectric constant of the semiconductor (ε_s), the dielectric constant of vacuum (ε_0) and the debye length (λ_n) as shown in the equation (2.8). GaN relative permittivity (ε_{GaN}) is defined as 9.5 [43].

$$C_{FB} = \frac{C_{OX} \times \frac{\varepsilon_s \varepsilon_0}{\lambda_n}}{C_{OX} + \frac{\varepsilon_s \varepsilon_0}{\lambda_n}} \tag{2.8}$$

The fixed charge density (N_F) is expressed by the equation (2.9) using the work function

difference of the gate electrode and the semiconductor (Φ_{ms}), V_{FB}, and C_{ox},

$$N_F = (\phi_{ms} - V_{FB})\frac{C_{ox}}{q} \quad (2.9)$$

Φ_{ms} is extracted using the work function of gate metal ϕ_m (Al), the electron affinity of GaN χ, and N_d as shown in the equation (2.10) [42]. ϕ_m is defined as 4.13 eV and χ is defined as 4.10 eV [36].

$$\phi_{ms} = \phi_m - \left(\chi + \left(\left(\frac{E_g}{2}\right) - \frac{kT}{q}\ln\left(\frac{N_d}{n_i}\right)\right)\right) \quad (2.10)$$

The hi-lo method is one of the measurement methods to analyze the interface state [34]. In the hi-lo method, trapped electrons follow low frequencies but cannot follow high frequencies, so the difference in response of electrons can be used. The high-frequency C–V curves are similar to $D_{it} = 0$ and the low-frequency C–V curves indicate $D_{it} \neq 0$. When the capacitance difference is small, it is judged that the interface state density is small. Figure 2-12 showed the equivalent circuit of low frequency and high frequency of MOS capacitor.

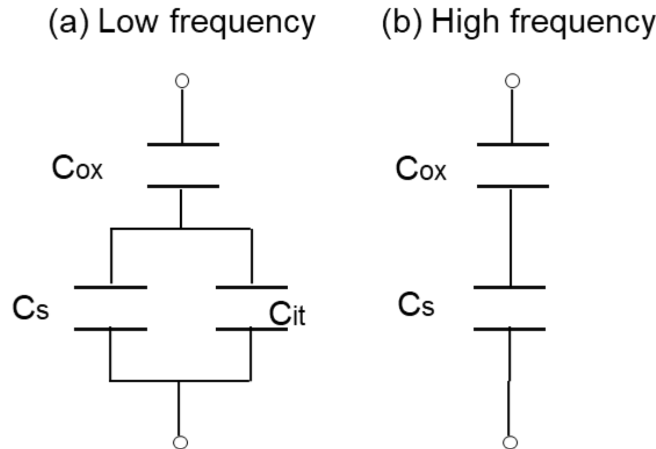

FIG. 2-12 (a) Low frequency equivalent circuit (b) High frequency equivalent circuit of MOS capacitor

C_{LF} (Capacitance the low-frequency) is extracted using the semiconductor capacitors

Cs and interface state capacitance C_{it} as shown the equation (2.11) [39].

$$C_{LF} = (C_S - C_{it})\frac{C_{OX}}{C_{OX}+C_S+C_{it}} \tag{2.11}$$

C_{HF} (Capacitance the high-frequency) is extracted as shown the equation (2.12),

$$C_{HF} = \frac{C_{OX}C_S}{C_{OX}+C_S} \tag{2.12}$$

The trap capacitance (C_{trap}) is calculated according to the equation (2.13).

$$C_{trap} = \left(\frac{1}{C_{LF}} - \frac{1}{C_{ox}}\right)^{-1} - \left(\frac{1}{C_{HF}} - \frac{1}{C_{ox}}\right)^{-1} \tag{2.13}$$

C_{ox}, C_{HF}, and C_{LF} are the oxide capacitance, high-frequency capacitance, and low-frequency capacitance, respectively. D_{it} is then obtained using the following the equation (2.14).

$$Dit = \frac{Cox}{q^2}\left(\frac{C_{LF}/Cox}{1-C_{LF}/C_{OX}} - \frac{C_{HF}/Cox}{1-C_{HF}/C_{OX}}\right) \tag{2.14}$$

It is important to pay attention to the range of sweep voltage because the bias applied and the number of electrons trapped depend on time in the insulation film with many traps in the film.

2.4.3 Experimental Apparatus

2.4.1.1 X-ray photoelectron spectroscopy (XPS)

XPS is a method that can perform not only a qualitative and quantitative analysis of elements present in a few nm surface but also the chemical bonding state [47]. In the photoelectron spectrum, the horizontal axis shows the binding energy for the electron nucleus, and the vertical axis shows the emitted photoelectron intensity. Because the binding energy is a value dependent on the elements and the electronic state, composition analysis of the material is possible from the value. The quantitative value is evaluated by

the relative sensitivity factor method using the sensitivity coefficient after calculating the area intensity of each peak intensity. Since XPS employs soft X-rays as a source, sample damage is small and charge of insulator can be easily removed. It is also possible to measure not only metals but also many materials such as polymer materials. When an element binds to another element, the electronic state changes and the peak position also changes. On the other hand, angle resolved XPS (ARXPS) is available as a method of layer analysis with thickness of several nm. In this method, the sample angle is set to an arbitrary angle in the vicinity of 0 ° to 90 ° and the emission angle of photoelectrons is changed as shown FIG. 2-12. If the specimen tilt angle is increased, the measurement depth becomes shallow and the vicinity of the surface can be measured.

X-ray photoelectron spectroscopy (XPS ; ULVAC-PHI PHI 5000 Versa Probe II) characterizations were carried out to study the chemical bonds of Al_2O_3/GaN interface. Monochromatic AlKα x-ray source with photon energy of 1486.6 eV was used. The take-off angles (TOA) to the surface plane were 20 ° and 90 ° to enhance the interface sensitivity and bulk sensitivity. A 2-nm-thick ALD-Al_2O_3 was deposited for XPS.

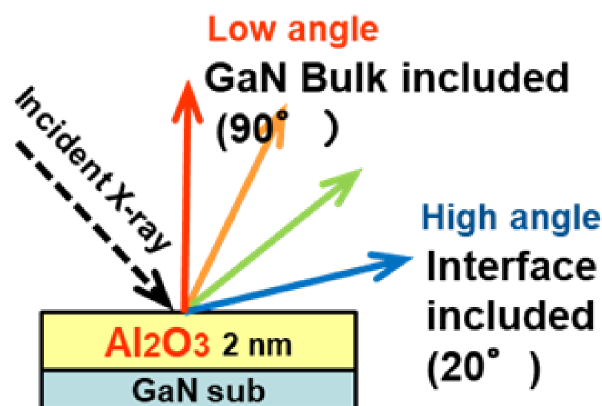

FIG. 2-12 Schematic diagram of XPS measurement. The take-off angles to the surface plane were 20 ° and 90 ° to enhance the interface sensitivity and bulk sensitivity.

2.4.1.2 Temperature-Programmed Desorption (TPD)

TPD is a mass spectrometry method that can monitor gas generated by vacuum heating and temperature rise [48]. TPD spectrum shows the temperature on the horizontal axis and the ion intensity on the vertical axis. It is possible to estimate the components of the gas generated from the samples. It is performed in a vacuum atmosphere. In addition, because only the sample can be heated, the background is low and high sensitivity analysis of low mass molecules such as hydrogen, water, oxygen and nitrogen is possible. Figure 2-13 shows the schematic diagram of TPD. The TPD measurements used TDS1200 were carried out with heating rate at 25 °C/min from room temperature to 1000 °C in vacuum.

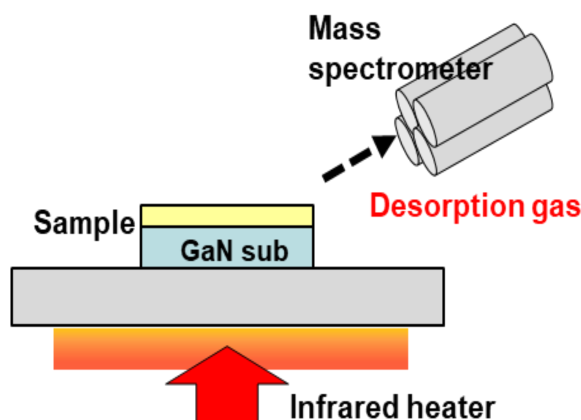

FIG. 2-13 Schematic diagram of TPD. The desorbed gases from the Al_2O_3/GaN samples through the heat treatment were measured by mass spectrometry.

2.4.1.3 Secondary Ion Mass Spectrometry (SIMS)

SIMS is a method of analyzing elements by irradiating the sample surface with an ion beam (primary ion) and mass analyzing ions (secondary ions) released from sputtering reduction from the sample surface as shown in FIG. 2-14 [47]. Because the surface is etched through sputtering, the concentration of elements in the depth profile from the surface can be measured with high sensitivity. Although it is an extremely sensitive

technique in surface composition analysis, the generation rate of secondary ions sometimes increases depending on factors such as the kind of element, the nature of the base material, and the surface condition. Furthermore, the generation rate of secondary ions has a matrix effect which is greatly affected by the sample composition. Therefore, SIMS is a sensitive microanalysis method, but it is necessary to pay attention to quantitative analysis. Elemental analysis was performed through ULVAC-PHI ADEPT-1010 with a Cs+ primary ion beam source and an accelerating voltage of 3 kV.

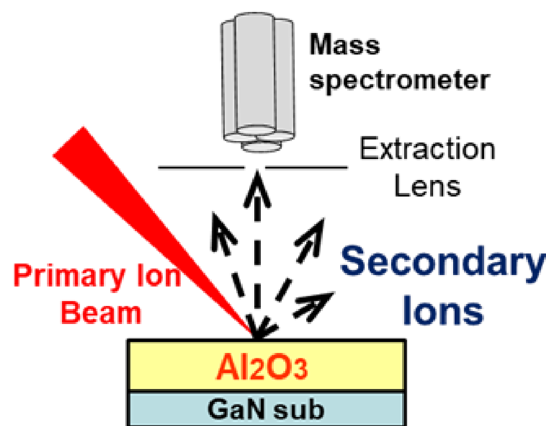

FIG. 2-14 Schematic diagram of SIMS. A primary ion was irradiated to the sample surface and secondary ions released from sputtering reduction from the sample surface

2.4.1.4 Atomic force microscopy (AFM)

Atomic force microscopy (AFM) is a method of using the atomic force between the probe and the sample surface as a probe to observe the surface directly at the nanoscale/atomic scale. To use atomic force, there is an advantage that the surface of insulating and organic materials can be measured. AFM consists of a displacement sensor that detects the deflection of the cantilever that converts the gravitational force and repulsion to the displacement of the probe. The 3D shape of the sample surface is imaged

from the z-axis control voltage of the piezoelectric element. In this study, a dynamic AFM (SPM-9600 : Shimadzu Corporation) was used to analyze the surface morphology. It detects the amount of change in the amplitude of the cantilever by periodically contacting the specimen surface and it is easy to obtain a clear image without surface treatment which makes it useful.

2.5 Electrical Characterization of GaN MOS Capacitor

2.5.1 C-V Characterization

Figure 2-15 (a) shows the frequency dispersion of the C-V characteristics of the ALD-Al_2O_3/GaN MOS capacitors of w/o HPWVA, with HPWVA (0.5 MPa), and with HPWVA at higher pressure (1.0 MPa). The sweep voltage was from + 2 to -2 V from the accumulation to the depletion and the frequency was varied from 1 MHz to 1 kHz. The measurement frequency is selected by Shockley-Read-Hall (SRH) process [49]. An electro diameter of 500 μm was used as a gate electrode. The gate voltage was swept from accumulation to depletion. The number of measured points is 5 points. Error of each points of the C-V curve was about ± 0.025 V, only one data is shown. It is confirmed that significant frequency dispersion occurs at around -0.5 V of w/o HPWVA. By applying HPWVA (0.5 MPa), the flat band voltage (V_{FB}) is very close to the ideal value. However, by applying HPWVA (1.0 MPa), a small frequency dispersion was obtained, but V_{FB} is disclose to the ideal value.

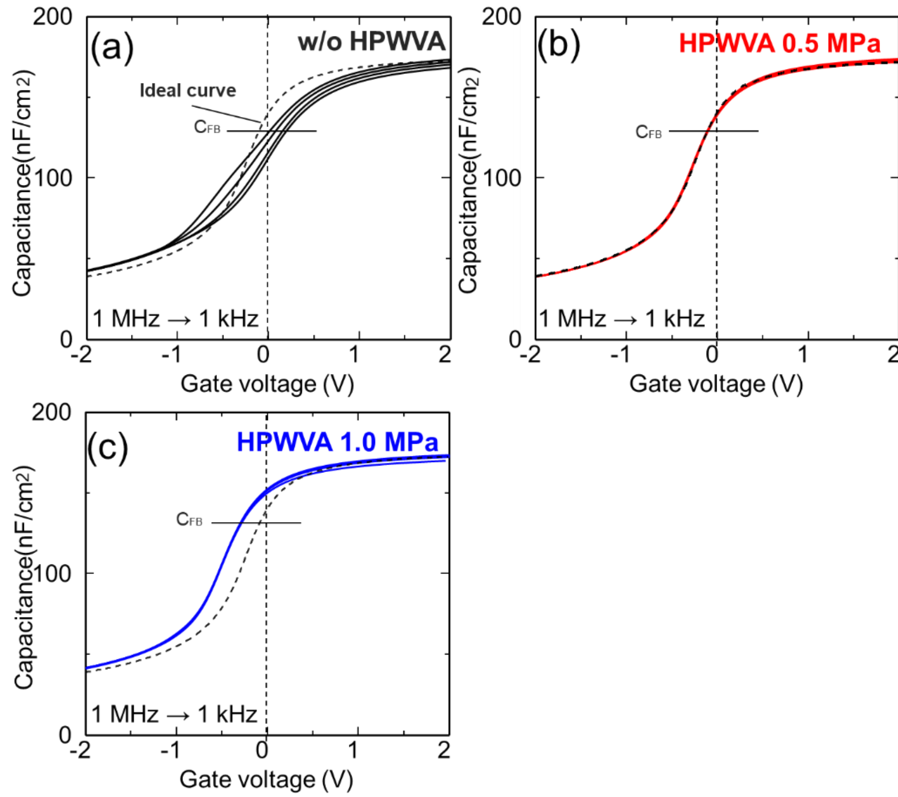

FIG. 2-15 Frequency dispersion of the C–V characteristics and (b) hysteresis of ALD-Al_2O_3/GaN MOS capacitors. The measurement frequency ranged from 1 kHz to 1 MHz, and the dashed line shows the ideal curve. The ΔV_{th} was extracted from the 1 MHz C–V curves. Solid line indicates a flat band capacitor (C_{FB}).

Figure 2-16 shows the hysteresis (ΔV_{th}) determined from the bidirectional C-V curve at 1 MHz. Hysteresis appears when electrons are captured at the interface trap or in the border trap which is near the interface. ΔV_{th} of w/o HPWVA is about 0.10 V and clearly shows a low quality interface and these of HPWVA between 0.5 and 1.0 MPa have a narrow hysteresis such as less than 0.02 V.

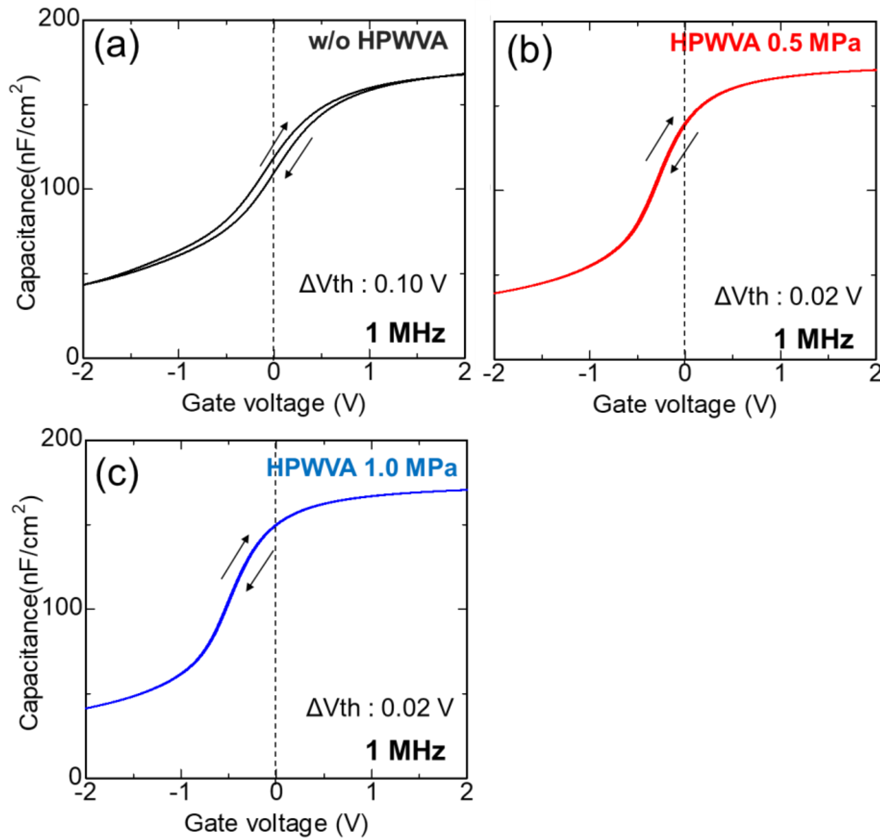

FIG. 2-16 Hysteresis characteristics of ALD-Al_2O_3/GaN MOS capacitors of (a)w/o HPWVA, (b)HPWVA (0.5 MPa) and (c)HPWVA (1.0 MPa).The C–V hysteresis was estimated from the 1 MHz C–V curves.

Table 2-1 shows the V_{FB} and N_F of Al_2O_3/GaN MOS capacitors both w/o HPWVA and with HPWVA. V_{FB} shifted from positive to negative by applying HPWVA and V_{FB} shifted further by increasing the pressure of HPWVA. The ideal V_{FB} is -0.11 V considering the condition of MOS capacitor. Therefore, HPWVA at 0.5 MPa is the closest to ideal voltage as shown in FIG 2-15. The HPWVA sample showed the smaller N_F. However, N_F of HPWVA of 1.0 MPa increased compared with 0.5 MPa. It is considered that new trap

site is formed due to increased pressure. HPWVA are effective for improving insulator characteristics of Al_2O_3 film in Al_2O_3/GaN MOS capacitors.

TABLE 2-1 Summary of V_{FB} shift and N_F of ALD-Al_2O_3/GaN MOS capacitors.

Sample Condition	V_{FB} (V)	N_F (cm^{-2})
w/o HPWVA	0.52	6.43×10^{11}
HPWVA 0.5 MPa	-0.21	1.25×10^{11}
HPWVA 1.0 MPa	-0.32	2.40×10^{11}

Figure 2-17 shows the C–V step-stress shift for ALD-Al_2O_3/GaN MOS capacitors with (a) w/o HPWVA and (b) HPWVA of 0.5 MPa and (c) HPWVA of 1.0 MPa. C-V curves were repeated by sweeping the gate voltage from accumulation to depletion with an increase in the accumulation voltage up to +10 V. The value of V_{FB} shifted in the positive direction with increasing gate voltage without stretch out by applying a positive bias. This shift was caused by the slow-charge trapping states to the Al_2O_3 film at higher electric fields and by negatively charged trap in the Al_2O_3 film [50, 51]. After HPWVA, the positive C–V shifts were approximately half the values of the V_{FB} shifts of the samples without HPWVA. There was also no difference between 0.5 MPa and 1.0 MPa. As shown in FIG. 2-17 (d), the V_{FB} change at each voltage decreases by applying HPWVA. Because in large electric fields, bulk traps far from the interface indicated the electron capture injected at a relatively fast rate, this indicates that the electron-trap density in the Al_2O_3 film was reduced by the HPWVA [50]. Therefore, high quality Al_2O_3 film by HPWVA leads to a small V_{FB} shift.

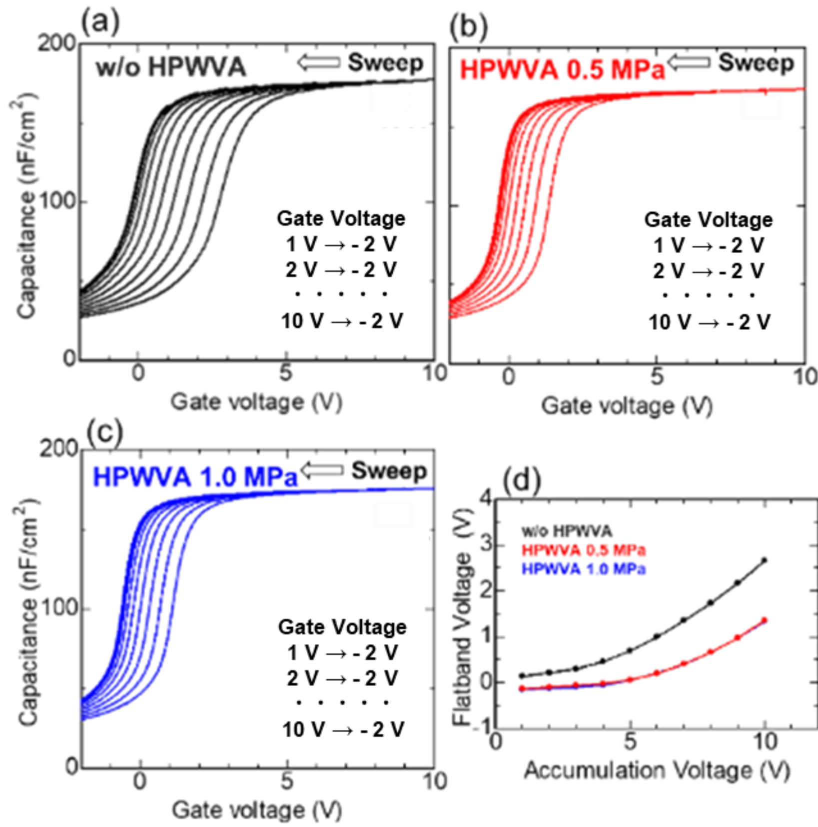

FIG. 2-17 Positive shift of the C–V step-stress measured for ALD-Al_2O_3/GaN MOS capacitors (a)w/o HPWVA and (b)HPWVA of 0.5 MPa and (c) HPWVA of 1.0 MPa. (d)Summary of V_{FB} shift plot per accumulation voltage. The C–V curves shifted positively with increasing accumulation voltage.

Figure 2-18 shows the comparison of the energy distribution of interface trap density of ALD-Al_2O_3/GaN MOS capacitors between w/o HPWVA, with HPWVA of 0.5 and 1.0 MPa. Here, E_c represents the conduction band edge of GaN. The detection band area determined that the deep level is E_c - 0.75 eV and the shallow level is E_c - 0.28 eV, assuming the capture cross section (σ_n) to be 10^{-16} cm ^{2} [52]. The D_{it} at an energy level of E_C - E = 0.3 eV was ~ 1.0×10^{12} cm^{-2} eV^{-1} for w/o HPWVA sample. In contrast, the D_{it} of the HPWVA sample was reduced to about 6×10^{10} cm^{-2} eV^{-1}. As shown FIG. 2-11, D_{it}

takes a U-shaped distribution that is higher for shallow levels at the band edge and lower for deeper levels near the mid-gap. The tendency was found in this result, and D_{it} was reduced by approximately one order of magnitude as closing mid-gap. At the interface between the insulator and GaN, trap levels related to nitrogen vacancy V_N have been reported near E_c - 0.5 eV [53-55]. A gentle peak distribution was observed around Ec 0.3 ~ 0.5 eV of the w/o HPWVA. Since this trap level is reduced by HPWVA, HPWVA is effective for reduction of discrete levels related to V_N at the interface. In addition, compared with HPWVA at 0.5 MPa and 1.0 MPa, it seems that these D_{it} is almost same. This investigation will be discussed in relation to the physical characteristics described in a later section. Therefore, it can be seen that HPWVA induced improvement of interface characteristics similar to insulator characteristics of Al_2O_3 film in Al_2O_3/GaN MOS capacitors.

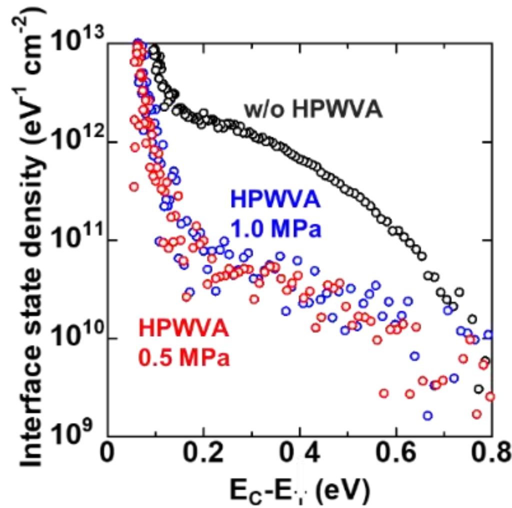

FIG. 2-18 Energy distribution of D_{it} of w/o HPWVA and with HPWVA 0.5 MPa and 1.0 MPa. E_C denotes the conduction band edge of GaN.

2.5.2 I-V Characterization

A time-zero dielectric breakdown test (TZDB) was performed using an Al_2O_3/GaN MOS capacitor. The leakage current was measured by sweeping the forward direction bias to the gate electrode and injecting majority carriers from the semiconductor layer into the Al_2O_3 film. Current density–electric field characteristics (J- E) are shown in FIG. 2-19. The breakdown electric field (E_{BD}) was defined at 10^{-3} A/cm^2 and after dielectric breakdown, an unrecoverable leak path was formed in the MOS capacitor. An electro diameter of 100 µm was used as a gate electrode and the J–E characteristics were obtained from 7 points. The E_{BD} is calculated considering the V_{FB} and GaN band bending [56]. The average oxide electric field Eox is given the equation (2.15).

$$E_{OX} = \frac{V_{OX}}{t_{OX}} = \frac{(V_G - V_{FB} - \Psi_s)}{t_{OX}} \tag{2.15}$$

In the calculation, Vox is the voltage drop across the Al_2O_3 film, V_{FB} is the voltage under the flat-band condition, and Ψ_s is the GaN band bending, which was estimated from an ideal C–V curve. tox is the Al_2O_3 thickness. In the Eox range from 0 to 3 MV/cm, J moderately increases. From 3 to 5 MV/cm, J significantly increases and at more than 6 MV/cm, the breakdown occurs. Initial failure destruction (A mode) around 0 MV/cm based on the initial defect did not appear and at 0 to 5 MV/cm, random failure (B mode) derived from the crystal quality of GaN was not observed.

Therefore, it was confirmed as intrinsic destruction (C mode) peculiar to the Al_2O_3 film in all the samples. Similar gate leakages were observed in the w/o HPWVA and HPWVA samples with range from 0 to 5 MV/cm. Fowler-Nordheim (FN) plots, Poole-Frenkel (PF) plots and Trap Assisted Tunneling (TAT) plots have been generally used as

leakage conduction analysis methods, however Hirawa recently reported that it is not fitted by a linear function in these plot [57]. These behaviors from 3 to 5 MV/cm indicate the possibility that the leakage current follows the new model, Space-charge-controlled field emission (SCC-FE) [45]. This is a current conduction model of a MOS capacitor assuming a field emission current considering the influence of two space charges of negative and positive bias on an insulator [57]. These results are related to the electron injection into the trap in the Al_2O_3 film and the electron trap density in the Al_2O_3 film with HPWVA was lowered. In addition, the E_{BD} average values of w/o HPWVA, HPWVA of 0.5 MPa and HPWVA of 1.0 MPa were 7.1, 7.9 and 6.2 MV/cm. The highest E_{BD} was obtained in HPWVA of 0.5 MPa. These results indicate that good quality Al_2O_3 film by HPWVA leads to high leakage current and high breakdown characteristics.

However, E_{BD} of HPWVA of 1.0 MPa was lower than w/o HPWVA. Because the leakage conduction mechanism of HPWVA of 1.0 MPa is shown in the same as other samples, it is unlikely that the Al_2O_3 film tends to leaky. Figures 2-20 show the energy band diagrams of the Al_2O_3/GaN interfaces with (a) w/o HPWVA and (b) HPWVA. Here, FIG. 2-20 (a) showed a higher trap density in the w/o HPWVA sample than the structure in FIG.2-20 (b). When a high positive voltage is applied to the gate electrode, electrons are injected into the Al_2O_3 films and go through the conduction band. Some injected electrons are trapped in the Al_2O_3 films, resulting in the formation of a low electric field near the Al_2O_3/GaN interface, which reduces the tunneling probability. Therefore, even with increasing gate voltage, the leakage current does not increase.

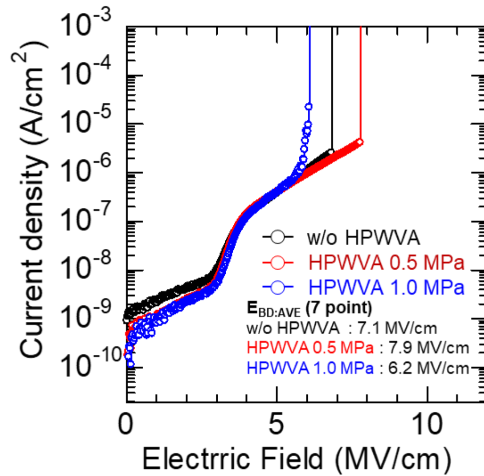

FIG. 2-19 J- E_{BD} of ALD-Al_2O_3/GaN MOS capacitors of w/o HPWVA and with HPWVA of 0.5 MPa and 1.0 MPa.

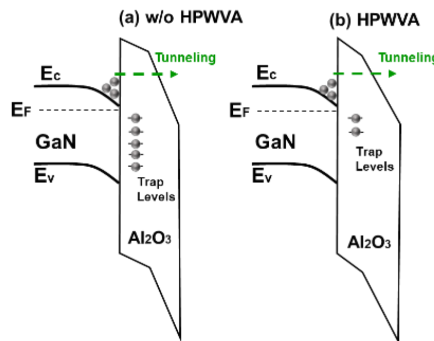

FIG. 2-20 Schematic energy band diagrams of the Al_2O_3/GaN structures with the trap levels in the Al_2O_3 film (a) w/o HPWVA and (b) with HPWVA

Time-dependent dielectric breakdown (TDDB) test was conducted as reliability evaluation of Al_2O_3/GaN MOS capacitor. It is an evaluation method of constantly applying various electrical stresses that do not cause hard breakdown and measure the dielectric lifetime until breakdown. Figure 2-21 shows the conduction currents in Al_2O_3/GaN MOS capacitor wihout HPWVA and with HPWVA of 0.5 MPa under constant voltages at room temperature. An electro diameter of 100 μm was used as a gate electrode. The number of measurement points is 5 points, and each points broke down due to hard

breakdown. Since the TZDB of HPWVA 1.0 MPa are worse than w/o HPWVA, only comparison with HPWVA of 0.5 MPa is measured. For the mechanism until breakdown, For the mechanism until breakdown, the gate leakage current firstly decreases with stress time, which is due to charging of deep traps at Al_2O_3/GaN interface [58]. Electrons injected in the oxide can be captured at oxide traps, rising the potential-barrier and suppressing leakage current. Current rises sharply because of the breakdown event and the formation of a conductive path. TDDB is abrupt, hard, and no early indicators of the breakdown event have been identified.

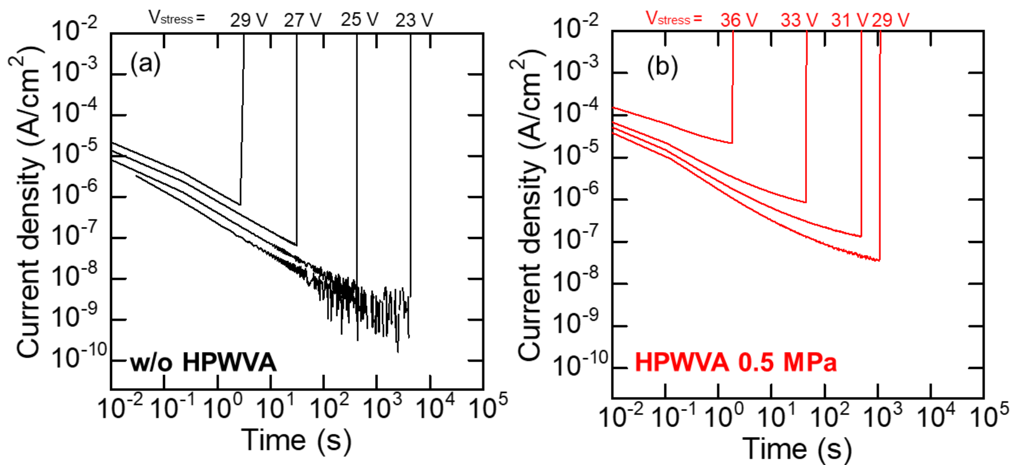

FIG. 2-21. Conduction currents in Al_2O_3/GaN MOS capacitor of (a)w/o HPWVA and (b)with HPWVA under constant voltages at room temperature. The abrupt increase in the currents is caused by dielectric breakdown.

The TDDB of w/o HPWVA and with HPWVA to gate voltage is depicted in FIG. 2-22. One plot point corresponds to the intermediate value of each voltage condition in the stress test. A straight line with the about same slope was obtained by linear approximation of these points using the least squares method. Normally, it is necessary to derive the true value of the plot under each voltage from the Weibull distribution showing the dominant mechanism of intrinsic failure from the measurement of many points (~30 points).

However in these results, there were few measurement points (~5 points) from the samples and note it as reference data. FIG. 2-22 showed that the maximum permissible electric field in 10 years of the HPWVA is 3.5 MV/cm compared with 2.1 MV/cm of w/o HPWVA. It is confirmed that the reliability is improved by HPWVA.

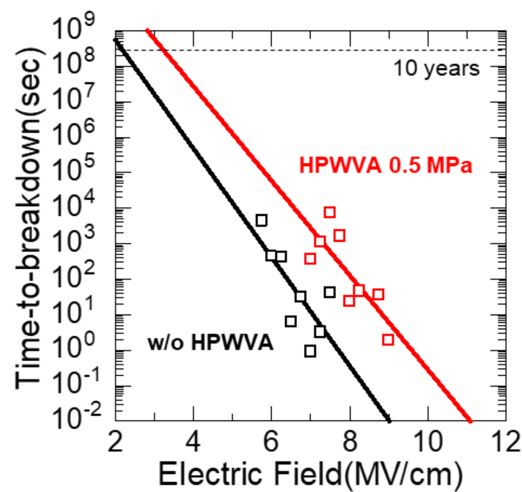

FIG. 2-22. TDDB without HPWVA and with HPWVA as a function of gate-voltage at room temperature. The dotted line indicates the time-to-breakdown in 10 years.

2.6 Investigation of HPWVA Effect with GaN MOS Capacitor

2.6.1 Change the ALD-Al_2O_3 film quality

The physical characteristics of the samples were evaluated to verify that the electrical characteristics were improved by HPWVA. Figures 2-23 shows Al2p XPS spectra of Al_2O_3 surface without and with HPWVA of 0.5 MPa. Peak intensity was normalized and the binding peak was calibrated with C1s. The Al2p peak fits only Al^{3+} for Al_2O_3 surface without and with HPWVA [59]. It follows that the peak, positioned at 74.2 eV, corresponds to Al^{3+} in ALD-Al_2O_3 [60, 61]. In additon, the peak, positioned at 75.2 eV, corresponds to Al^{3+} formed AlO(OH) and $Al(OH)_3$ by the connection with OH

or H_2O ligands [60, 61, 62]. XPS spectra of Al_2O_3/GaN showed an increase in the ratio of Al-OH or Al-O(OH) bonds derived from the HPWVA.

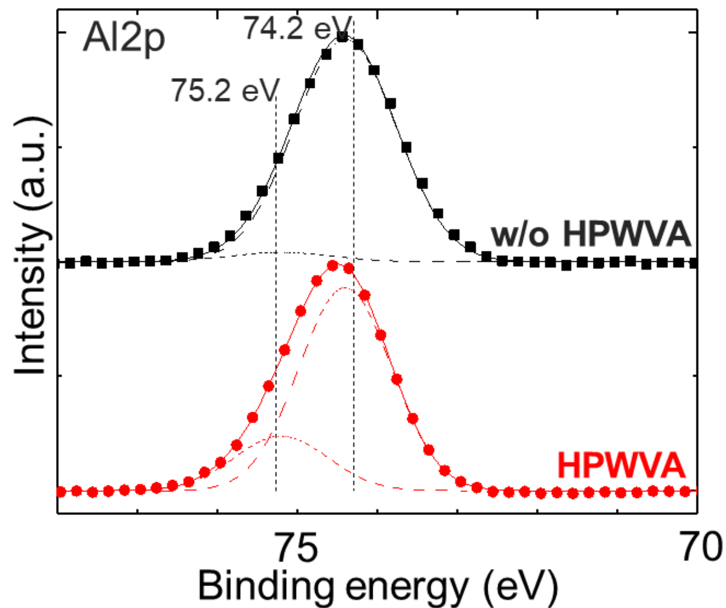

FIG. 2-23 Al 2p XPS spectra of Al_2O_3 surface without and with HPWVA. The dashed lines represent the fitted peaks, the dots represent the raw spectrum, and the solid lines represent the cumulative sum of the fitted peaks.

O 1s XPS spectra of Al_2O_3/GaN samples without and with HPWVA were shown in FIG. 2-24. The peak at 531.2 eV represents the bonding between oxygen atoms and Al atoms, and the peak at 532.3 eV represents hydroxyl groups, and the peak at 533.2 eV represents adsorbed water [63]. The peak intensites were normalized by Al2p spectra. The peak intensity of Al-O-Al increased by HPWVA. Also, it was confirmed the ratio of Al-OH bonds increased as well as the results of Al2p spctra.

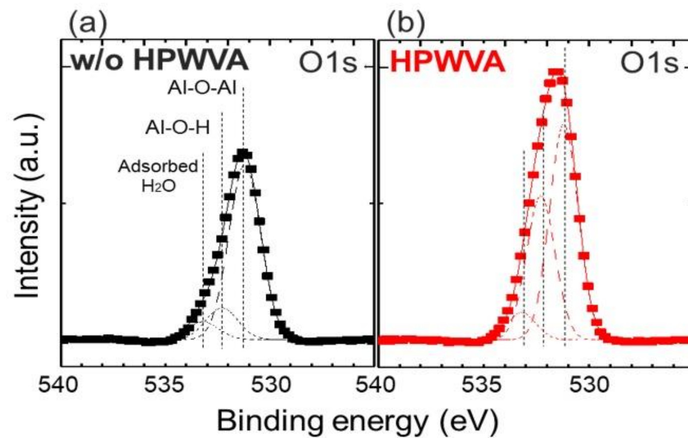

FIG. 2-24 O 1s XPS spectra of of Al_2O_3/GaN samples (a) without and (b) with HPWVA. The dashed lines represent the fitted peaks, the dots represent the raw spectrum, and the solid lines represent the cumulative sum of the fitted peaks.

Figure 2-25 shows the TDS at a mass-to-charge ratio m/z = 18 (corresponding to H_2O) for samples with and without HPWVA and for the GaN substrate. The TDS results show a desorption peak at around 100 °C both for the sample without HPWVA and for the GaN substrate. This is primarily caused by molecular water physically adsorbed on the surface ($H_2O(\alpha)$) [64, 65]. On the other hand, the desorption peak of the HPWVA samples at around 200 °C corresponds to desorption of tightly bound water, in which molecular water is bonded to hydrogen at –Al-OH ($H_2O(\beta)$). In addition, the desorption peak from 300 °C to 500 °C corresponds to desorption of bound water derived from OH (Al-OH(γ)). The $H_2O(\alpha)$ on the Al_2O_3 surface is dissociated by the annealing process [31-33]. The H_2O monomer derived from HPWVA is formed the $H_2O(\beta)$ in the interior or at the surface of the Al_2O_3 film. In particular, a desorption peak for the samples both with and without HPWVA at 500 was observed. However, the desorption gradually increases from 200 °C to 500 °C for the HPWVA sample. This shows that a large amount of Al-

OH(γ) exists in the Al_2O_3 film. The Al-OH(γ) increased by about 20% by HPWVA compared to the without HPWVA sample.

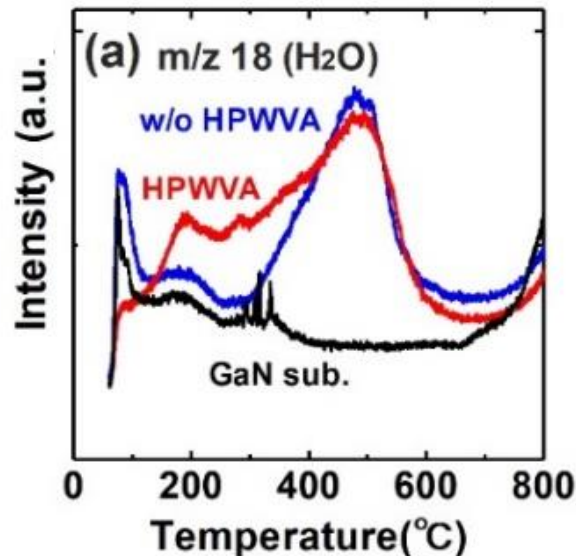

FIG. 2-25 Thermal-desorption spectra at m/z =18 without HPWVA, with HPWVA, and for the GaN substrate.

2.6.2 Diffusion of active species derived from HPWVA

The distribution of diffused oxygen into the sample during HPWVA was investigated. Figure 2-26 shows the SIMS observations of the samples, using water containing the ^{18}O isotope ($H_2{}^{18}O$) for the HPWVA. Because oxygen atom is a constituent element of the Al_2O_3 film, it is necessary to distinguish it from the oxygen acquired during the ALD process. A clear diffusion of ^{18}O in the HPWVA samples was observed. Because the same results of SIMS for ^{18}O were obtained both the GaN-on-Si substrate and the Si substrate for ALD-Al_2O_3 samples with HPWVA for 30 min, an Si substrate was used. The diffusion depth of oxygen (^{18}O) increases as the processing time is increased, as shown in FIG. 2-26 (b) and (c). From the results of the sample with HPWVA at 0.5 MPa for 10 minutes,

the diffusion coefficient for H_2O into the ALD-Al_2O_3 film was 2.2×10^{-20} m^2/s. The diffusion coefficient was calculated using the equation for the diffusion coefficient [66]. This diffusion coefficient is equivalent to that for O_2 in a dry annealing process at about 700°C.[34)] As shown in FIG. 2-26 (c), performing HPWVA for at least 30 minutes induces the diffusion of oxygen throughout the Al_2O_3 film, and this accounts for the high diffusion ability of H_2O by HPWVA at low temperatures.

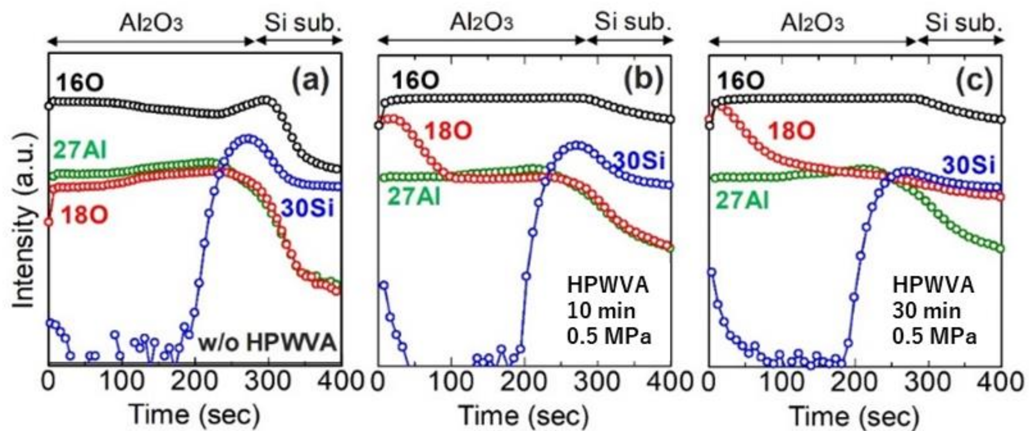

FIG. 2-26 SIMS depth-profile analysis for ^{27}Al (27Al), ^{30}Si (30 Si), ^{18}O (18O), and ^{16}O (16O) for ALD-Al_2O_3 samples (a) without HPWVA, (b) with HPWVA for 10 min, and (c) with HPWVA for 30 min at 0.5 MPa. The HPWVA used $H_2{}^{18}O$.

Deuterated water (D_2O) for the HPWVA for the SIMS was used. As shown in FIG. 2-27 of the SIMS analysis, the HPWVA diffused deuterium (^2H = D, labeled 2H in the figures) through the entire Al_2O_3 film. The curve labeled 1H is hydrogen derived from the precursor remaining from the ALD process [67]. Since the hydrogen species have relatively small sizes, unlike oxygen, they can easily move into the Al_2O_3 film. However, it is important to note that 2H has almost twice mass than 1H and diffusivity and chemical reaction with Al_2O_3 film may be different [68]. As for the diffusing power, it is suggested that the mass of 1H is less than that of 2H and even in the original HPWVA used 1H,

hydrogen diffused throughout the Al_2O_3 film. A previous report found that the hydrogen or deuterium—but not the oxygen—from the diffusing water molecules exchange with the OH groups in the oxide film, as a diffusion reaction mechanism when water enters the film [69]. Thus, it is considered that this diffused 2H shows hydride species such as Al-OD in the Al_2O_3 film. Also, it is conceivable that the D_2O reacted with the Al_2O_3 film and formed hydrogen. The hydrogen remains in the Al_2O_3 film after HPWVA.

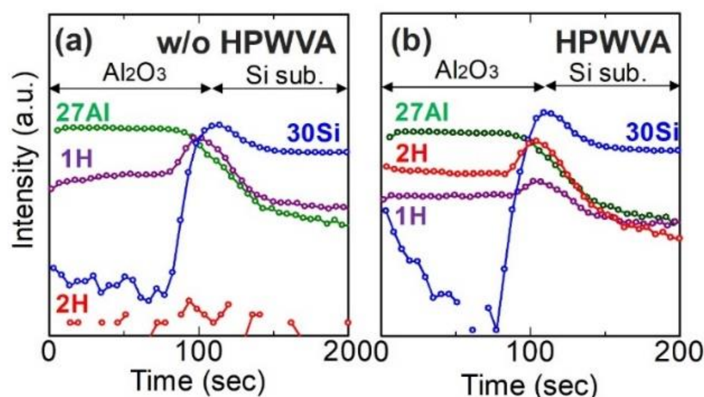

FIG. 2-27 SIMS depth-profiles of ^{27}Al (27Al), ^{30}Si (30Si), ^{1}H (1H), and ^{2}H = D (2H) for ALD-Al_2O_3 samples (a) without and (b) with HPWVA of 0.5 MPa using D_2O.

2.6.3 Oxidation of GaN in Al_2O_3/GaN Interface

Figures 2-28 show the Ga 2p XPS spectra of the interface and the bulk of the ALD-Al_2O_3 samples (a)without HPWVA, with HPWVA (0.5 MPa) and with HPWVA (1.0 MPa). Since Ga 2p is shallower in penetration length than Ga 3d, more sensitive interface information can be obtained from it. The Ga–N peak occurs at 1117.8 eV in ALD-Al_2O_3/GaN, the Ga-O peak at 1118.7 eV represents the oxide of GaN at the Al_2O_3/GaN interface, and the Ga-Ga peak at 1116.3 eV represents the bonding between Ga atoms in the GaN crystal [70, 71]. In the interface sensitive XPS spectra of Al_2O_3/GaN, the peak of the Ga-O bond was increased for samples both with and without HPWVA, as compared with the bulk-sensitive spectra. As shown in FIG. 2-28 (b), there was a tendency for the

Ga-O binding at the interface to be increased slightly for the HPWVA sample. It is difficult to observe the binding peak due to Ga-OH around 1120 eV from these results [71]. In addition, compared with HPWVA between 0.5 MPa and 1.0 MPa, Ga-O binding at the interface was increased slightly. This suggests that reaction between Ga and oxygen occurs at the interface after HPWVA and that gallium oxide is formed at the Al_2O_3/GaN interface. Ga-O binding increased by rising pressure of HPWVA.

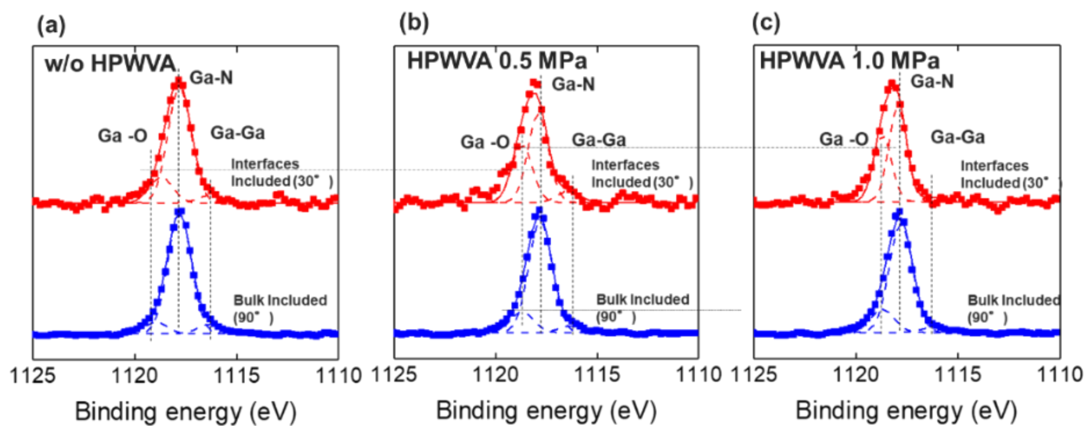

FIG. 2-28 Ga 2p XPS spectra for the interface and the bulk of ALD-Al_2O_3 films (a) without and (b) with HPWVA. The dashed lines represent the fitted peaks, the dots represent the raw spectrum, and the solid lines represent the cumulative sum of the fitted peaks.

Figure 2-29 shows the AFM image of Al_2O_3/GaN structure (a)without HPWVA, with HPWVA (0.5 MPa) and HPWVA (1.0 MPa). Three points are measured and the maximum error is ± 0.005 nm at a range of 2 μm. The square average roughness (root mean square, RMS) of HPWVA of 0.5 MPa was 0.22 nm and slightly increased surface roughness compared with 0.20 nm of w/o HPWVA. RMS of HPWVA (1.0 MPa) is 0.26 nm and surface roughness increased with increasing pressure. In addition, Some protrusions that were not confirmed at 0.5 MPa were confirmed at 1.0 MPa. Therefore, it

can be seen that the surface morphology is changing through increasing pressure of HPWVA. This increase in surface irregularities is undesirable because of the local electric field concentration. It was confirmed that the TZDB characteristics deteriorated in HPWVA of 1.0 MPa, as shown in FIG. 2-19. It is cosidered the local electric field concentration was caused by generating such a surface projection. In the next chapter, the investigation of the surface flatness and surface projections under higher pressure conditions in HPWVA will be discussed.

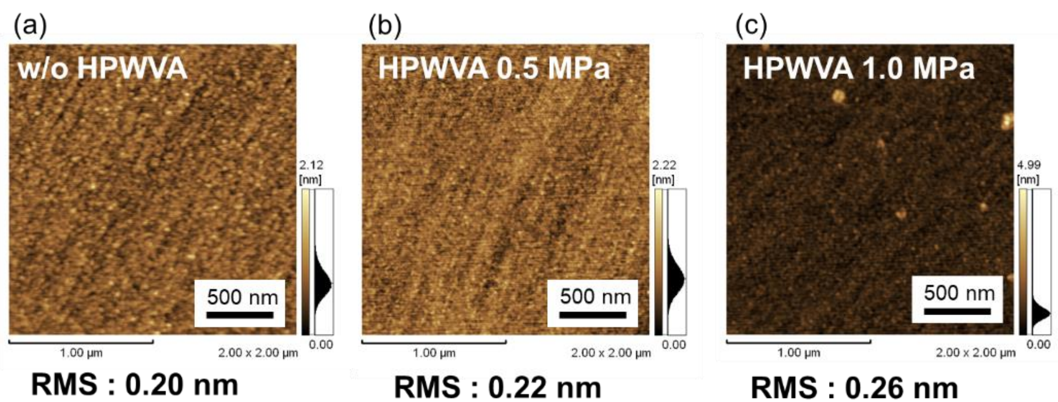

FIG. 2-29 AFM image of Al_2O_3/GaN structure (a)without HPWVA, (b)with HPWVA (0.5 MPa) and (c) HPWVA (1.0 MPa) (top view).

2.7 Grain Growth of GaOx in HPWVA under High Pressure

Surface of Al_2O_3/GaN MOS structure under higher pressure condition of 1 MPa or more was investigated by using the new supercritical apparatus. Figure 2-30 shows the pressure dependence of surface roughness of HPWVA in Al_2O_3/GaN structure. The surface roughness at each pressure condition (300 °C and 400 °C) are also shown. The sample was Al_2O_3 (40nm)/GaN structure and the Al_2O_3 surface was observed with AFM. It was observed that the surface roughness exceeded 5 nm rapidly at 400 °C and 300 °C

with pressures of 2.0 MPa or more, suggesting that the oxidation reaction at the interface rapidly changes at 2 MPa or more. In addition, when it exceeds 2 MPa, the initial failure (A mode) around 0 MV/cm was shown in the TZDB characteristics. Figure 2-31 shows the annealing time dependence of surface roughness at each pressure condition of HPWVA in Al_2O_3/GaN structure. Even at an annealing time of 3 hours, time dependence of surface roughness was not observed and it was found that the time dependence of surface roughness was not very large.

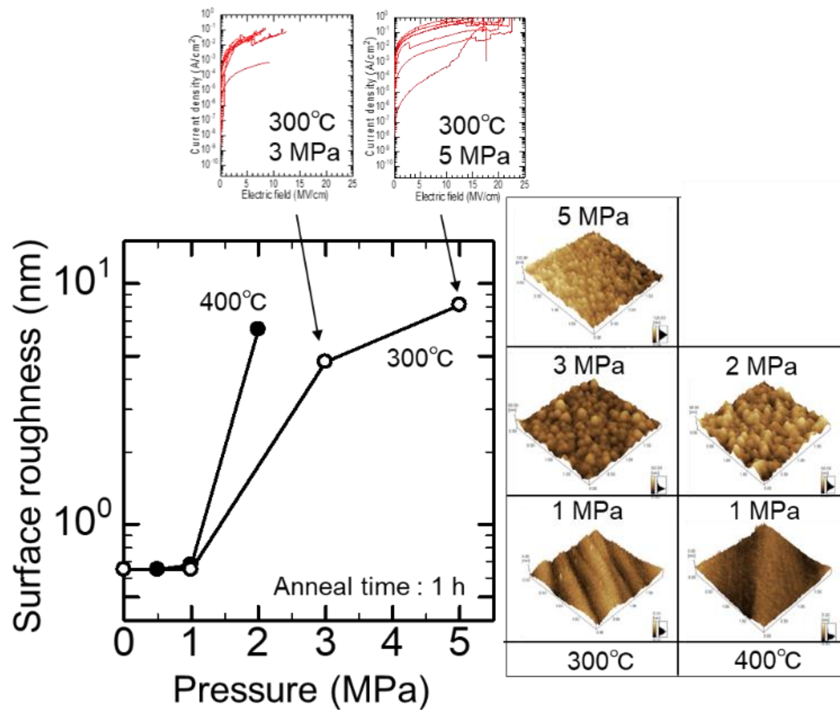

FIG. 2-30 Pressure dependence of surface roughness of HPWVA in Al_2O_3/GaN structure. The surface shape at each pressure condition (300 °C. and 400 °C) are also shown. When it exceeds 2 MPa in the HPWVA, initial failure (A mode) around 0 MV/cm occurs.

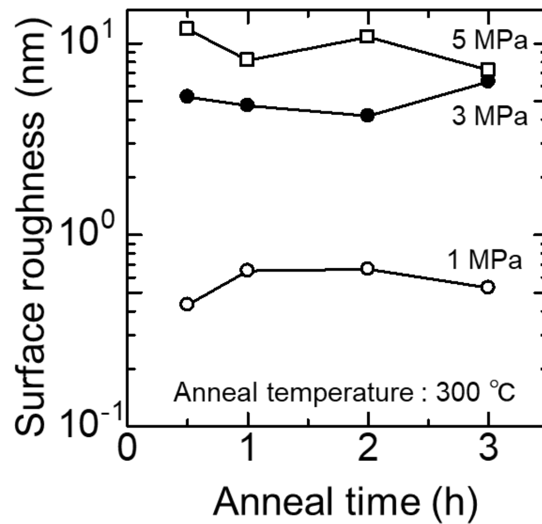

FIG. 2-31 Anneal time dependence of surface roughness at various pressure condition of HPWVA in Al_2O_3/GaN structure. The pressure condition of 300 °C **is 1 MPa, 3 MPa and 5 MPa as function of annealing time.**

It was investigated whether this surface was made of Al_2O_3 or GaN. Figure 2-32 shows Scanning Electron Microscope (SEM) image of the Al_2O_3 surface in Al_2O_3/GaN MOS structure with HPWVA. The HPWVA of this sample was processed at 6 MPa for 1 hour at 300 °C. It has been confirmed that rod-shaped crystal growth substances of micron sizes locally grow through the Al_2O_3 film and the surrounding round shape is also a crystal growth material. FIG 2-33 shows the composition analysis of the bar-shaped crystal growth product. Ti, Cu, etc. indicate peaks derived from Transmission Electron Microscope (TEM) grid. W is a cover metal in cross-section etching. It is confirmed a Ga-derived peak from the crystal growth. The point analysis was carried out at an accelerating voltage of 20 kV, and light elements such as oxygen were hardly detected. It could not confirmed a oxygen peak, but carbon which is light element was detected and it is a possibility that Ti and O may be over raped.

Thus, Energy dispersive X-ray spectrometry (EDS) mapping of oxygen was

observed with an acceleration voltage of 5 eV. As shown in the FIG. 2-34, it was found that the crystal growth is composed of oxygen. Since Ti is derived from the TEM grid, it should be observed throughout in the EDS mapping, however it is observed at specific locations such as the Al_2O_3 film and crystal growth, it is highly probable that these mapping is derived from oxygen. It is reported that oxidation progresses preferentially from GaN surface defects due to dry oxygen annealing at high temperature (800 °C ~) and generated crystal growth of Ga oxide [72, 73]. In addition, the surface roughness is caused by oxidation of GaN at the Al_2O_3/GaN interface. Therefore, it was considered that this crystal growth product is a Ga oxide derived crystal growth material and the HPWVA under higher pressure (2 MPa~) promotes the crystal growth of Ga oxides and greatly deteriorates the electrical characteristics of the Al_2O_3/GaN MOS capacitor.

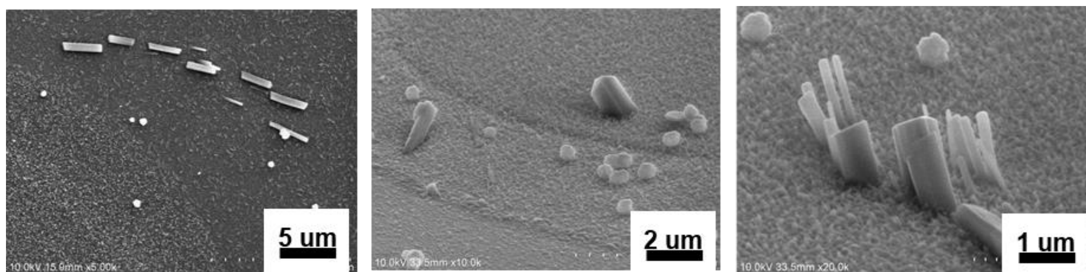

FIG. 2-32 SEM image of the Al_2O_3 surface in Al_2O_3/GaN MOS structure with HPWVA. The HPWVA of this sample processed 6 MPa for 1 hour at 300 °C. Rod-shaped crystal growth of micron sizes locally grows through the Al_2O_3 film.

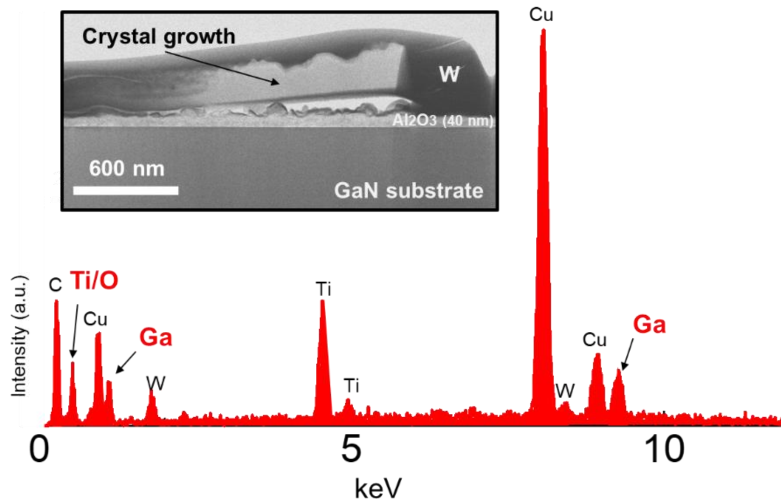

FIG. 2-33 The composition analysis of the bar-shaped crystal growth material at 20 keV. Ti, Cu, etc. indicate peaks derived from TEM grid. W is a cover metal in cross-section etching.

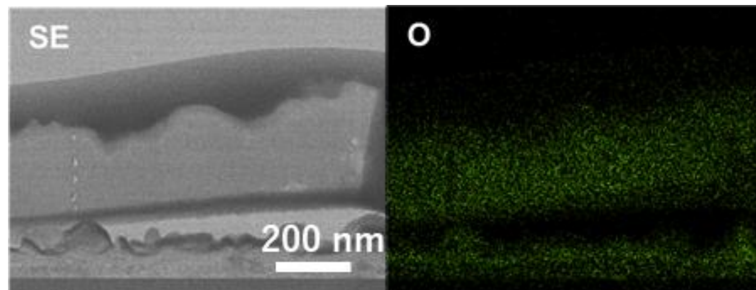

FIG. 2-34 EDS mapping spectra of oxygen at 5 keV. It was observed oxygen derived the crystal growth and Al_2O_3 film.

2.8 Discussion on Reaction Model of HPWVA

The effect of HPWVA on Al_2O_3/GaN capacitors from these results was summarized. Figure 2-35 shows the mechanism model of the HPWVA effect (~ 0.5 MPa) on Al_2O_3/GaN MOS structure. From these results, a reaction model of HPWVA for Al_2O_3/GaN MOS capacitors was proposed. Under the condition of HPWVA (400°C, 0.5MPa, 30min), active H_2O monomers can be diffused into Al_2O_3 film.

From the SIMS and TDS results, the diffused H_2O monomer to the Al_2O_3 film was

distributed as $H_2O(\beta)$ in the vicinity of the surface. The diffused H_2O monomer also reacted with the defective Al_2O_3 film and formed Al-O-Al and Al-OH bonds. It is suggested that hydrogen observed from the SIMS result of ^2H is derived from the reaction product of the active H_2O with the Al_2O_3 film. As shown in the XPS results of Al 2p and O 1s, the ratio of Al-OH bond at the Al_2O_3 surface is increased about 2 times by HPWVA and the peak intensity of Al-O-Al is also slightly increased. On the other hand, from the TDS results, it was found that the Al-OH (γ) signal from the whole Al_2O_3 film was only increased by about 20%. These differences of the Al-OH results were related to the gradient of H_2O concentration in the Al_2O_3 film. Therefore, it is considered that these reactions of the active H_2O are relevant to the modification of defective Al_2O_3 film and the improvement of the electric characteristics, such as the N_F and the stress shifts.

However, it could not be determined from results whether hydrogen is related to the improvement of Al_2O_3 film. HPWVA is effective not only for improving the Al_2O_3 film but also for improving the Al_2O_3/GaN interface. From the XPS results for Ga2p, it was confirmed that the Ga-OH bond was not observed and the intensity of the Ga-O bond was increased by HPWVA. The gallium oxide thickness estimated from AR-XPS of Ga2p is about 1 ~ 2 atomic layers. The active H_2O, which reached the Al_2O_3/GaN interface, was only a small number at this condition of HPWVA as shown SIMS results. It is considered that even a small number of H_2O can react with the interface and form a thin gallium oxide. Consequently, the generation of gallium oxide affects the termination of the Ga dangling bonds. This termination was also reported in high temperature dry annealing [74-76]. However, previous reports indicated that the high temperature dry oxidation annealing of 800 °C causes the electrical characteristics to deteriorate due to the crystallization of the Al_2O_3 film [77]. Therefore, HPWVA has the advantage to form

the gallium oxide at a low temperature (400 °C). Thus, it is effective in reducing the D_{it} significantly.

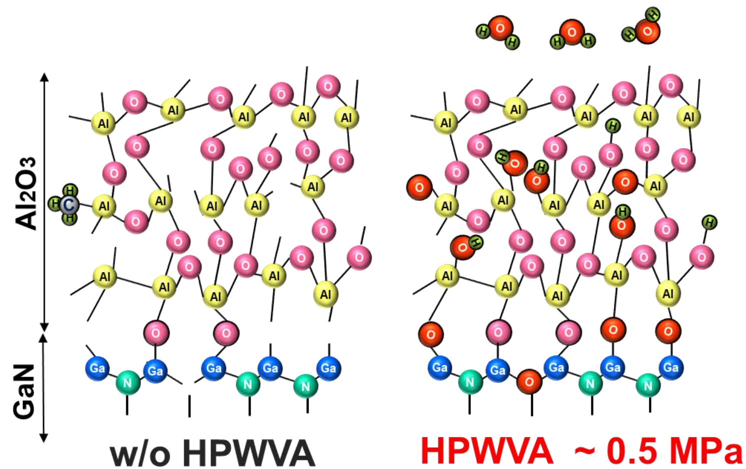

FIG. 2-35 Effect model of HPWVA (~ 0.5 MPa) on Al_2O_3/GaN MOS structure.

At 1 MPa or more, surface roughness increased with pressure rise, it was confirmed that the deterioration of D_{it} and E_{BD}. When the pressure was further raised to 2 MPa, only the the initial failure occurred in TZDB measurement and other electrical characteristics could not be obtained. under high pressure condition of 6 MPa, micro-sized GaOx crystal growth developed and it penetrated the Al_2O_3 surface. Therefore, HPWVA is sensitive to pressure conditions and it was found that improvement of electrical characteristics can be expected within the range where surface roughness does not occur.

2.9 Electrical Characterization in High Temperature Condition

2.9.1 I-V Characterization

Main problem of the high power modules is high electric power loss, which requires the water cooling system. For the future power devices, very low on-resistance and high temperature operation above 200 °C are expected to simplify the cooling system of the

inverter, as introduced in Chapter 1. Therefore, electrical characteristics were evaluated in a high temperature range.

Figure 2-36 shows the temperature dependence of J- E of Al_2O_3/ GaN MOS devices between w/o HPWVA and HPWVA. Temperatures are set at RT, 100 °C and 200 °C. An electro diameter of 100 μm was used as a gate electrode. The number of measurement points at each temperature are 5 points, and each points broke down due to hard breakdown. This shows that the E_{BD} of both samples. decreased due to the temperature rise and the leak current increased. In addition, the E_{BD} improved by HPWVA at each temperatures. The leakage conduction mechanisms of Al_2O_3/GaN capacitors are SCC-FE at 3~5 MV/cm and Schottky emission (SE) at 0 ~ 3 MV/cm. SE conduction mechanism is a bulk-limited conduction process and occurs due to defect states and carriers follow the over barrier. Electron emission requires thermal excitation. In the high temperature (200 °C), SE which the carrier absorbs thermal energy is released across the potential barrier of the interface increased [78]. SE occurs at the barrier of interface between Al_2O_3 and GaN and SCC-FE occurs via a trap in the bulk of the Al_2O_3. As a result of the temperature dependence of the leakage current, it is considered that the SE became dominant from the FE due to the temperature rise. As described in chapter 2-19, it is considered that defects were reduced by HPWVA and this was attributed to an increase in dielectric breakdown voltage.

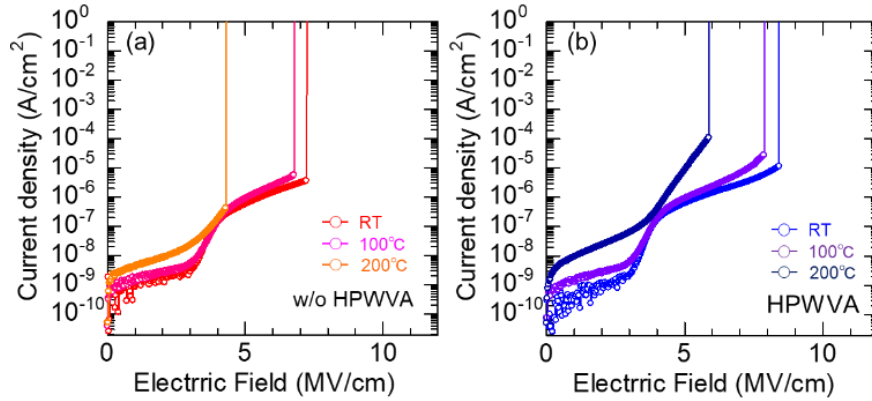

FIG. 2-36 Temperature dependence of J- E_{BD} of GaN MOS devices with ALD-Al_2O_3 (a) wihout HPWVA and (b)with HPWVA. The temperature condition is RT, 100°C and 200 °C.

In order to investigate the lifetime of Al_2O_3/GaN MOS capacitors, TDDB measurement was carried out at 200 °C compared with room temperature. Figure 2-37 shows the results of Al_2O_3/GaN MOS capacitor wihout HPWVA and with HPWVA at 200 °C . In general, TDDB is evaluated at 3 MV/cm for Si power devices for automotive applications [79]. Therefore, tBD is defined as 3 MV/cm. The TDDB of the w/o HPWVA was estimated to be over 30 years at room temperature. The TDDB at temperature of 200 °C was about 10^3-10^4 seconds, It was reported that it is necessary to have a service life of more than 20 years at 200 °C for automotive applications. The TDDB at 200 °C. is much lower than the required value. TDDB decreases as the leakage current of the Al_2O_3 film increases. The Al_2O_3 film had a relatively large leakage current due to trapping to bulk defect and the short TDDB may be due to the large leakage current. In order to increase the lifetime, it is necessary to reduce the trap density by optimizing the deposition condition of ALD - Al_2O_3.

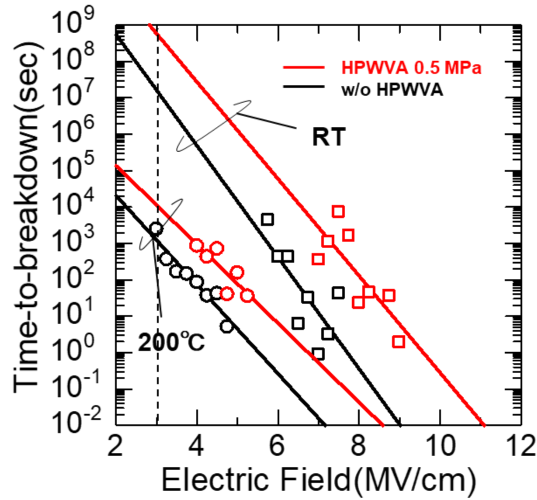

FIG. 2-37 TDDB wihout HPWVA and with HPWVA (0.5 MPa) at 200 °C compared with room temperature. The dotted line indicates the electrical field is 3 MV/cm.

2.9.2 C-V Characterization

Figure 2-38 shows C–V characteristics of ALD-Al_2O_3/GaN MOS capacitors of both w/o HPWVA and HPWVA (0.5 MPa) as a function of frequency. Temperature ranges are set at 100 °C and 200 °C. Increasing temperature leads to: increasing V_{FB} shift in the positive voltage direction and C-V curve stretch-out. These indicate that electron capture and emission associated to traps located close to the Al_2O_3/GaN interface increase and enhanced activity of electronic states at high temperature and are not negligible in the measured positive V_{FB} shift. The effect of HPWVA was maintained even in the high temperature range. From the results of TDS, desorption of H_2O began when the temperature exceeded 100 °C. Although deterioration of the electric characteristics was concerned at >100 °C, such influence was not seen in the C-V characteristic. There is a possibility of reoxidation in the Al_2O_3 film due to water desorption.

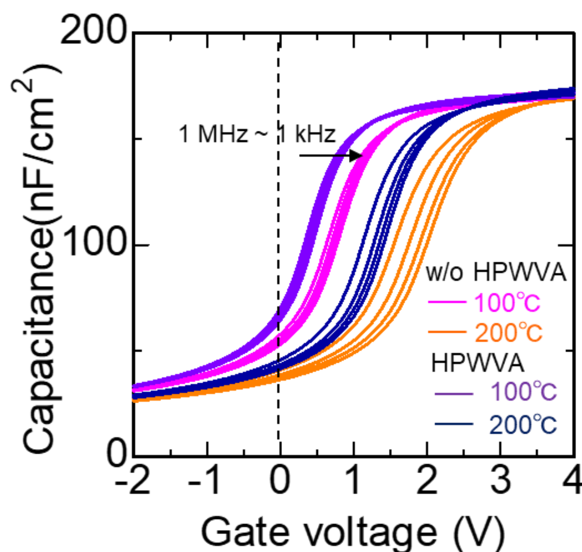

FIG. 2-38 Frequency dispersion of the C–V characteristics of ALD-Al_2O_3/GaN MOS capacitors. The measurement frequency ranged from 1 kHz to 1 MHz. Temperature condition is 100 °C and 200 °C.

Figure 2-39 show positive shift of C–V step-stress measured for ALD-Al_2O_3/GaN MOS capacitors with w/o HPWVA and HPWVA of 0.5 MPa at each temperatures. At high temperature such as 100 °C and 200 °C, V_{FB} shifted in the positive direction along the gate voltage without stretch out and positive C–V shifts of HPWVA showed smaller V_{FB} shift than that of the w/o HPWVA. More interestingly, temperature increase shifts the C–V curve towards more positive gate voltages. The origin of the temperature-induced Vth shift indicate the electron capture by the Al_2O_3/GaN interface traps or Al_2O_3 bulk traps [80]. As well as RT, the Vth shift was about 1/2 times even at 100 °C and 200 °C and HPWVA is also effective at high temperature.

The relationship between the electrical and the physical characteristics in the high temperature of 200 °C will be proposed. As the shown in TDS results of FIG. 2-25, it was confirmed that desorption of H_2O at 200 °C due to the hydrogen bonds bonded to Al-OH

in the film and on the surface. It is considered that H_2O is desorbed during the measurement of electrical properties, however this desorption does not affect the deterioration of the electrical characteristics. Therefore, it is suggested that the Al - OH bond derived from 300 °C to 500 °C is attributed to the modification of Al_2O_3 film and the electric characteristics at 200 °C were improved by HPWVA.

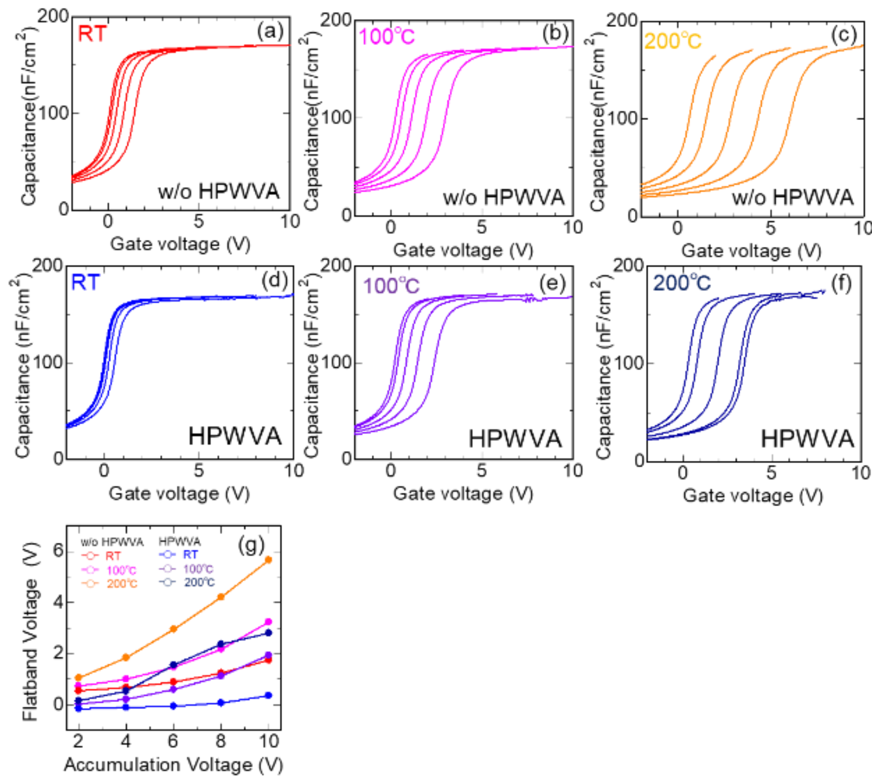

FIG. 2-39 Positive shift of C–V step-stress measured for ALD-Al_2O_3/GaN MOS capacitors with w/o HPWVA and HPWVA at temperature ranging of (a,d)RT, (b,e)100 °C and (c,f)200 °C. (g)Summary of V_{FB} shift plot per accumulation voltage.

2.10 Summary

In this chapter, HPWVA using high temperature and high pressure steam for Al_2O_3/GaN MOS capacitor was proposed. The effect of HPWVA on the Al_2O_3/GaN MOS structure was evaluated for electrical characteristics and physical characteristics. The

tendency of the electrical characteristics regarding the pressure dependence of HPWVA is reproducible. By processing HPWVA with 0.5 MPa, improvement of the E_{BD} of HPWVA samples was confirmed in TZDB and TDDB showed the lifetime of the HPWVA sample tends to increase compared with w/o HPWVA. From the C-V evaluation, reduction of N_F in Al_2O_3 film and reduction of the D_{it} in the HPWVA sample were observed.

However, at 1 MPa, the E_{BD} decreased compared with w/o HPWVA. N_f and D_{it} improved better than w/o HPWVA, however these decreased as compared with 0.5 MPa. In the physical evaluation, XPS showed that the Ga-O bonding at the interface increased, and the Ga-O bond tended to increase further than the pressure rise (~ 1.0 MPa). In the TDS and XPS evaluation, the Al-OH bond increased in the Al_2O_3 film. In SIMS, it was confirmed that oxygen and hydrogen in the water vapor were diffused. In addition, HPWVA at 400 °C and 0.5 MPa was shown to have the same diffusion coefficient as dry anneal at 700 °C, indicating that it has high oxidizing power.

From the above, the main points of physical characteristics and electrical characteristics was summarized. By HPWVA, the oxygen termination at the interface caused the effect of reducing D_{it} by reducing the discrete level related to nitrogen vacancy V_N. In addition, HPWVA promotes dangling bond termination of Al by -OH and reoxidation of Al_2O_3 film, which is considered to have the effect of reducing defects in the film. However, in the case of 1.0 MPa, the surface of Al_2O_3 was roughened and protrusions were confirmed. Therefore, it is considered that the E_{BD} decrease is attributed to the electric field concentration due to the protrusions formed on the GaN interface. In addition, D_{it} increased due to an increase in defects existing at the interface by interface roughness.

Furthermore, the electrical characteristics of HPWVA treated at higher pressure (2 MPa~) tended to deteriorate. In the case of 2 MPa, the Al_2O_3 surface roughly roughed and only the initial breakdown occurred in the J-E characteristic, and C - V curve was not observed. Furthermore, when exceeding 6 MPa, a crystal growth product of 1 μm size was confirmed through the Al_2O_3 film from the GaN interface. STEM revealed that this crystal growth product was derived from Ga oxide. Therefore, it is considered that crystal growth starts at 1 MPa or more and protrusions derived from Ga oxide formed at the initial stage grow with increasing pressure. This suggests that HPWVA is sensitive to pressure conditions. It is known that the density of water greatly changes due to slight fluctuation of pressure near the critical point, and it is conceivable that the oxidizing power of HPWVA changes greatly. Paradoxically, it means that hydrothermal reactions can be generated freely if control of both temperature and pressure is possible.

The operation at high temperature of 200 °C which is an essential in practical application was evaluated. It was possible to maintain reliability in HPWVA samples even at 200 °C. It is suggested that the Al - OH bond derived from 300 °C to 500 °C is attributed to the modification of Al_2O_3 film. However, it is confirmed that the leakage current greatly increases from the TZDB characteristic, and it is necessary to improve the characteristics under high temperature conditions in the future.

Finally, in this study, the HPWVA effect in Al_2O_3/GaN MOS capacitor was achieved. Some reports have shown that HPWVA improved the electrical characteristics of $HfSiO_2$/Si and CVD-SiO_2/ Si MOS structure, and also, in my group, it was confirmed that electrical characteristic of SiO_2/GaN MOS capacitor improved by HPWVA [14]. Therefore, it is suggested that HPWVA as PDA is effective for improvement of insulating films.

However, HPWVA is sensitive to control such as pressure, annealing time and temperature. Thus, the optimum condition for improving characteristics may vary greatly depending on the kind of MOS capacitor consisted of insulators and substrates. For example, it is confirmed the characteristics degradation of $HfSiO_2$/Si MOS capacitors with long time annealing (~3h) and HPWVA effect of $HfSiO_2$/Si MOS capacitors had an optimum annealing time to improve the film quality [14]. In this study, only the pressure dependence of HPWVA for Al2O3/GaN MOS capacitors is evaluated and it is necessary to evaluate the time dependence and the temperature dependence.

On the other hand, at more than 1.0 MPa, the GaN substrate began a surface roughness and the HPWVA condition may be limited to improve the electrical characteristic. However, it is possible to take advantage of this high oxidizing power for the formation technology of sacrificial oxide film as etching damage removal [81]. It was found that HPWVA controlling the condition can be expected to have a large effect of improving characteristics as PDA process in GaN MOS capacitor as well as with other process [82].

References

[1] T. Kachi, M. Kanechika and T. Uesugi, Proc. Compound Semicond. Integr. Circuit Symp., 2011, pp. 1-3.

[2] S. Chowdhury, Physica Status Solidi (a) **212**, 1066 (2015).

[3] T. Kachi, Jpn. J. of Appl. Phys. **53**, 10 (2014).

[4] R. Chu, A. Corrion, M. Chen, Li Ray, D. Wong, D. Zehnder, B. Hughes, and K. Boutros, IEEE Electron Device Lett. **32**, 632 (2011).

[5] Y. Hori, C. Mizue, and T. Hashizume, Jpn. J. Appl. Phys., **49**, 080201 (2010).

[6] X. Liu, R. Yeluri, J. Lu, and U. K. Mishra, J. of Electron. Mater. **42**, 33 (2012).

[7] C. M. Jackson, A. R. Arehart, E. Cinkilic, B. McSkimming, J. S. Speck, and S. A. Ringel, J. of Appl. Phys. **113**, 204505 (2013).

[8] S. Ozaki, T. Ohki, M. Kanamura, T. Imada, N. Nakamura, N. Okamoto, T. Miyajima and T. Kikkawa, CS-MANTECH Technical Digests, 311 (2012).

[9] K. Mitsuishi, K. Kimoto, Y. Irokawa, T. Suzuki, K. Yuge, T. Nabatame, S. Takashima, K. Ueno, M. Edo, K. Nakagawa, and Y. Koide, Jpn. J. Appl. Phys., **56**, 110312 (2017).

[10] T. Sameshima, M. Satoh, K. Sakamoto, K. Ozaki, and K. Saitoh, Jpn. J. Appl. Phys. **37,** 4254 (1998).

[11] M. Uenuma, K. Takahashi, S. Sonehara, Y. Tominaga, Y. Fujimoto, Y. Ishikawa, Y. Uraoka, AIP Adv. **8**, 105103 (2018)

[12] T. Sameshima and M. Satoh, Jpn. J. Appl. Phys. **36**, L687 (1997).

[13] T. Sameshima, K. Sakamoto and K. Asada, Appl. Phys. A, **69,** 221 (1999).

[14] P. Punchaipetch, M. Miyashita, Y. Uraoka, T. Fuyuki, T. Sameshima, and S. Horii, Jpn. J. Appl. Phys. **45**, L120 (2006).

[15] M. Fujii, Y. Ueoka, H. Yamazaki, M. Horita, Y. Ishikawa, and Y. Uraoka, The 8th Int.Thin-Film Transistor Conf., 2012.

[16] G. Ch. Lin, W. Lei, Z. Y. Rong, Z. H. Feng, L. Feng, Y. Z. Hui, Y. D. Ren, Chin. Phys. Lett. **31**, 108501 (2014).

[17] K. Yoshitsugu, T. Umehara, M. Horita, Y. Ishikawa, and Y. Uraoka, IEICE Tech. Rep., **113**, 7 (2013).

[18] H. M. Manasevit and W. I. Simpson, J. Electrochem. Soc., **116**, 1725 (1969).

[19] D. J. Schlyer and M. A. Ring, J. Organomet. Chem., **114**, 9 (1976).

[20] T. Katouda, Semiconductor epitaxy technology, pp. 2-5. (1982).

[21] S. M. George, Chem. Rev. **110**, 111 (2010).

[22] O. Sneh, R. C. Phelps, A. Londergan, J. Winkler, T. Seidel, Thin film atomic layer deposition equipment for semiconductor processing. Thin Solid Films. **402**, 248 (2002)

[23] I. Perez, E. Robertson, P. Banerjee, L. H. Lecordier, S. Son, S. Lee, G. Rubloff, Small, **4**, 1223, (2008)

[24] P. Banerjee, I. Perez, L. H. Lecordier, S. Lee, G. Rubloff, Nat Nanotechnol. **4**, 292, (2009)

[25] J. P. Mannaerts, M. Hong, K. K. Ng, and J. Bude, Appl. Phys. Lett., **83**, 180 (2003).

[26] Y. Hori, C. Mizue, and T. Hashizume, Phys. Stat. Sol. C, **9**, 1356 (2012).

[27] S. Huang, Q. Jiang, S. Yang, Z. Tang, and K. J. Chen, IEEE Elec. Dev. Lett., **34**, 2 (2013).

[28] H. Watakabe, and T. Sameshima, Jpn. J. Appl. Phys., **41**, L974 (2002).

[29] Y. Yano, D.Takeda, T. Hatayama, Y. Uraoka, T. Fuyuki, IEICE Tech. Rep., SDM2007 28 (2007).

[30] K. Mizuno, Physical properties and utilization of supercritical water, Zairyo-to-Kankyo, **47**, 298 (1998).

[31] A. N. Hattori, F. Kawamura, M. Yoshimura, Y. Kitaoka, Y. Mori, K. Hattori, H. Daimon, K. Endo, Surface Science, 604, 1247 (2010)

[32] A. N. Hattori, K. Endo, K. Hattori, H. Daimon, Appl. Surf. Sci., 256, 14 (2010)

[33] A. N. Hattori, T. Okamoto, S. Sadakuni, J. Murata, K. Arima, Y. Sano, K. Hattori, H. Daimon, K. Endo, K. Yamauchi, Surf. Sci., 605, 597 (2011)

[34] Y. Ogawa and Y. Horiike, Hajimete no handotai senjo gijutsu, Kogyo chosa-kai, (2002)

[35] T. Kawamura, A. Kitamoto, M. Imade, M. Yoshimura, Y. Mori, Y. Morikawa, Y. Kangawa, K. Kakimoto, and T. Akiyama, Jpn. J. Appl. Phys. **57**, 115504 (2018)

[36] S. M. Sze, Physics of Semiconductor Devices, Wiley, New York, (1981).

[37] E. H. Nicollian and J. R. Brews, MOS Physics and Technology, Wiley, New York (1982).

[38] L. M. Terman, Solid State Electron. 5, 285 (1962).

[39] T. Hashizume, S. Ootomo, T. Inagaki, and H. Hasegawa, J. Vac. Sci. Technol. B, **21**, 1828 (2003).

[40] C. T. Sah, A. B. Tole, and R. F. Pierret, Solid State Electron. **12**, 689 (1969).

[41] M. Miczek, C. Mizue, T. Hashizume, and B. Adamowicz, J. Appl. Phys. **103**, 104510 (2008).

[42] D K. Schroder, Semiconductor Material and Device Characterization Third Edition, pp.319-352 2006.

[43] S.M. Sze, Kwok. K. NG, Physics of Semiconductor Device, Willy, pp 135 (2006)

[44] M. Choi, A. Janotti, and C. G. Van de Walle, Journal of Applied Physics, **113**, 044501

(2013)

[45] J. Neugebauer and C. G. Van de Walle, Phys. Rev. B **50**, 8067 (1994).

[46] M. L. Huang, Y. C. Chang, Y. H. Chang, T. D. Lin, J. Kwo, and M. Hong, Appl. Phys. Lett. **94,** 052106 (2009).

[47] Japan Surface Science Association, X-ray photoelectron spectroscopy, Maruzen, (1998).

[48] N. Hirashita, T. Ajioka, Y. Hinaga SCAS technical news, **34**, 813 (1991).

[49] W. Shockley and T. Read, Phys. Rev **87,** 835 (1952)

[50] D. Bisi, S. H. Chan, M. Tahhan, O. S. Koksaldi, S. Keller, M. Meneghini, G. Meneghesso, E. Zanoni, U. K. Mishra, Proc. Int. Symp. Power Semiconductor Devices ICs, pp. 119-122. (2016).

[51] K. Watanabe, D. Terashima, M Nozaki, T. Yamada, S. Nakazawa, M. Ishida, Y. Anda, T Ueda, A. Yoshigoe, T. Hosoi1, T. Shimura, and H. Watanabe, Jpn. J. Appl. Phys., **57**, 06KA03 (2018).

[52] H. Hasegawa, and T. Sawada, J. Vac. Sci. Technol., **16**, 1478 (1979).

[53] A. Hiraiwa, T. Sasaki, S. Okubo, K. Horikawa, and H. Kawarada, J. Appl. Phys. **123**, 155303 (2018).

[54] T. Hashizume, and R. Nakasaki, Appl. Phys. Lett., **80**, 24 (2002).

[55] T. Hashizume, and H. Hasegawa, Appl. Sur. Sci., **234**, 387 (2004).

[56] N. X. Truyen, N. Taoka, A. Ohta, K. Makihara, H. Yamada, T. Takahashi, M. Ikeda, M. Shimizu, and S. Miyazaki, Jpn. J. Appl. Phys. **57**, 04FG11 (2018).

[57] A. Hiraiwa, T. Sasaki, S. Okubo, K. Horikawa, and H. Kawarada, J. of Appl. Phys. **123**, 155303 (2018).

[58] E. Yamaguchi, and M. R. Junnarkar, J. Crystal Growth, **190**, 570 (1998).

[59] K. Shimizu, C. Phanopoulos, R. Loenders, M.L. Abela and J. F.Wattsa, Surf. Interface Anal., **42,** 1432 (2010)

[60] R.A. Andreeva, E.A. Stoyanova, A.S.Tsanev, D.S. Stoychev, Bulgarian Chemical Communications, **48,** 96 (2016)

[61] A. V. Naumkin, A. K. Vass, S. W. Gaarenstroom, and C. J. Powell, NIST X-ray Photoelectron Spectroscopy Database 20, Version 4.1 (2012)

[62] T. L. Duan, J. S. Pan, and D. S. Ang, Appl. Phys. Lett. **102**, 201604 (2013).

[63] A. Abidli, S. Hamoudiab and K. Belkacemi, J. Chem. Soc. Dalton. Trans. 44, 9823 (2015)

[64] K. Kulyk, B. Palianytsia, J. D. Alexander, L. Azizova, M. Borysenko, M. Kartel, M. Larsson, and T. Kulik, Chemphyschem **18**, 1943 (2017).

[65] N. Hirashita, S. Tokitoh and H. Uchida, Jpn. J. Appl. Phys., **32**, 1787 (1993).

[66] T. Nabatame, T. Yasuda, M. Nishizawa, M. Ikeda, T. Horikawa, and A. Toriumi, Jpn. J. Appl. Phys., **42**, 7205 (2003).

[67] K. E. Lapham, J. R. Holloway, J. R. Delaney, J. non-cryst. Solids **67**, 179 (1984).

[68] R. L. Murray : nuclear engineering Maruzen pp70-71, (1955)

[69] B. Visweswaran, P. Mandlik, S. H. Mohan, J. A. Silvernail, R. Ma, J. C. Sturm, and S. Wagner, J. of Vac. Sci. & Technol. A: Vac. Surf. and Films **33**, 031513 (2015).

[70] N. Ramanan, B. Lee, C. Kirkpatrick, R. Suri, and V. Misra, Semicond. Sci. and Tech. **28**, 074004 (2013).

[71] S. J. Wilkins, T. Paskova, and A. Ivanisevic, Appl. Surf. Sci. **327**, 498 (2015).

[72] T. Yamada, J. Ito, R. Asahara, K. Watanabe, M. Nozaki, T. Hosoi, T. Shimura, and H. Watanabe, Appl. Phys. Lett. 110, 261603 (2017)

[73] T. Yamada, K. Watanabe1, M. Nozaki, H. Yamada, T. Takahashi, M. Shimizu, A.

Yoshigoe, T. Hosoi, T. Shimura, and H. Watanabe, Appl. Phys. Express 11, 015701 (2018)

[74] D. Das and P. Mondal, RSC Advances **6**, 6144 (2016).

[75] V. V. Afanas'ev, A. Stesmans, B. J. Mrstik, and C. Zhao, Appl. Phys. Lett. 81, 1678 (2002)

[76] K. Mitsuishi, K. Kimoto, Y. Irokawa, T. Suzuki, K. Yuge, T. Nabatame, S. Takashima, K. Ueno, M. Edo, K. Nakagawa, and Y. Koide, Jpn. J. Appl. Phys., **56**, 110312 (2017).

[77] T. Hashizume, and R. Nakasaki, Appl. Phys. Lett., 80, 24 (2002).

[78] M. Reddy, P. Puneerha, V. Reddy, J. H. Lee, S. H. Jeong, and C. Park, J. Elect. Mat., **45**, 11, (2016).

[79] D. Kikuta, T. Narita, K. Kutsuki, T. Uesugi and T. Kachi, Jpn. J. Appl. Phys., **52**, 08JN19 (2013).

[80] M Tapajna, K Čico, J Kuzmik, D Pogany, G Pozzovivo, G Strasser, J-F Carlin, N Grandjean and K Frohlich, Semi. Sci. and Tech., **24**, 3, (2009)

[81] M. Kodama, M. Sugimoto, E. Hayashi, N. Soejima, O. Ishiguro, M. Kanechika, K. Itoh, H. Ueda, T. Uesugi and T. Kachi, Appl. Phys. Express, **1**, 2 (2008)

[82] S Kaneki, J. Ohira, S. Toiya, Z. Yatabe, Joel T. Asubar, and T. Hashizume, Appl. Phys. Lett. **109**, 162104 (2016).

Chapter 3

Investigation of Atomic Structure in Al_2O_3/GaN interface

3.1 Introduction

The control of MOS interfaces remains one of the key issues. As described in Chapter 2, HPWVA for MOS interface control and succeeded in improving the Al_2O_3 film quality and the quality of the Al_2O_3/GaN interface was suggested.

However, the atomic structure at the interface of Al_2O_3/GaN is not yet well understood in detail. Therefore, it is necessary to clarify the interfacial structure at the interface of Al_2O_3/GaN for a better understanding and improvement of the device performance of GaN MOSFETs.

As a detail investigation of the Al_2O_3/GaN interface, photoelectron diffraction was used. The photoelectron diffraction is a powerful element-selective and non-destructive technique for the analysis of atomic structure, surface, and interface structure [1-3]. By utilizing the photoelectron diffraction phenomenon, it is possible to obtain element-specific X-ray photoelectron spectroscopy by analyzing the photoelectron intensity angular distribution (PIAD) that can provide direct access to the local atomic structure of selected elemental atom sites and their neighboring atoms [4-6]. Until recently, in the research on SiC, which is a promising power semiconductor like GaN, the atomic structure analyses of interfaces of insulator/SiC have been extensively reported and analyzed in detail [2, 4, 7, 8]. In particular, D. Mori recently reported the important interface information on the N local atomic arrangement at the amorphous

SiO_2/SiC(000-1) interface for improving the performance of SiC MOSFETs [9]. On the other hand, the detailed structure between insulator and GaN is still unclear and the study on insulator/GaN interface also needs to be promoted. Therefore, this atomic site-specific photoelectron diffraction patterns using a circularly polarized soft X-ray beam line of SPring-8 was applied to analyze and clarify the interface structures of the Al_2O_3/GaN interface.

3.2 Two-dimensional photoelectron spectroscopy

Figure 3-1 (a) shows the schematic diagram of photoelectron diffraction. Photo electronic waves generated from atoms are scattered by surrounding atoms to emit scattered waves. The phenomenon wherein the scattered wave and the photoelectron wave overlap makes the photoelectron diffraction. The atom from which the photoelectron wave is derived by X-ray irradiation is the "emitted atom", the derivative photoelectron wave is called the "direct wave", and the wave generated by scattered atom is called the "scattered wave". Forward focusing peaks (FFP) are formed in regions where the intensity of photoelectrons is strong in the direction of scattered atoms observed from emitted atoms. From the polar angle at which the FFP appears and its symmetry, the atomic arrangement around a specific atom can be observed and the interatomic distance can be evaluated from the diffraction ring [10].

Photoelectron-diffraction measurements were carried out using a circularly polarized soft X-ray beam line at BL25SU of SPring-8, Japan [11]. PIAD is most efficiently measured using two-dimensional photoelectron spectrometer Display-type Spherical Mirror Analyzer (DIANA), which enables the acquisition of a two-dimensional angular distribution snapshot of a specific kinetic energy electron.

Beam Line BL25SU uses a synchrotron light source. Because the energy of synchrotron light is white light having continuity, it is possible to extract only X-rays of specific energy using a spectroscope. Therefore, it is possible to arbitrarily change the incident energy, acquire high-quality data with good SN in a short time, control the kinetic energy and the depth of detection of the photoelectrons excited, and perform detailed analysis.

As shown in FIG. 3-1 (b), DIANA has two concentric hemispherical electrodes as main components [12]. The photoelectron passing through the electrode mesh of the inner hemisphere is bent by the electric field generated in the inner hemisphere electrode and the outer hemisphere electrode. At this time, those above the photoelectric kinetic energy to be detected are blocked by the outer sphere (obstacle ring), and those below the pass energy are removed by the blocking potential grid of the outlet (aperture). Therefore, only photoelectrons with some energy converge on the aperture. By observing the angular distribution of photoelectrons coming out through the aperture on the screen, it is possible to obtain the PIAD of the sample.

In this evaluation, the sample at an azimuth angle of 360 ° was scanned and collected PIAD data [13-16]. The sample was introduced into the ultra-high vacuum chamber, and no further sample surface treatment was carried out. All experiments were carried out at room temperature. The PIAD by 360° rotation in 9° step size was obtained. The PIADs of right and left circularly polarized light are integrated. PIADs of Ga3p, Al2p were obtained with photoelectric kinetic energy of 800 eV and N1s was obtained with a photoelectric kinetic energy of 540 eV and displayed in stereographic projection.

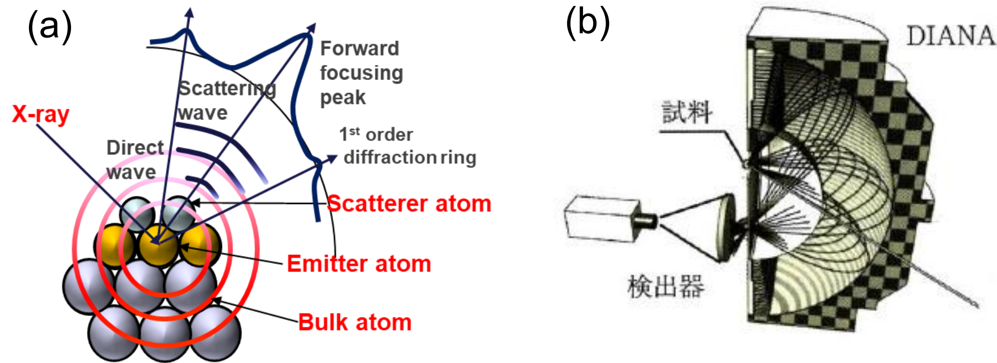

FIG. 3.1. (a) Schematic diagram of photoelectron diffraction. The atom from which the photoelectron wave is derived by X-ray irradiation is the emitted atom, the derivative photoelectron wave is called the direct wave, and the wave generated by scattered atom is called the scattered wave. (b) Diagram of the DIANA used in this work. The angular distribution of photoelectrons from the sample is projected on the screen without distortion [17].

3.3 Device fabrication

Homoepitaxial layer (2 μm, Si :5 × 10^{16} cm^{-3}) on c-plane free-standing GaN substrates with surface tilted toward m-axis [1-100] direction by 0.4 °off was utilized. After the standard RCA cleaning process, Al_2O_3 film with a nominal thickness of 20 nm was deposited on the n^+-GaN(0001) surfaces by T-ALD. The Al_2O_3 film was deposited at 300°C by repeating TMA supply as aluminum precursor and O_2 supply. The deposition rate of the Al_2O_3 film was 0.91 Å/cycle. The sample was then subjected to HPWVA under a constant pressure of 0.5 MPa and to annealing temperatures of 400 °C for 30 min. The sample was dipped slowly (dipping rate : 9 sec/mm) into diluted HF (0.1 mMol/L) and wedged Al_2O_3 layers were formed by etching. The wedged structure enabled us to analyze Al_2O_3/GaN interface. The purpose of the inclined etching is to measure under the conditions for device application wherein insulator film thickness of Al_2O_3 is deposited at least 20 nm. For the measurement point, the point where the Al_2O_3 film thickness corresponds to about 1.2 nm was specified by scanning the intensity of Ga3p toward the

etching direction.

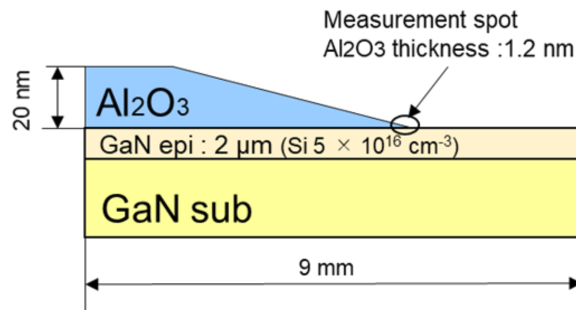

FIG. 3-2. Cross section of inclined Al_2O_3/GaN sample. The measurement point which Al2O3 thickness is 1.2nm is a part where the intensity of Ga3p is halved.

3.4 Investigation of atomic structure in Al_2O_3/GaN interface

3.4.1 Scanning transmission electron microscopy (STEM)

To focus on interface phase morphology determination by electron microscopy methods, structural characterization was performed by using annular bright-field scanning transmission electron microscopy (ABF-STEM) by using the JEM-ARM200CF (Kyusyu Uni. Nano. Tech. platform) operated at 200 keV .

Figure 3-3 shows the cross sectional image of the interfaces of Al_2O_3 (2 nm)/GaN substrate observed by ABF-STEM. Amorphous Al_2O_3 layer and GaN (0001) substrate can be confirmed. The samples with the cross-section cut out in the (01-10) direction and could not confirm the offset step was observed. However, these images indicate that relatively steep interfaces are formed, although 2, 3 layers of GaN. Mitsuishi et al. reported that there is a layer of crystalline gallium oxide (Ga_2O_3) having epitaxial relation with very thin GaN of about 1.5 nm in SiO_2/GaN [18, 19]. Plasma damage is caused when CVD SiO_2 is deposited on GaN substrate. Therefore, in the case of the Al_2O_3/GaN interface, the excessive damaged layer of Al_2O_3/GaN interface after Al_2O_3 deposition by thermal ALD was not found and a sharp and distinct interface was formed.

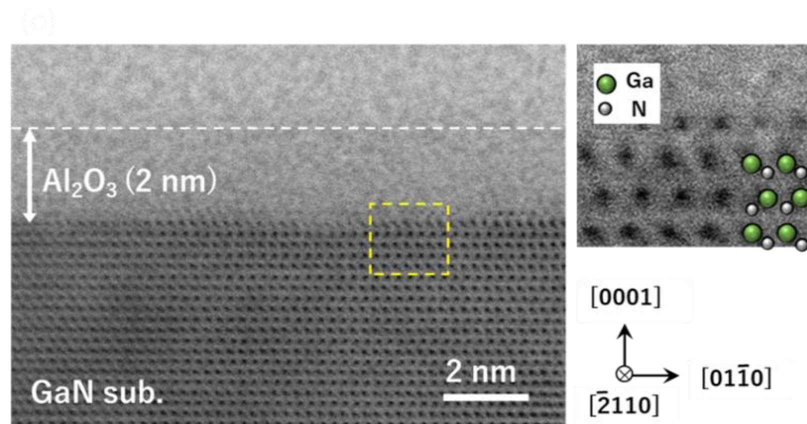

FIG. 3-3. The cross section image of ABF-STEM observed interfaces with Al_2O_3/GaN (0001) substrate. The pattern on the GaN substrate corresponds to Ga atom and nitrogen atom. The ALD-Al_2O_3 film is amorphous.

3.4.2 Photoelectron Diffraction Pattern (PIAD)

To analyze the atomic structure of Al_2O_3/GaN interface in detail, two-dimensional photoelectron-diffraction measurements was carried out. Figure 3-4 showed the PIADs of Ga3p and N1s from c–plane GaN surface of GaN substrate, respectively. The PIADs of Ga3p and N1s is six-fold symmetry. As shown in FIG 3-5, GaN has a pair of local atom sites of mirror image of Ga atoms and N atoms against (1-100) planes. The obtained PIADs is superimposed with information of Ga atoms and N atoms present at each layer, wherein both layer 1 (Ga 1 and N 1) and layer 3 (Ga 3 and N 3) are same, and both layer 2 (Ga 2 and N 2) and layer 4 (Ga 4 and N 4) are same.

Figures 3-6 and 3-7 show the atomic arrangement and direction of atoms around Ga atoms and N atoms at each layer. The FFP caused by the direction of the second closest Ga atom indicated by the red circle in the Ga3p PIAD is six-fold symmetric. Similarly, FFP indicated by a blue triangle in the PIAD of N1s is the direction of the second neighboring N atom viewed from the N atom and the red triangle indicate the direction of the Ga atom closest to the first. Superimposition of FFP is six-fold symmetric by

superimposing three-fold symmetric PIAD which is a mirror image in relation to (1-100) plane. In addition, as shown in FIG 3-6, FFP in the Ga3p PIAD is attributed to the third neighboring N atom and FFP forms a six-fold symmetric PIAD at the same position. Therefore, the PIADs of Ga3p and N1s at have six-fold symmetry PIADs. It is concluded that the PIADs of Ga3p and N1s PIADs reflect the GaN crystal structure.

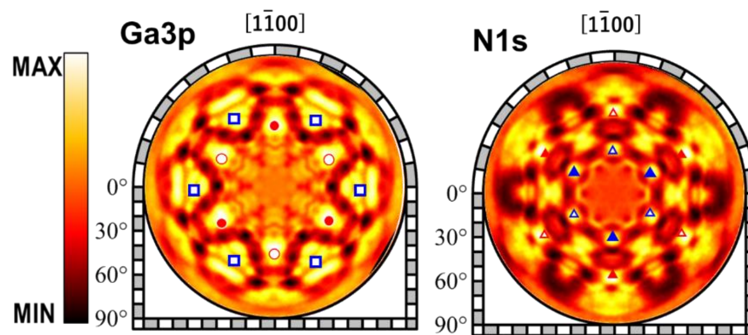

FIG. 3-4. PIADs of Ga3p and N1s from c–plane GaN surface. The marks indicate the position of FFP (direction of adjacent atoms). The structure diagram of each adjacent atom is shown in FIG. 3-5 and FIG. 3-6.

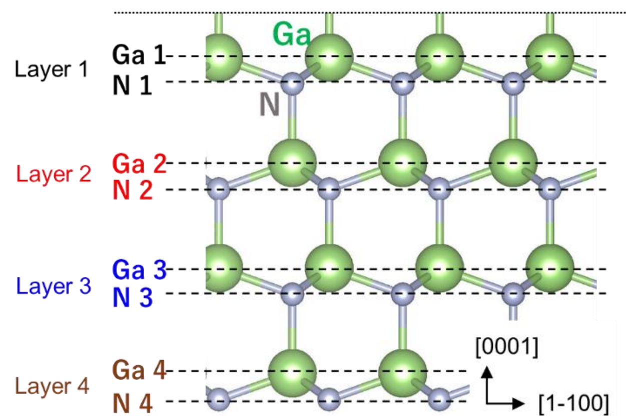

FIG. 3-5. Crystal structure of GaN observed from [1-100] direction. The Ga atom and N atom at Layer 1 - 4 are shown.

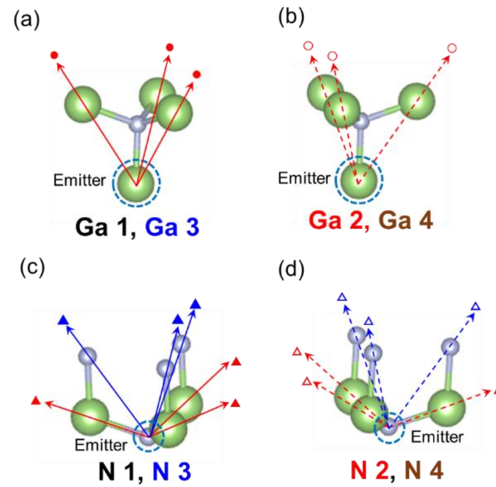

FIG. 3-6. The atomic arrangement around the photoelectron emitting atom (Emitter) and the direction of the surrounding atoms as observed from the emitter

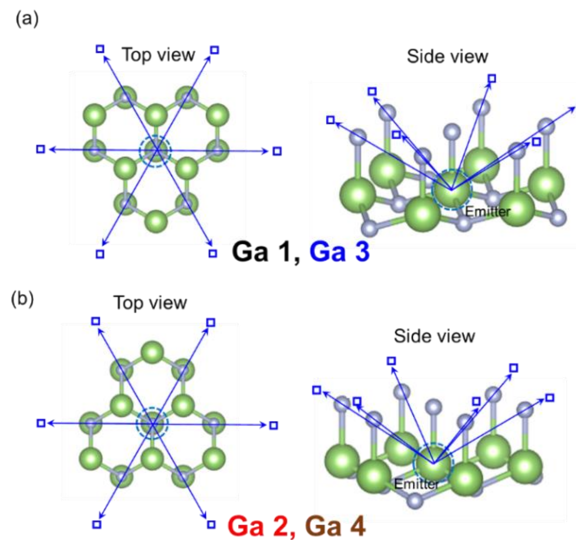

FIG. 3-7. The atomic arrangement around the photoelectron emitting atom (Emitter) and the direction of the surrounding atoms as observed from the emitter

As shown in FIG 3-8, these results indicate that Ga3p and N1s PIADs with and without HPWVA have the PIADs derived the GaN bulk crystals. Both PIADs show no difference. As shown FIG.3-4, PIADs of Ga3p and N1s become a six-fold symmetry with three-fold symmetry PIADs superimposed.

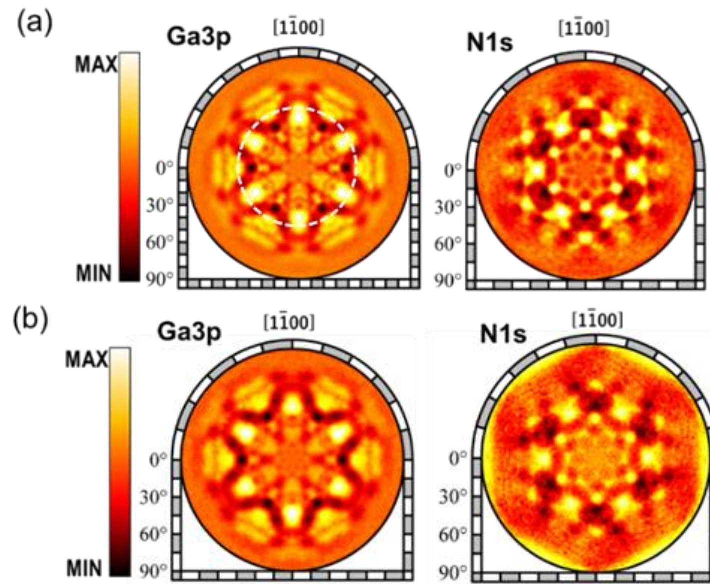

FIG. 3-8. PIADs of Ga3p and N1s of Al_2O_3/GaN interface from c–plane GaN surface of (a) HPWVA and (b) w/o HPWVA

Figure 3-9 (a) and (b) shows the Al2p PIADs of Al_2O_3/GaN interface with and without HPWVA. FIG 3-9 (c) shows the line scan profile of Al2p and Ga3p for the white dashed lines in FIG. 3-8 (a) and FIG. 3-9 (a). These results show that the tendency which Al2p PIAD has a three-fold symmetry for FFPs at a polar angle of 120° is strong. The PIADs of both with and without HPWVA show no difference. The trend shows similar results with the PIAD of Ga3p. The Al_2O_3 film deposited by T-ALD is typically amorphous as also shown in the STEM image and no PIADs should be observed (PIAD of O1s was not observed). The PIADs indicated by the black circles, as well as open circles, correspond to adjacent Ga or Al atoms which is second closest to the Al emitter atoms, (FIG. 3-10).

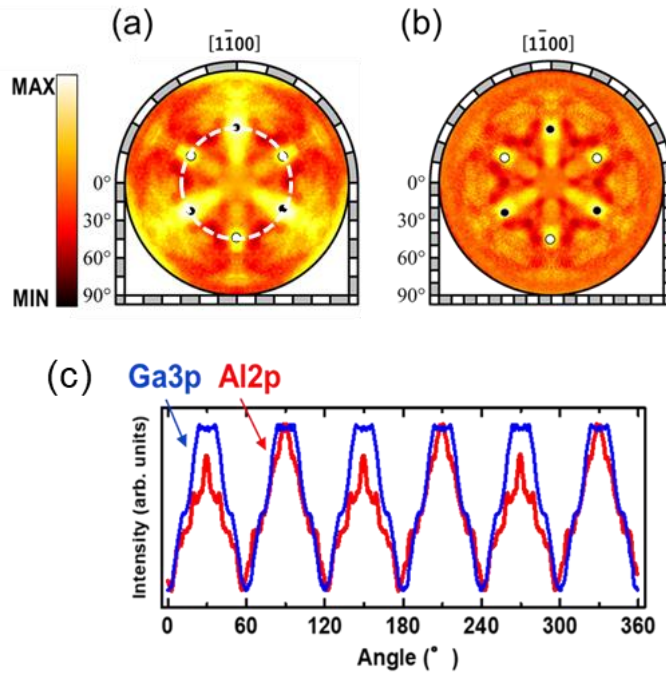

FIG. 3-9. Al2p PIADs of Al_2O_3/GaN interface (a) with HPWVA and (b) w/o HPWVA (c) the line scan profile of Al2p and Ga3p for the white dashed lines in FIG. 3-8 (a) and FIG. 3-9 (a).

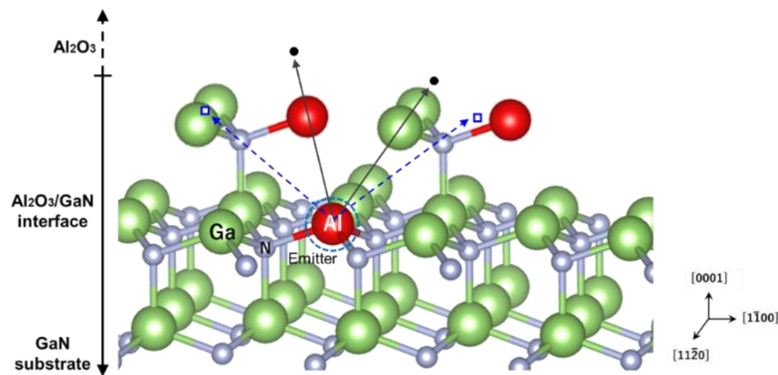

FIG. 3-10. The schematic model of Al_2O_3/GaN interface. The FFPs from Al emitter correspond to adjacent Ga or Al atoms indicated by the black circles.

3.5 Discussion on interfacial atomic structure model

The similarity of PIADs between Ga3p and Al2p shows that Al atoms are located in the Ga site of the GaN crystal structure in the vicinity of the uppermost surface. Therefore, it shows that an extremely thin Al_2O_3/GaN multiphase layer was formed at the Al_2O_3/GaN interface. FIG. 3-11 shows a model where Al penetrated or replaced at the Al_2O_3/GaN interface. The PIAD from the Al emitter that are in the first layer on the outermost surface has only information of atom located on the same layer and pattern can not be obtained. In the second and subsequent layers, as shown in FIG. 3-5, the three-fold symmetry is reversed for each layer and can be obtained alternately. The PIAD of Al2p shows stronger three-fold symmetry matching to Ga 1 and 3 (Layers 1 and 3) than PIADs of Ga 2 and 4 (Layers 2 and 4). Therefore, the PIAD of Al2p which is three-fold symmetry and is dominant means that Al atoms are up to the third layer, but many Al atoms are up to the second layer. Because the PIAD of Al2p was confirmed regardless of the presence or absence of HPWVA, it is considered that Al was formed during ALD process.

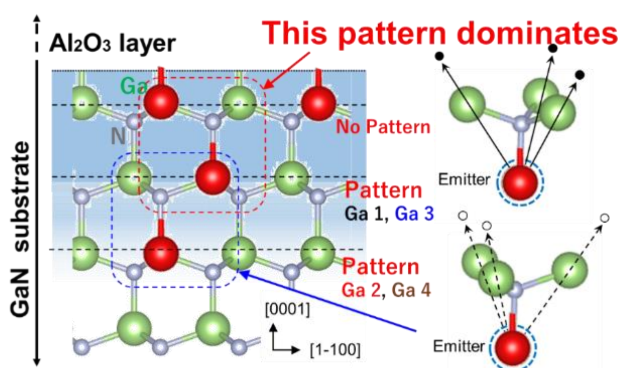

FIG. 3-11. Relationship between PIAD from Al emitter in Ga site and element model. In the PIAD of Al2p (FIG. 3-9), the black circle is linked with the PIADs of Ga 1 and 3 (FIG. 3-8). On the other hand, open circles are linked with PIADs of Ga 2 and 4. A PIAD can not be obtained from the outermost Al emitter at Al_2O_3/GaN interface.

Furthermore, because an off angle of 0.4° is actually formed on the GaN substrate, a model considering this GaN step surface will be considered. As shown in FIG. 3-12, the GaN substrate has a step formed in the m-axis [1-100] direction. From the results of AFM, it was confirmed that the step height was mainly 0.5 nm, forming a step in which the Ga atomic layer fell down by two steps. Three-fold symmetry (the same PIAD as Ga 1 and Ga 3) derived from Al atoms of the second layer from the outermost surface of GaN has no relation with the presence or absence of a step. However, in the third layer from the outermost surface, it is considered that Al easily was replaced with the Ga site at the boundary of the step surface, and the opposite three-fold symmetry (the same PIAD as Ga 2 and Ga 4) is confirmed. These Al atoms are supposed to compensate for Ga defects in the GaN crystal, which may contribute to reduction of Dit, however further investigation is necessary.

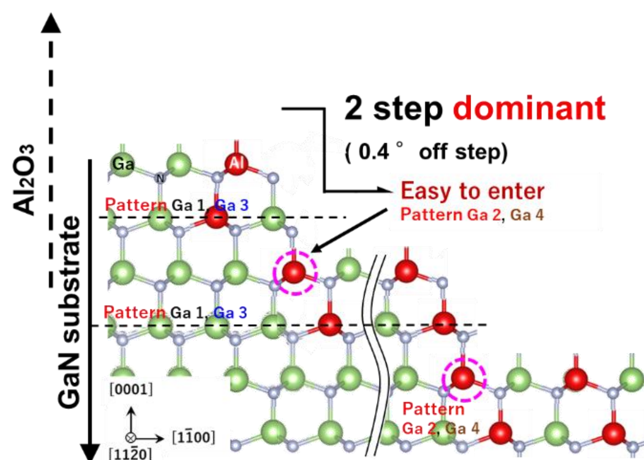

FIG. 3-12. Schematic model of the transition layer in consideration of the GaN step face (off angle 0.4°) at the Al_2O_3/GaN interface.

Figures 3-13 shows the schematic model of GaN substrate, MOS interface after deposition of Al_2O_3 film and MOS interface after HPWVA. When an ALD-Al_2O_3 film is

deposited on a GaN substrate with vacancies, Al predominantly penetrates into the second layer of the Ga vacancy site. After HPWVA, a thin oxide layer was formed on the interface between GaN and Al_2O_3, but it did not reflect on the PIAD patterns.

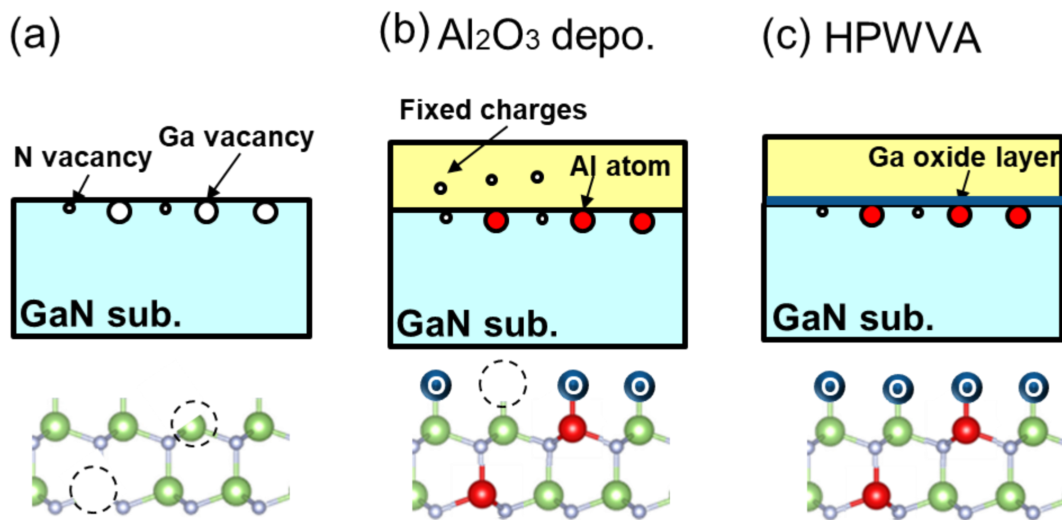

FIG. 3-13. Schematic model of (a) GaN substrate, (b) MOS interface after deposition of Al_2O_3 film and (c) MOS interface after HPWVA.

3.6 Summary

The atomic structure at the Al_2O_3/GaN interface was investigated. ABF-STEM, and PIAD that can provide direct access to the local atomic structure of selected elemental atom sites and their neighboring atoms were carried out. PIAD from the sample was carried out using Two-dimensional photoelectron spectrometer, Display-type Spherical Mirror Analyzer (DIANA) at BL25SU of SPring-8, Japan. The cross section image of the interfaces of Al_2O_3 (2 nm)/GaN substrate was observed by ABF-STEM. Amorphous Al_2O_3 layer and GaN (0001) substrate can be confirmed. These images indicate that an excessively damaged layer of Al_2O_3/GaN interface after Al_2O_3 deposition was not found.

The PIAD of Ga3p and N1s by identifying the part where the Al_2O_3 thickness is

1.2 nm was measured. PIADs of Ga3p and N1s were confirmed and these PIADs showed that Ga3p and N1s incident PIAD derived the GaN bulk crystals. The PIADs of both with and without HPWVA show no difference. Specifically, PIAD of Al2p is similar to the Ga3p PIAD. Although the Al_2O_3 film deposited by ALD should has no PIAD as it has an amorphous structure, this showed that Al atoms fixed in Ga atomic sites in the vicinity of the uppermost surface of GaN substrate during the ALD deposition. Therefore, it shows that an extremely thin Al_2O_3/GaN multiphase layer was formed at the Al_2O_3/GaN interface.

Furthermore, when a model with GaN step surface will be considered, Al easily replaces the Ga site at the boundary of the step surface. The Al_2O_3/GaN multiphase layer may contribute to the reduction of the D_{it}.

References

[1] N. Maejima, M. Horita, H. Matsui, T. Matsushita, H. Daimon, and F. Matsui, Jpn. J. Appl. Phys. **55**, 085701 (2016).

[2] N. Maejima, F. Matsui, H. Matsui, K. Goto, T. Matsushita, S. Tanaka, and H. Daimon, J. Phys. Soc. Jpn. **83**, 044604 (2014).

[3] F. Matsui, T. Matsushita, M. Hashimoto, K. Goto, N. Maejima, H. Matsui , Y. Kato, and H. Daimon, J. Phys. Soc. Jpn. **81,** 013601 (2012).

[4] F. Matsui, N. Nishikayama N. Maejima, H. Matsui, K. Goto, M. Hashimoto, T. Hatayama, T. Matsushita, Y. Kato, S. Tanaka, and H. Daimon, J. Phys. Soc. Jpn. **80**, 013601 (2011).

[5] S. Takahashi, S. Kono, H. Sakurai, T. Sagawa, J. Phys. Soc. Jpn., **51**, 3296 (1982).

[6] J. Osterwalder, T. Greber, E. Wetli, J. Wider, H.J. Neff, Prog. Surf. Sci. **64**, 65 (2000).

[7] M. Schürmann, S. Dreiner, U. Berges, and C. Westphal, Phys. Rev. B **74**, 035309 (2006).

[8] F. Varchon, R. Feng, J. Hass, X. Li, B. Ngoc Nguyen, C. Naud, P. Mallet, J.-Y. Veuillen, C. Berger, E. H. Conrad, and L. Magaud, Phys. Rev. Lett., **99**, 126805 (2007).

[9] D. Mori, Y. Oyama, T. Hirose, T. Muro, and F. Matsui, Appl. Phys. Lett. **111**, 201603 (2017).

[10] M. Muntwiler, J. Zhang, R. Stania, F. Matsui, P. Oberta, U. Flechsig, L.Patthey, C. Quitmann, T. Glatzel, R. Widmer, E. Meyer, T. A. Jung, P. Aebi, R. Fasel and T. Greber, J. Synchrotron Rad., **24**, 354, (2017).

[11] Y. Saitoh, H. Kimura, Y. Suzuki, T. Nakatani, T. Matsushita, T. Muro, T. Miyahara, M. Fujisawa, K. Soda, S. Ueda, H. Harada, M. Kotsugi, A. Sekiyama, and S. Suga,

Review of Scientific Instruments **71**, 3254 (2000).

[12] H. Daimo and Y. Sasaki, Kinoukouzou kagaku-nyumon, Maruzen, (2016).

[13] S. Fukami, M. Taguchi, Y. Adachi, I. Sakaguchi, K. Watanabe, T. Kinoshita, T. Muro, T. Matsushita, F. Matsui, H. Daimon, and T. Suzuki, Phys. Rev. **7**, 064029 (2017)

[14] H. Matsui, F. Matsui, N. Maejima, T. Matsushita, T. Okamoto, A. N. Hattori, Y. Sano, K. Yamauchi, H. Daimon, Surf. Sci. **632**, 98 (2015)

[15] H. Daimon, T. Nakatani, S. Imada, S. Suga, Y. Kagoshima, and T. Miyahara, Review of Scientific Instruments **66**, 1510 (1995).

[16] H. Daimon, Rev.Sci.Instrum, **59,** 4 (1988).

[17] H. Daimo and Y. Sasaki, Kinoukouzou kagaku-nyumon, Maruzen, (2016).

[18] S. Arulkumaran, T. Egawa, H. Ishikawa, T. Jimbo, and M. Umeno, Appl. Phys. Lett. **73**, 809 (1998).

[19] K. Mitsuishi, K. Kimoto, Y. Irokawa, T. Suzuki, K. Yuge, T. Nabatame, S. Takashima, K. Ueno, M. Edo, K. Nakagawa, and Y. Koide, Jpn. J. Appl. Phys.**56**, 110312 (2017).

[20] P. L. J. Gunter, A. M. de Jong and J. W. Niemantsverdriet, Surf. and Interface Anal., **19**, 161 (1992).

Chapter 4 Effect of ALD precursor on Al_2O_3/GaN MOS capacitors

4.1 Introduction

ALD-Al_2O_3 films are expected as gate insulator materials in GaN-based electronic devices. TMA having high volatility and thermal stability is widely used as an Al raw material for ALD-Al_2O_3 and the process has been established. However, because TMA is bound to three methyl groups, carbon impurities tend to remain in the ALD cycle and monomolecular adsorption is difficult due to large steric hindrance. As a result, carbon impurities and oxygen defect which are sources of fixed charges and trap remain in the Al_2O_3 film.

In this study, dimethyl aluminum hydride (DMAH : C_2H_7Al) in which one of the methyl groups is bonded to hydrogen compound to replace TMA was used and tried to form an ALD-Al_2O_3 film with DMAH and evaluate electrical characteristics. In addition, HPWVA described in Chapter 2 was applied to ALD-Al_2O_3 with DMAH/GaN MOS capacitors and the influence on the characteristics of ALD-Al_2O_3/GaN MOS capacitors was evaluated.

4.2 DMAH Precursor for ALD-Al_2O_3

ALD is capable of forming pinhole-free oxide with precise thickness control by simple layer-by-layer deposition mechanism and proved to be effective in various oxide film deposition techniques such as Al_2O_3, ZnO_2 [1]. Usually, the ALD process of Al_2O_3 includes TMA and an oxidant. TMA is widely used in Al_2O_3 gate insulators and

passivation layers [2-4]. As shown FIG. 4-1, new metalorganic precursor, DMAH in which one of the methyl groups is bonded to hydrogen compound to replace TMA was used for Al_2O_3/GaN MOS capacitors.

The success of ALD process depends critically on the availability of volatile, thermally stable precursors that exhibit high and constant vapor pressures, because poor performance affects the film characteristics [5, 6]. compared with TMA precursors, new DMAH chemistry has a high vapor pressure of 2 Torr at room temperature and a potential to form Al_2O_3 films with low carbon impurity owing to the following disproportionation reaction [7],

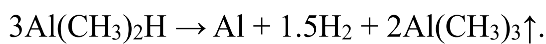

$$3Al(CH_3)_2H \rightarrow Al + 1.5H_2 + 2Al(CH_3)_3\uparrow.$$

Usually, carbon residue incorporated in ALD derived films can deteriorate film electrical characteristics. CVD of aluminum with DMAH has been extensively studied for integrated circuits because of its potential to form aluminum films with low carbon impurity and excellent gap-filling characteristics [8-10]. DMAH have been used for the first time as the source for photo-CVD of aluminum at a low carbon level [11]. This gas was used originally to grow AlGaAs films with low carbon concentration by MOCVD [12].

Conventionally, ALD is a process in which the layer deposition rate is slow. By using DMAH, the number of deposition cycles can be reduced by a deposition rate (1.31 Å/cycle) higher than that of TMA (0.91 Å/cycle). The higher deposition rate is due to the reduction of steric hindrance from the less bulky ligand and the number of available reaction sites is higher [2]. However, there has been no report on Al_2O_3/GaN MOS

capacitors using DMAH and O_3 as precursor and oxidant, respectively. The low number of methyl groups in DMAH potentially reduces carbon due to the high quality Al_2O_3 gate insulator for Al_2O_3/GaN MOS capacitors.

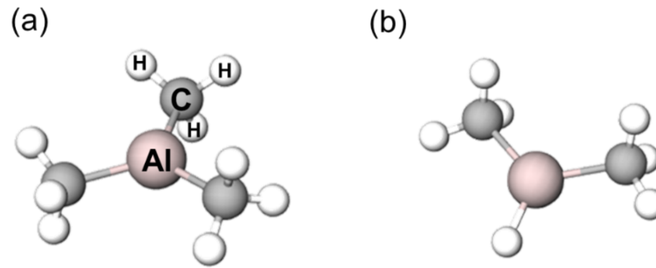

FIG. 4-1. Molecular model of (a) TMA and (b) DMAH. DMAH in which one of the methyl groups is bonded to hydrogen compound to replace TMA.

4.3 Device Fabrication

Homoepitaxial layer (2 μm, Si :5 × 10^{16} cm^{-3}) on c-plane free-standing GaN substrates was utilized. After performing the standard RCA cleaning process, An Al_2O_3 film with a nominal thickness of 40 nm on the n^+-GaN (0001) surface using T-ALD was deposited. The Al_2O_3 film at 300 °C was deposited by repeating cycles of introducing TMA and DMAH as the aluminum precursor and then supplying O_3. The deposition rate of the Al_2O_3 film was 0.91 Å/cycle and 1.31 Å/cycle, respectively. Time cycle of ALD process using both TMA and DMAH was same. Then, HPWVA under a constant pressure of 0.5 MPa at an annealing temperature of 400 °C for 30 min was subjected. In addition, the samples to N_2 PDA and O_2 PDA at an annealing temperature of 400 °C for 30 min were subjected. As the top electrode, a 100-nm-thick layer of Al using electron-beam deposition was evaporated. After removing the oxide from the back of the GaN substrate,

a 10/100-nm-thick Ti/Al layer as the bottom electrode used as the back side ohmic contact was deposited.

4.4 Electrical Characterization of MOS Capacitor with DMAH

4.4.1 Comparison of Characteristics of ALD-Al_2O_3 between TMA and DMAH

Figure 4-2 shows C–V characteristics of ALD-Al_2O_3 with TMA and DMAH/GaN MOS capacitors with and without HPWVA as a function of frequency. The measurement frequency ranged from 1 MHz to 1 kHz. The frequency dispersion was small for DMAH samples compared with TMA. The number of measured points is 5 points. Error of each points of the C-V curve was about ± 0.025 V, only one data is shown. Frequency dispersion was small even for DMAH samples w/o HPWVA. This indicated that the density at interface was low even for DMAH samples of w/o HPWVA.

Table 4-1 shows the V_{FB} and N_F of TMA and DMAH samples with and without HPWVA. The ideal flat band voltage is -0.11 V in condition. The V_{FB} of TMA sample w/o HPWVA is positive, whereas the V_{FB} of DMAH is a negative. This indicates that the presence of positive charges either at the interface or in the Al_2O_3 film of the DMAH samples, and TMA samples have positive fixed charges. Thus, the results is related to the carbon contents. These results are consistent with the previous studies, reporting that the residual carbon acts as traps and forms negative fixed charges in the Al_2O_3 film [13]. The N_F of DMAH sample w/o HPWVA is smaller than the N_F of TMA sample w/o HPWVA. It is also found that defects and traps in the film are lower in DMAH than in TMA. In addition, DMAH samples with HPWVA is the closest to ideal voltage compared with TMA sample. N_F of DMAH sample with HPWVA (4.50×10^{10} cm^{-2}) decreases more than

that of TMA sample with HPWVA (1.25×10^{11} cm^{-2}). The V_{FB} of DMAH samples with HPWVA becomes close to the ideal value, and HPWVA was effective also in DMAH sample.

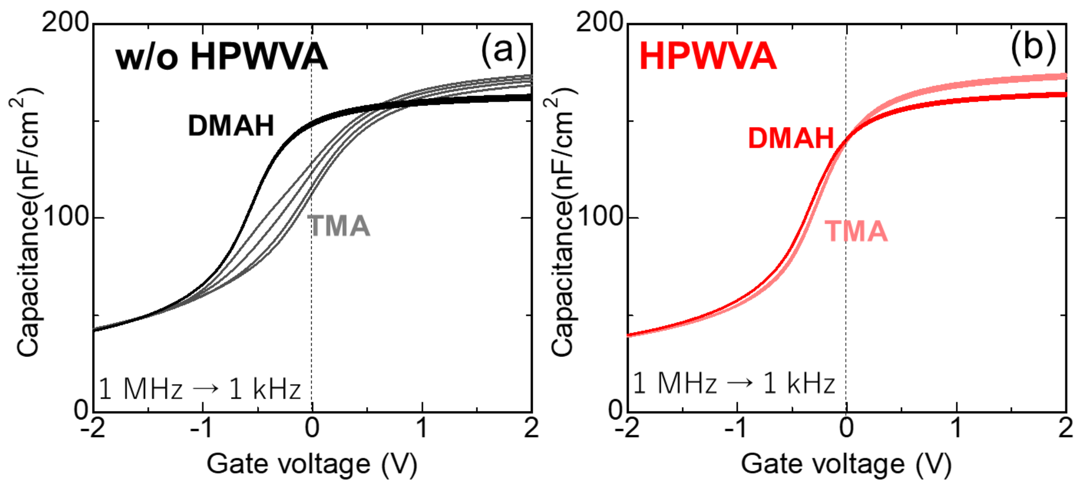

FIG. 4-2 Frequency dispersion of the C–V characteristics of ALD-Al_2O_3 with TMA and DMAH/GaN MOS capacitors without HPWVA and with HPWVA. The measurement frequency ranged from 1 MHz to 1 kHz.

TABLE 4-1 Summary of V_{FB} shift and N_f of ALD-Al_2O_3/GaN MOS capacitors.

Sample Condition	V_{FB} (V)	N_F (cm^{-2})
DMAH : w/o HPWVA	-0.34	2.30×10^{11}
DMAH : HPWVA	-0.16	4.50×10^{10}
TMA : w/o HPWVA	0.52	6.43×10^{11}
TMA : HPWVA	-0.21	1.25×10^{11}

Figure 4-3 shows the comparison of the energy distribution of interface trap density of ALD-Al_2O_3 with TMA and DMAH/GaN MOS capacitors with and without HPWVA. The D_{it} of DMAH sample w/o HPWVA at an energy level of E_C - E = 0.3 eV was ~ 1.0 $\times 10^{11}$ cm^{-2} eV^{-1} compared with ~ 1.0×10^{12} cm^{-2} eV^{-1} of TMA samples. At the interface

between the insulator and GaN, trap levels related to nitrogen vacancy V_N have been reported near Ec - 0.5 eV and the distribution of 0.5 eV with TMA sample is not confirmed for the DMAH sample. This result confirms that interface traps can be reduced by using DMAH. D_{it} of the DMAH and TMA samples with HPWVA was obtained to be very low below 10^{11} $cm^{-2}eV^{-1}$. D_{it} of both DMAH and TMA samples with HPWVA were 10^{10} $eV^{-1}cm^{-2}$ order and were almost same. The 10^{10} $eV^{-1}cm^{-2}$ order is almost the detection limit of the hi-lo method and these indicated that a very good interface is formed [14-17].

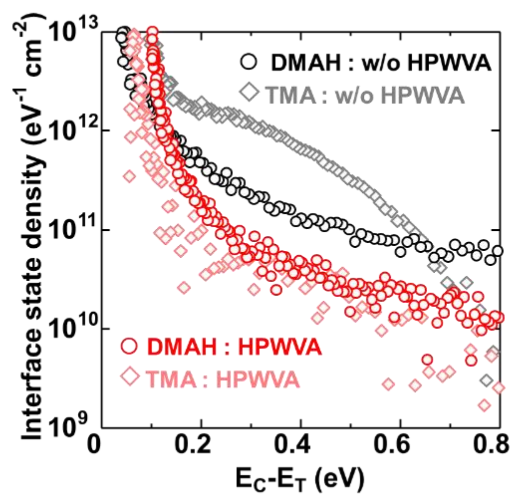

FIG. 4-3 Energy distribution of interface trap density of ALD-Al_2O_3 with TMA and DMAH/GaN MOS capacitors without HPWVA and with HPWVA. E_C denotes the conduction band edge of GaN.

Figure 4-4 shows the J-E characteristics of ALD-Al_2O_3 /GaN MOS capacitors using TMA and DMAH with and without HPWVA. The number of measurement points at each temperatures are 5 points, and each points broke down due to hard breakdown. The leakage currents of both TMA and DMAH samples sharply increased above 3 MV/cm and E_{BD} were observed between 7 and 9 MV/cm. The E_{BD} of DMAH samples w/o HPWVA and w/ HPWVA were 7.8 and 8.3 MV/cm, respectively, and DMAH

samples showed higher E_{BD} than TMA samples. These results indicate that the DMAH samples lead to good breakdown properties, which could be due to the densification of the Al_2O_3 network. The J-E curve of the DMAH sample with HPWVA shifted a little toward a high electric direction. These results could be interpreted by the electron injection into the traps in the Al_2O_3 films, as described in section 2.5.2 [18, 19]. The leakage current in the DMAH sample was slightly higher than that in the TMA sample. The difference of leakage current between TMA and DMAH can be explained by SCC-FE model [6]. Hiraiwa et al. reported that the difference in the leakage current was affected mostly by the substrate-side effective electron affinity and the sheet of charge near the substrate.

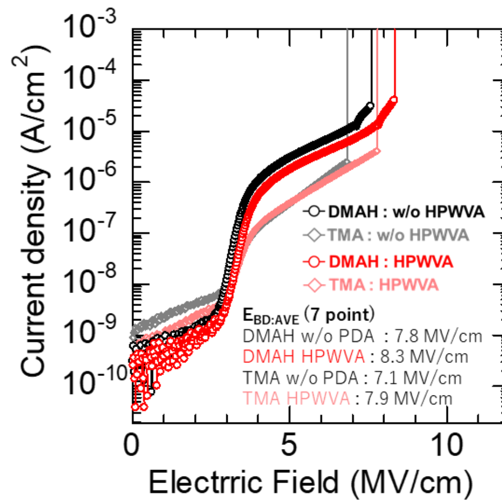

FIG. 4-4 J- E_{BD} of ALD-Al_2O_3 with TMA and DMAH/GaN MOS capacitors without HPWVA and with HPWVA.

4.4.2 Comparison of Characteristics of DMAH samples with PDA

In the previous section, the effect of HPWVA has been compared with a sample w/o HPWVA. This section shows the results of comparison with various conditions in dry

PDA. J- E_{BD} of ALD-Al_2O_3 with DMAH /GaN MOS capacitors is shown in FIG. 4-5. The leakage current of N_2 PDA and O_2 PDA sample showed almost no change compared to that w/o PDA and slight decrease was confirmed in HPWVA sample. In addition, the E_{BD} was 7.6 V and 7.7 V for the N_2 PDA and O_2 PDA samples, respectively.

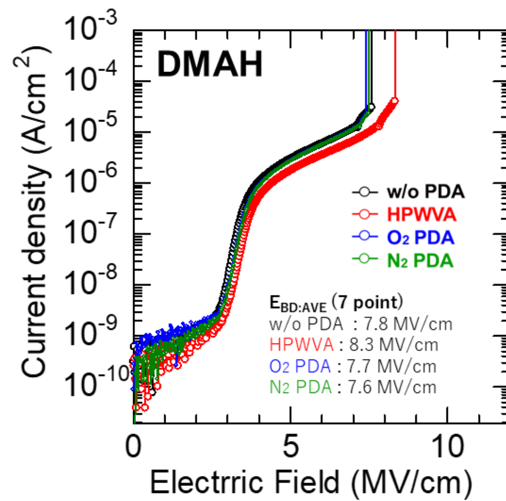

FIG. 4-5 J- E_{BD} of of ALD-Al_2O_3 with DMAH /GaN MOS capacitors of w/o PDA, HPWVA, O_2 PDA and N_2 PDA.

Figure 4-6 shows C–V characteristics of ALD-Al_2O_3 with DMAH/GaN MOS capacitors of w/o PDA, HPWVA (0.5 MPa), O_2 PDA and N_2 PDA as a function of frequency. The frequency dispersion was small for all samples. V_{FB} shifted in the positive direction by applying N_2 PDA, O_2 PDA and HPWVA. As shown in Table 4-2, the N_F improvement by O_2 PDA and N_2 PDA were small. However, HPWVA had a further reduction effect than N_2 PDA and O_2 PDA.

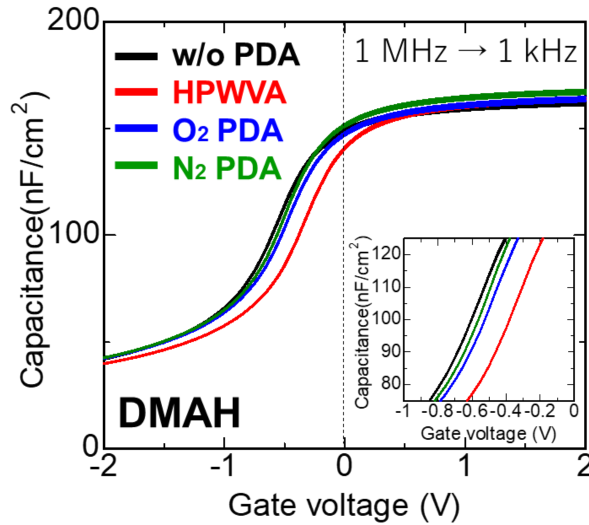

FIG. 4-6 Frequency dispersion of the C–V characteristics of ALD-Al_2O_3 with DMAH / GaN MOS capacitors of w/o PDA, HPWVA (0.5 MPa), O_2 PDA and N_2 PDA.

TABLE 4-2 Summary of flat-band shift and fixed charge density of ALD-Al_2O_3 with DMAH / GaN MOS capacitors.

Sample Condition	V_{FB} (V)	N_F (cm^{-2})
w/o PDA	-0.34	2.30×10^{11}
HPWVA	-0.16	4.50×10^{10}
O2 PDA	-0.24	1.36×10^{11}
N2 PDA	-0.35	2.40×10^{11}

Figure 4-7 shows positive shift of C–V step-stress measured for ALD-Al_2O_3 with DMAH/GaN MOS capacitors of w/o PDA, HPWVA (0.5 MPa), O_2 PDA and N_2 PDA. C–V measurement was performed by sweeping the gate voltage from to depletion. As shown in FIG. 4-6 (e), summary of positive C–V shifts of HPWVA showed that the stress shift was improved in the order of HPWVA, O_2 PDA, N_2 PDA. This trend correlates with the reduction of N_F in Table 4-2.

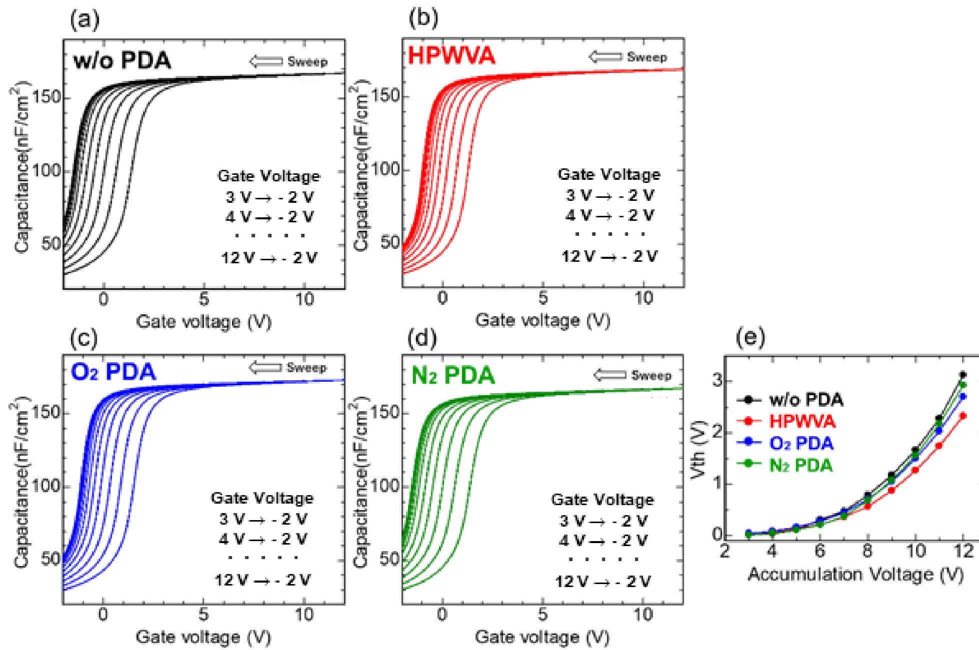

FIG. 4-7 Positive shift of C–V step-stress measured for ALD-Al_2O_3 with DMAH/GaN MOS capacitors with (a)w/o PDA, (b)HPWVA, (c)O_2 PDA, (d)N_2 PDA (e)Summary of V_{FB} shift plot per accumulation voltage. C–V measurements were performed by sweeping the gate voltage from accumulation to depletion. (e0 Summary of positive C–V shifts as a function of accumulation voltage.

Figure 4-8 shows the comparison of the energy distribution of interface trap density of ALD-Al_2O_3 with DMAH/GaN MOS capacitors of w/o PDA, HPWVA, O_2 PDA and N_2 PDA. D_{it} of the DMAH sample with HPWVA was lowest and D_{it} of N_2 PDA and O_2 PDA have no different significantly. These results indicate HPWVA is effective to reduce the traps such as oxygen defect of the Al_2O_3 film and interface trap with DMAH and Al_2O_3/GaN MOS structure. As a reason why HPWVA is superior to other dry heat treatments, the high oxidizing power of the HPWVA was effective, as mentioned in section 2.6.2, and reoxidation of defects in the Al_2O_3 film and oxidation of the interface were effective for improving electrical properties.

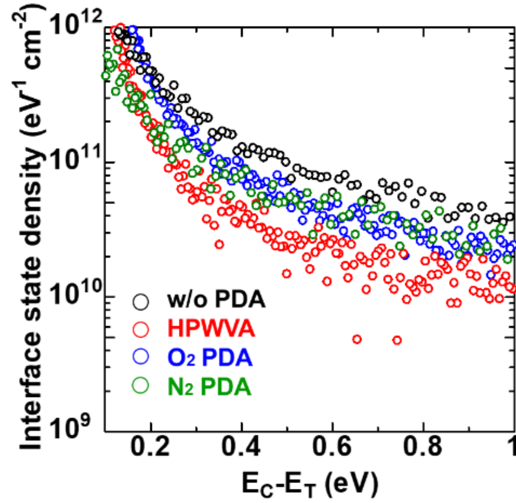

FIG. 4-8 Energy distribution of interface trap density of ALD-Al_2O_3 with DMAH /GaN MOS capacitors of w/o PDA, HPWVA, O_2 PDA and N_2 PDA. E_C denotes the conduction band edge of GaN.

4.5 Investigation of the Effect with the ALD-Al_2O_3 with DMAH

Figure 4.9 shows the depth profile of 1H and 16O+1H in the ALD-Al_2O_3 film with TMA and DMAH measured by SIMS. The amount of residual hydrogen in the Al_2O_3 film of DMAH is almost the same as TMA. Although it was thought that there is a difference in the amount of residual hydrogen due to the hydrogen group of DMAH, the result was different from the hypothesis, and the hydrogen residue of Al_2O_3 film of DMAH showed an almost same with that of TMA. The reason why the residual hydrogen of DMAH is the same as TMA is considered to be related that the bond dissociation energies of Al - C and Al - H are about the same [20]. Therefore, it is considered that hydrogen is desorbed from the Al_2O_3 film during the ALD process like the methyl group.

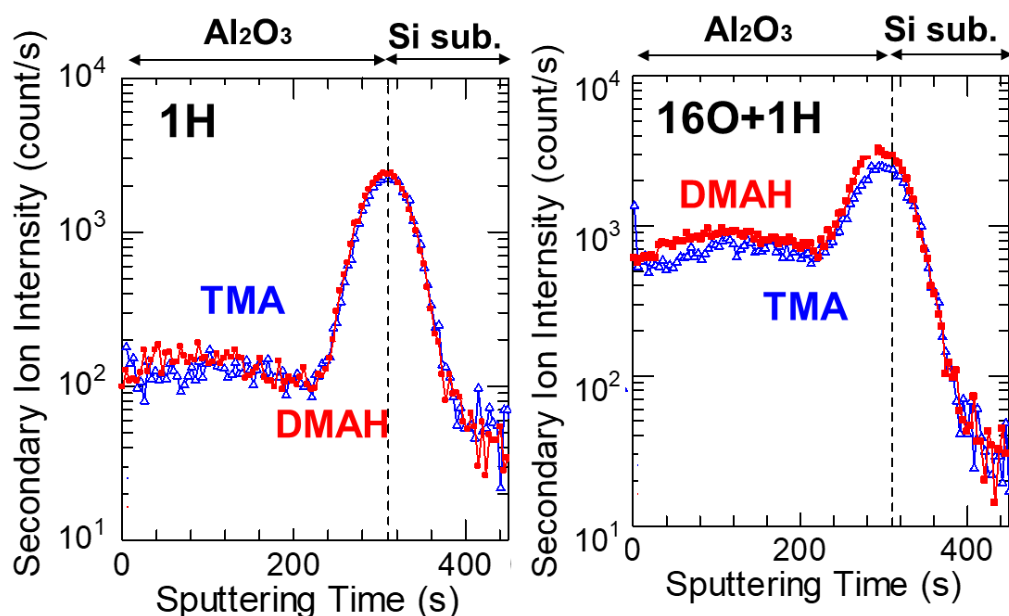

FIG. 4-9. Depth profile of 1H and 16O+1H in the ALD-Al_2O_3 film with TMA and DMAH measured by SIMS.

Figure 4.10 shows depth profile of carbon in the ALD-Al_2O_3 film of between TMA and DMAH measured by SIMS. This results showed that reduction of residual carbon of ALD-Al_2O_3 was achieved by the use of DMAH as a precursor. The reduction in residual carbon was approximately 50%. One of the methyl groups is bonded to hydrogen in the molecular model of DMAH compared with TMA. Comparing DMAH with two methyl groups and TMA with three methyl groups, a 66% decrease was expected. However, the difference in residual carbon concentration between the two samples was even higher. The residual carbon concentration is not only dependent on the precursor but also on the chemical reactions occurring during the ALD process. It was not confirmed the reduction of carbon impurities in TMA and DMAH samples by HPWVA in SIMS. The error in SIMS is approximately 2% and it could not be determined the reduction of carbon impurities [21].

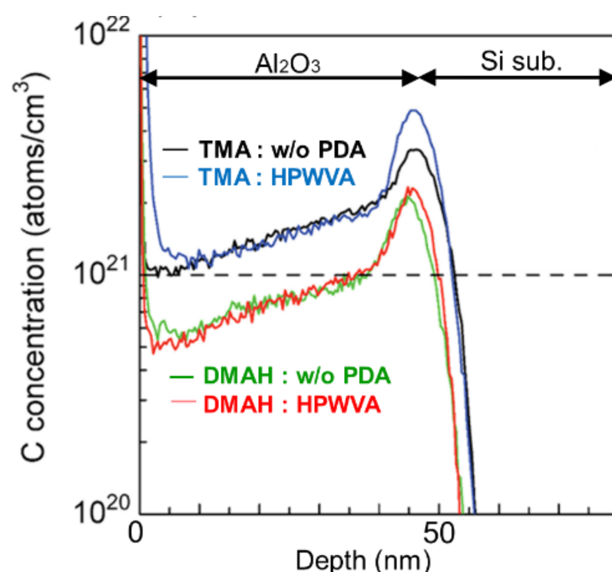

FIG. 4-11. Depth profile of carbon in the ALD-Al_2O_3 film measured with TMA and DMAH by SIMS.

Figure 4-12 shows the TDS at a mass-to-charge ratio m/z = 44 (corresponding to fragment ion C_XH_y and CO_2) for samples with and without HPWVA, O_2 PDA at 400 °C for 30 min and for the GaN substrate. The desorption peak from 100 °C to 400 °C corresponds to desorption of hydrocarbon fragment ions from the Al_2O_3 film or GaN surface [22]. In addition, the desorption peak at 500°C corresponds to desorption of CO_2. Thus, these desorption is attributed to residual carbon derived from precursor of the Al_2O_3 film. These results shows that residual carbon of HPWVA decreased compared with w/o HPWVA. In addition, HPWVA reduces residual carbon more than O_2 PDA. It suggested that higher oxidizing power of HPWVA was influenced compared with O_2 PDA at the same anneal temperature. As the results of TDS was a more sensitive detection than results of SIMS, it seems that HPWVA have the effect to reduce a few carbon, which could not be measured the difference of residual carbon between w/o HPWVA and HPWVA by SIMS.

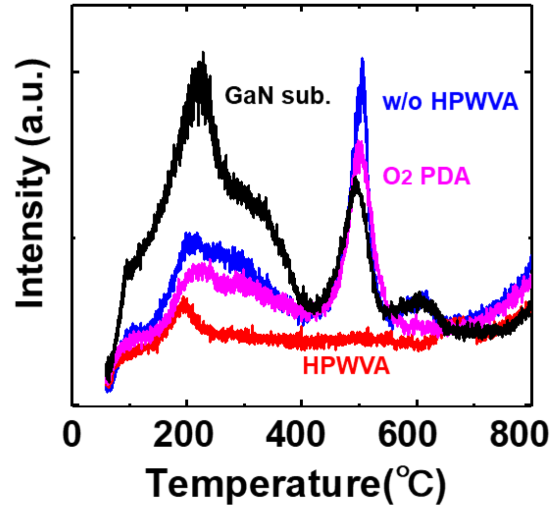

FIG. 4-12 Thermal-desorption spectra at m/z =44 without HPWVA, with HPWVA, O_2 PDA and for the GaN substrate.

Figure 4-13 showed N_F versus carbon concentration for the TMA, TMA with HPWVA, DMAH and DMAH with HPWVA samples. Comparing TMA and DMAH samples, N_F decreased as the carbon concentration decreased. In addition, N_F of both these samples with HPWVA became lower by improving the film quality due to a decrease in oxygen defects. Thus, the traps are influenced both by carbon impurities and dangling bonds in the Al_2O_3 film. Therefore, the residual carbon in the Al_2O_3 film was reduced by using DMAH and Al_2O_3 with DMAH has better quality than that with TMA. Furthermore, by reoxidation of the Al_2O_3 and compensation of the dangling bonds, further improvement was achieved in the DMAH with HPWVA.

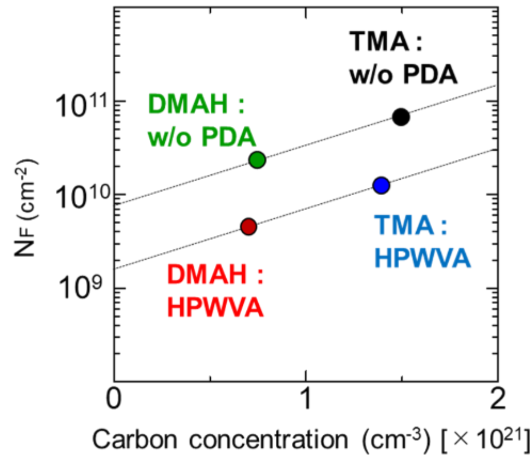

FIG. 4-13 N_F versus carbon concentration for the TMA, TMA with HPWVA, DMAH and DMAH with HPWVA samples.

4.6 Summary

In this study, the effect of ALD precursor type between TMA and DMAH and HPWVA on the Al_2O_3/GaN MOS capacitors was investigated. The comparison with various dry PDA on the Al_2O_3/GaN MOS capacitors was also investigated. The tendency of the electrical properties with TMA and DMAH samples is reproducible. Reduction of residual carbon using DMAH as ALD precursor was confirmed and N_F and D_{it} are strongly affected by carbon impurities at the Al_2O_3/GaN MOS structure. The amount of residual hydrogen in the Al_2O_3 film of DMAH is almost the same as TMA. In addition, it was also observed that there is an improvement in N_F at the DMAH-Al_2O_3/GaN MOS structure by the compensation of the dangling bonds due to HPWVA effect. HPWVA is more effective in improving the film quality and interface with the use of DMAH and for Al_2O_3/GaN MOS structure than N_2 and O_2 PDA. Furthermore, for the improvement of D_{it} at the Al_2O_3/GaN interface, it is preferable to reduce carbon impurity in addition to oxidation of the interface.

References

[1] R. W. Johnson, A. Hultqvist, and S. F. Bent, Mater. Today **17**, 236-246 (2014).

[2] R. L. Puurunen, J. Appl. Phys. **97**, 121301 (2005).

[3] Y. H. Chang, M.-J. Yu, R.-P. Lin, C.-P. Hsu, and T.-H. Hou, Appl. Phys. Lett. **108**, 033502 (2016).

[4] X. Ding, H. Zhang, J. Zhang, J. Li, W. Shi, X. Jiang, and Z. Zhang, Mater. Sci. Semicond. Process **29**, 69-75 (2015).

[5] D. C. Corsino, J. P. S. Bermundo, M. N. Fujii, K. Takahashi, Y. Ishikawa, and Y. Uraoka, Appl. Phys. Express **11**, 061103 (2018).

[6] M. Uenuma, K. Takahashi, S. Sonehara, Y. Tominaga, Y. Fujimoto, Y. Ishikawa, Y. Uraoka, AIP Adv. **8**, 105103 (2018).

[7] G. He, X. Wang, M. Oshima, and Y. Shimogaki, Jpn J. Appl. Phys., **49**, 031502 (2010).

[8] M. Sugiyama, H. Itoh, J. Aoyama, H. Komiyama, and Y. Shimogaki: Jpn. J. Appl. Phys. **39**, 1074 (2000).

[9] M. Sugiyama, T. Iino, T. Nakajima, T. Tanaka, Y. Egashira, K. Yamashita, H. Komiyama, and Y. Shimogaki: Thin Solid Films **498**, 30 (2006).

[10] M. Sugiyama, T. Nakajima, T. Tanaka, H. Itoh, J. Aoyama, Y. Egashira, K. Yamashita, H. Komiyama, and Y. Shimogaki: Jpn. J. Appl. Phys. **39**, 6501 (2000).

[11] T. Cacouris, G. Scelsi, P. Shaw, R. Scarmozzino, and R. M. Osgood, Appl. Phys. Lett. **52**, 1865 (1988).

[12] R. Bhat, M. A. Koza, C. C. Chang, and S. A. Schwars: J. Cryst. Growth **77**, 7 (1986).

[13] M. Choi, J. L. Lyons, A. Janotti, and C. G. Van de Walle, Appl. Phys. Lett. **102**, 142902 (2013).

[14] A. N. Hattori, F. Kawamura, M. Yoshimura, Y. Kitaoka, Y. Mori, K. Hattori, H.

Daimon, K. Endo, Surface Science, 604, 1247 (2010)

[15] A. N. Hattori, K. Endo, K. Hattori, H. Daimon, Appl. Surf. Sci., 256, 14 (2010)

[16] A. N. Hattori, T. Okamoto, S. Sadakuni, J. Murata, K. Arima, Y. Sano, K. Hattori, H. Daimon, K. Endo, K. Yamauchi, Surf. Sci., 605, 597 (2011)

[17] Y. Ogawa and Y. Horiike, Hajimete no handotai senjo gijutsu, Kogyo chosa-kai, (2002)

[18] N. X. Truyen, N. Taoka, A. Ohta, K. Makihara, H. Yamada, T. Takahashi, M. Ikeda, M. Shimizu, and S. Miyazaki, Jpn. J. Appl. Phys. **57**, 04FG11 (2018).

[19] H. Hasegawa, and T. Sawada, J. Vac. Sci. Technol., **16**, 1478 (1979).

[20] K. Chokawa, E. Kojima, M. Araidai, K. Shiraishi, Phys. Status Solidi B 2018, 255, 1700323

[21] Y. Honma, Surf. Sci. **24**, 239 (2003)

[22] J. H. Han, M. Takenaka, and S. Takagi, Jpn. J. Appl. Phys. **55**, 04EC06 (2016)

Chapter 5　Conclusions

5.1 Conclusions

In order to develop high-performance GaN power devices and power electronics, investigation of the electronic and physical properties in GaN MOS capacitors is one of the most critical issue, as described in Chapter 1. In this study, the influence of insulating film quality and Al_2O_3/GaN interface and local interfacial structure evaluated by various techniques. This thesis mainly described the highest quality Al_2O_3 film and interface on Al_2O_3/GaN MOS capacitors among the previous studies were achieved by annealing process and deposition process. In addition, it is established the Al_2O_3/GaN interface atomic model and revealed the reforming process of Al_2O_3 and its interface. The results obtained in this study are important from both a scientific and an engineering point of view.

In Chapter 2, HPWVA using high temperature and high pressure steam as a PDA process for Al_2O_3/GaN MOS capacitors was proposed. In order to investigate the trapping state at the Al_2O_3/GaN interface and mechanism of HPWVA, electrical properties evaluation and physical characteristics evaluation were used. Improvement of the E_{BD} and lifetime from I-V characteristic and reduction of N_F and D_{it} from C-V characteristic was confirmed by processing HPWVA with 0.5 MPa. It produces high-quality Al_2O_3 films with reduced values of N_F by the reaction of H_2O monomer derived from HPWVA. The low D_{it} is thought to result from the formation of gallium oxide at the Al_2O_3/GaN interface due to oxidization caused by the HPWVA. However, electrical properties of HWPVA more than 1.0 MPa came worsted because high oxidation power of HPWVA become promotion oxidation of GaN substrate and increase defects near the interface by GaOx

formation. This suggests that HPWVA is sensitive to pressure conditions. Actually, exceeding 6 MPa, a crystal growth product of 1 μm size was confirmed through the Al_2O_3 film from the GaN interface. In additon, it was possible to maintain reliability in HPWVA capacitors even at high temperature of 200 ° C.

In Chapter 3, the atomic state and atomic structure at the Al_2O_3/GaN interface was investigated. ABF-STEM images indicate that an excessively damaged layer of Al_2O_3/GaN interface after Al_2O_3 deposition was not found. The surface-sensitive Al2p on the GaN surface where the Al_2O_3 film was etched was slightly detected and this major peak is clearly the Al-N bond. Quantitative analysis of XPS revealed that the Al element was substituted by up to ~10% in the GaN surface. In addition, it is found that PIAD of Al2p is similar to the Ga3p PIAD. This showed that Al atoms fixed in Ga atomic sites in the vicinity of the uppermost surface of GaN substrate during the ALD deposition. An extremely thin Al_2O_3/GaN multiphase layer was formed at the Al_2O_3/GaN interface. Al easily replaces the Ga site at the boundary of the step surface. This report is the result that became clear for the first time.

In Chapter 4, the effect of ALD precursor between trimethyl aluminum (TMA) and dimethyl aluminum hydride (DMAH) on the Al_2O_3/GaN MOS capacitors was investigated. The DMAH comprises fewer methyl groups compared to TMA. The comparison with dry PDA on the Al_2O_3/GaN MOS capacitors was also investigated. Reduction of residual carbon using DMAH was confirmed and N_F and D_{it} are strongly affected by carbon impurities. Also, film quality with DMAH and HPWVA of Al_2O_3/GaN MOS capacitor is better than TMA and HPWVA. Therefore, to improve of film quality and interface for Al_2O_3/GaN MOS structure, DMAH is optimal precursor compared with TMA.

Finally, the influence of film quality and Al_2O_3/GaN interface and local interfacial structure were evaluated by various techniques. The high quality Al_2O_3 film and Al_2O_3/GaN interface were achieved by applying HPWVA and using DMAH precursor due to the reduction of residual carbon and the reaction with H2O monomer. Furthermore, Al atoms were fixed in Ga sites in the uppermost surface of GaN substrate during the ALD process. It suggested that an extremely thin AlGaN transition layer was formed at the Al_2O_3/GaN interface.

The position of these results for application of the GaN MOS device are summarized. The results of this study shows that N_F was 4.5×10^{10} $cm^{-2}$and D_{it} was 5×10^{10} $eV^{-1}cm^{-2}$ at 0.3 eV for ALD-Al_2O_3/n-type GaN (0001) MOS capacitor. In particular, high temperature anneal at about 800 °C is mainly used as the PDA and the reduction effect of N_F and D_{it} was up to 10^{11} order [1,2]. However, by a simple method such as changing the ALD precursor and applying HPWVA at a low temperature of about 400 °C, it was possible to achieve a good electric characteristic of MOS capacitor. The 10^{10} cm^{-2} is an enough for properties of GaN MOS capacitor [3-6]. Recently, it has been reported that good electrical properties as well as this results are achieved only by post metallization anneal (PMA) of about 300 °C [7].

However, there is a concern that the electrical properties change due to the kinds of GaN substrate such as p-type and m-plane used for the MOS capacitor. Furthermore, reducing the defect density of GaN substrates and the development of ion implantation technology are also issues for development of GaN MOSFET, but it is unknown how much improvement of the vertical type GaN MOSFET contributes by improving the MOS characteristic used HPWVA and DMAH.

5.2 Suggestions for future work

There are still many challenges for realization of high performance GaN based power device and problems preventing a deeper understanding of MOS interface. The following are suggested as future work.

1. Investigation of characteristics of Al_2O_3/GaN in heterogeneous GaN substrates

In this study, the free-standing GaN substrate which is n-type and c plane (0001) was used. However, for development of fabricating a vertical-type GaN MOSFET, investigation of MOS capacitors used p-type GaN substrate is necessary. Furthermore, assuming that a gate recess structure in GaN MOS devices is applied, it is also necessary to investigate the Al_2O_3/GaN interface at the m-plane GaN [8]. Otherwise, p-type GaN is generally grown by using Mg as an acceptor and there is a problem that a large amount of impurity hydrogen is contained [9]. Thus, hydrogen diffusion towards the insulating film is a concern due to the annealing process and so on, and it is possible to appear different characteristics from Al_2O_3/GaN MOS capacitors used n-type GaN. Both subjects are indispensable for developing vertical GaN MOSFET.

2, Deep understanding of hydrothermal reaction

Improvement of characteristics of Al_2O_3/GaN MOS capacitor by applying HPWVA and the construction of a reforming model was achieved. Also, the pressure dependence of HPWVA was investigated and negative effect such as increase of roughness delivered from GaN substrate was seen under high pressure. Therefore, optimization of pressure is very sensational in improving film quality and interface quality.

Currently, research on time dependence and temperature dependence in HPWVA is

under way. It is necessary to further study how the characteristics by changing HPWVA parameters such as temperature, time and pressure and the hydrothermal reaction such as the ion product ($[H^+]$ $[OH^-]$) and radical reaction are linked with each other. As one of the methods, by applying reaction simulation such as gas molecular dynamics, it is possible to study an improvement process of reaction of H_2O monomer by HPWVA. In addition, it is necessary to study in detail the generation mechanism of the crystal growth product grown from the GaN surface. This is an important issue to develop research on hydrothermal reaction not only in organic chemistry but also in application physics and semiconductor processes.

3, Development of application to GaN MOS HEMT and vertical- GaN MOSFET

In this study, only a simple GaN MOS capacitor was used. Thus, there is a need for demonstration of the GaN MOS devices such as GaN HEMT and MOSFET. As described in Chapter 1, the problems of fabrication process of MOSFET is included not only the MOS interface but also crystal defects and doping technique such as p-GaN and so on, so there is concern that evaluation will be difficult. However, However, it is indispensable to study how improvement of MOS characteristics affects device performance of MOSFET for development of power device. The roadmap of GaN based devices shows the breakdown voltage of 1200 V and on resistance of 1 mΩ・A are aimed until 2021 and the improvement of the MOS characteristics is academically and industrially important.

References

[1] Nguyen Xuan Truyen, Noriyuki Taoka, Akio Ohta, Katsunori Makihara, Hisashi Yamada, Jpn J Appl. Phys. **57**, 04FG11 (2018)

[2] Yujin Hori, Chihoko Mizue, and Tamotsu Hashizume, Jpn J Appl. Phys.**49**, 080201 (2010)

[3] A. N. Hattori, F. Kawamura, M. Yoshimura, Y. Kitaoka, Y. Mori, K. Hattori, H. Daimon, K. Endo, Surface Science, 604, 1247 (2010)

[4] A. N. Hattori, K. Endo, K. Hattori, H. Daimon, Appl. Surf. Sci., 256, 14 (2010)

[5] A. N. Hattori, T. Okamoto, S. Sadakuni, J. Murata, K. Arima, Y. Sano, K. Hattori, H. Daimon, K. Endo, K. Yamauchi, Surf. Sci., 605, 597 (2011)

[6] Y. Ogawa and Y. Horiike, Hajimete no handotai senjo gijutsu, Kogyo chosa-kai, (2002)

[7] T. Hashizume, S. Kaneki, T. Oyobiki, Y. Ando, S. Sasaki and K. Nishiguchi, Appl. Phys. Express **11**, 124102 (2018)

[8] K. Fujito, K. Kiyomi, T. Mochizuki, H. Oota, H. Namita, S. Nagao and I. Fujimura, **205**, 1056 (2008).

[9] I. waki, doctoral paper, Tokyo Uni. No. 16667.

Achievements

I. Academic journals

1) Yuta Fujimoto, Mutsunori Uenuma, Tsubasa Nakamura, Masaaki Furukawa, Ishikawa Yasuaki and Yukiharu Uraoka, "The physical and electrical properties of ALD-Al_2O_3/GaN MOS annealed with high pressure water vapor", Jpn. J. Appl. Phys. Lett. Rapid comm. (Accepted)

2) Mutsunori Uenuma, Kiyoshi Takahashi, Sho Sonehara, Yuta Tominaga, Yuta Fujimoto, Yasuaki Ishikawa, and Yukiharu Uraoka, "Influence of carbon impurities and oxygen vacancies in Al_2O_3 film on Al_2O_3/GaN MOS capacitor characteristics", AIP ADVANCES **8**, 105103 (2018)

Referenced paper

1) Yuta Fujimoto, Mutsunori Uenuma, Yasuaki Ishikawa, Yukiharu Uraoka, " Thermoelectric Devices Fabricated Using Amorphous Indium Gallium Zinc Oxide", ECS Trans., 575, 213-216, (2016) (invited)

2) Yuta Fujimoto, Mutsunori Uenuma, Yasuaki Ishikawa, Yukiharu Uraoka, "Thermoelectric Properties of a-InGaZnO Thin Film", AIP Advances, 5, 097209 (2015).

3) Yuta Fujimoto, Mutsunori Uenuma, Yasuaki Ishikawa, Yukiharu Uraoka, "Improvement of Thermoelectric Properties of a-InGaZnO Thin Film by Optimizing Carrier Concentration", Journal of electric material, 45, 1377–1381.(2015)

II. Presentations at conference

Presentations at international conference

1) Yuta Fujimoto, Mutsunori Uenuma, Hiroshi Ota, Fumihiro Matsui, Yasuaki Ishikawa and Yukiharu Uraoka "Analyses of Electronic and Atomic Structures of Insulator/GaN Interface by Photoelectron Diffraction and Spectroscopy", International Workshop on Nitride Semiconductors 2018, TuP-CR-13, Ishikawa, Japan, September 2018

2) Tsubasa Nakamura, Mutsunori Uenuma, Yuta Fujimoto, Yasuaki Ishikawa and Yukiharu Uraoka "Effects of Annealing Time in High Pressure Water Vapor Annealing for ALD- Al_2O_3/GaN MOS", International Workshop on Nitride Semiconductors 2018, TuP-ED-2, Ishikawa, Japan, September 2018

3) Masaaki Frukawa, Mutsunori Uenuma, Yuta Fujimoto, Yasuaki Ishikawa and Yukiharu Uraoka "Improvement of SiO_2/GaN Interface Characteristics by High Pressure Water Vapor Annealing", International Workshop on Nitride Semiconductors 2018, MoP-CR-24, Ishikawa, Japan, September 2018

4) Mutsunori Uenuma, Kiyoshi Takahashi, Sho Sonehara, Yuta Tominaga, Yuta Fujimoto, Yasuaki Ishikawa, and Yukiharu Uraoka "Effects of ALD-Precursor on Al_2O_3/GaN MOS Characteristics", International Workshop on Nitride Semiconductors 2018, TuP-ED-7, Ishikawa, Japan, September 2018

5) Yuta Fujimoto, Mutsunori Uenuma, Tsubasa Nakamura, Masaaki Frukawa, Yasuaki Ishikawa and Yukiharu Uraoka "Physical and Electrical Properties of ALD- Al_2O_3/GaN MOS Annealed by High Pressure Water Vapor", Materials Research Society 2018, EP.08.10., Boston, September 2018

Presentations at domestic conference

1) 冨永雄太，上野勝典，上沼睦典，藤本裕太，石河泰明，浦岡行治 "高圧水蒸気処理による SiO_2/GaN MOS 界面制御および絶縁膜の改質", 2016 年度先進パワー半導体分科会第 3 回講演会, P109, つくば国際会議場, 11 月, 2016 年

2) 上沼 睦典、高橋 清、曽根原 翔、赤野 拓哉、藤本 裕太、石河 泰明、浦岡行治" DMAH を用いて成膜した Al_2O_3/GaN MOS の評価" 第 78 回応用物理学会秋季学術講演会, 6p-PA8-7, 福岡国際会議場, ９月, (2017)

3) 藤本裕太，上沼睦典，太田紘志，松井文彦，石河泰明，浦岡行治 "光電子回折・分光法を用いた絶縁膜/GaN 界面の電子状態と原子構造の評価", 78 回応用物理学会秋季学術講演会, 6p-PA8-4, 福岡国際会議場 9 月, 2017 年

4) 安藤領汰，上沼睦典，藤本裕太，石河泰明，浦岡行治 "高圧水蒸気処理によ

る SiO_2 膜の物性および電気的特性変化", 第 65 回応用物理学会春季学術講演会, 17p-P12-7, 早稲田大学, 3 月, 2017 年

5) 古川暢昭，上沼睦典，藤本裕太，石河泰明，安田昌弘，浦岡行治 "SiO_2/n-GaN 界面に対する高圧水蒸気処理条件の検討"，第 65 回応用物理学会春季学術講演会, 17p-P12-6 早稲田大学, 3 月, 2017 年

6) 曽根原 翔，上沼睦典，藤本裕太，石河泰明，浦岡行治 "積層構造による Al_2O_3/GaN MOS 特性の改善"，第 65 回応用物理学会春季学術講演会, 17p-P12-13 早稲田大学, 3 月, 2017 年

7) 中村翼，上沼睦典，藤本裕太，石河泰明，浦岡行治 "ALD-Al_2O_3/GaN MOS 構造における高圧水蒸気処理の圧力依存性", 第 65 回応用物理学会春季学術講演会, 17p-P12-11, 早稲田大学, 3 月, 2017 年

8) 中村翼，上沼睦典，藤本裕太，石河泰明，浦岡行治 "ALD-Al_2O_3/GaN MOS における高圧水蒸気処理の時間依存性", 第 79 回応用物理学会秋季学術講演会, 18p-PA6-17, 名古屋国際会議場, 9 月, 2018 年

Acknowledgements

First of all, I would like to express my gratitude to Prof. Yukiharu Uraoka, my principal adviser, for his supervision, continuous guidance, and kind encouragement through discussions throughout the duration of this work. I want to give you heartfelt thanks for what you did.

I am very indebted to Prof. Tsuyosi Kawai and Prof. Ken Hattori for their supervision and critical comments for improving this thesis. I wish to express my deepest thanks to Assoc. Prof. Yasuaki Ishikawa for helpful discussions and valuable advice. He gave me precise advices and enthusiastic guidance at the progress report.

I am also indebted to Assistant Prof. Mutsunori Uenuma for technical support and helpful advice. He took a lot of time in discussing and consulting the experiment results and research plan kindly. In addition, I was heavily influenced in overall research such as attitude toward the research. It was impossible without Mr. Mutsunori Uenuma to carry out my research. I sincerely appreciate your time and consideration. To Associate Profs. Mami Fujii, Associate Profs. Juan Paolo Soria Bermundo and Associate Profs. Mime Kobayashi for their helpful support.

I would like to express my appreciation of Ms. Yukiko Morita for their great support and kindness in my daily work. I would also like to express my appreciation of Mr. Hirotoshi Kawahira and Mr. Akio Watakabe for their technical support of our laboratory. Thanks to them, I could received the guidance and cooperation such as handling of experimental equipment and improvement of research environment. I would also like to extend my gratitude to Mr. Noritaka Koike, Mr. Kazuhiro Miyake, and Mr. Yasuo Okajima for technical help. I could received the support to facilitate my research such as Management and guidance of common use equipment facilities.

The synchrotron radiation experiments were performed at the BL25SU of SPring-8 with the approval of the Japan Synchrotron Radiation Research Institute (JASRI) (Proposal No. 2017A1594). I thank Associate Prof. Fumihiko Matsui of the Green Nanosystem Laboratory, Mr. Hiroshi Ohta, all members of the Green Nanosystem Laboratory and the Surface and Materials Science Laboratory for technical support and valuable discussions on my experiments conducted at SPring-8.

I would like to extend my great appreciation to Mr. Koji Yoshitsugu of Mitsubishi electronics and Mr. Yuta Tominaga of Hitachi Corporation for their pioneering work and instruction. I deeply thank Mr. Lin Tenfda, Mr.Yuki Tada, Mr.Masaaki Frukawa, Mr. Ryota Ando, Mr. Tsubasa Nakamura and Mr. Masato Higashi of the powor device group for helpful discussions and technical help. I thank them the actively discussion about the research and deepening the knowledge by informing ideas.

I would like to extend my great appreciation to colleague in tis laboratory, Dr. Shunsuke Uchiyama, Dr. Itaru Raifuku. We spent a lot of time in our research life. This research life has been enriched by supporting each other and working hard. In addition, we became an irreplaceable friends by going out and consulting a lot in our life. I would like to express my appreciation of Dr. shun Fukami of Surface and Materials Science Laboratory. I spent a total of 9 years with him at university and graduate school. At our private life and my research life, we could consult anything and saved when we encountered problems that can not be solved. I was able to spend a fulfilling student life with his existence.

Thanks also go to Dr. Hiromi Okada, Dr. Yang Liu, Dr. Yuma Karaki, Dr. Yuki Hashima, Dr. Michael Paul Jallorina, Dr. Nguyen Chung Dong, Dr. Yuki Tada, Xudongfang Wang, Dr. Jenichi Clairvaux Felizco, Hiroto Murakami, Dr.Muhammad Arif

and Dr. Dianne Corsino for their helpful advice and valuable discussions. I wish to acknowledge, Mr. Daisuke Kobayashi, Mr. Yuta Miyagoshi, Mr. Ryosuke Mochii, Ms. Sachiko Morioka, Ms. Aimi Syairah Binti Safaruddin, Mr. Ryosuke Sato, Mr. Takanori Takahashi, Mr. Naoyoshi Noda, Mr. Hoshito Murakawa, and Mr. Daichi Yoshii and all members in the various laboratories for their understanding and for sharing good times during this research work.

Finally, I would really like to thank my parents and all my friends for their understanding, support, and encouragement.

March, 2019

Yuta Fujimoto